Multiscale and Stabilized Methods

Thomas J. R. Hughes[1], Guglielmo Scovazzi[2], and Leopoldo P. Franca[3]

[1] *Professor of Aerospace Engineering and Engineering Mechanics, and Computational and Applied Mathematics Chair III, Institute for Computational Engineering and Sciences, The University of Texas at Austin,201 E. 24th Street, ACE 6.412, 1 University Station C0200, Austin, Texas 78712-0027, U.S.A.*
[2] *Graduate Research Assistant, Mechanics and Computation Division, Mechanical Engineering Department, Stanford University, and Institute for Computational Engineering and Sciences, The University of Texas at Austin,*
[3] *Department of Mathematics, University of Colorado, P.O. Box 173364, Campus Box 170, Denver, Colorado 80217-3364, U.S.A.*

ABSTRACT

This article presents an introduction to multiscale and stabilized methods, which represent unified approaches to modeling and numerical solution of fluid dynamic phenomena. Finite element applications are emphasized but the ideas are general and apply to other numerical methods as well. (They have been used in the development of finite difference, finite volume, and spectral methods, in addition to finite element methods.) The analytical ideas are first illustrated for time-harmonic wave-propagation problems in unbounded fluid domains governed by the Helmholtz equation. This leads to the well-known Dirichlet-to-Neumann formulation. A general treatment of the variational multiscale method in the context of an abstract Dirichlet problem is then presented which is applicable to advective-diffusive processes and other processes of physical interest. It is shown how the exact theory represents a paradigm for subgrid-scale models and *a posteriori* error estimation. Hierarchical p-methods and bubble function methods are examined in order to understand and, ultimately, approximate the "fine-scale Green's function" which appears in the theory. Relationships among so-called residual-free bubbles, element Green's functions, and stabilized methods are exhibited. These ideas are then generalized to a class of non-symmetric, linear evolution operators formulated in space-time. The variational multiscale method also provides guidelines and inspiration for the development of stabilized methods (e.g., SUPG, GLS, etc.) which have attracted considerable interest and have been extensively utilized in engineering and the physical sciences. An overview of stabilized methods for advective-diffusive equations is presented. A variational multiscale treatment of incompressible viscous flows, including turbulence is also described. This represents an alternative formulation of Large Eddy Simulation which provides a simplified theoretical framework of LES with potential for improved modeling.

KEY WORDS: Stabilized Methods, Multiscale Methods, Turbulence, Dirchlet-to-Neumann Formulation, Variational Methods, Residual-free Bubbles, Space-time Formulations, Hierarchical p-refinement, Subgrid-scale Models, Galerkin's Method, Finite Elements, Advective-Diffusive Equations, Boundary-value Problems, Incompressible Navier-Stokes Equations, Smagorinsky Model, Eddy Viscosity Models, Exterior Problems.

Report Documentation Page

1. REPORT DATE **2004**	2. REPORT TYPE	3. DATES COVERED **-**

4. TITLE AND SUBTITLE **Multiscale and Stabilized Methods**	5a. CONTRACT NUMBER
	5b. GRANT NUMBER
	5c. PROGRAM ELEMENT NUMBER

6. AUTHOR(S)	5d. PROJECT NUMBER
	5e. TASK NUMBER
	5f. WORK UNIT NUMBER

7. PERFORMING ORGANIZATION NAME(S) AND ADDRESS(ES) **Office of Naval Research,One Liberty Center,875 North Randolph Street Suite 1425,Arlington,VA,22203-1995**	8. PERFORMING ORGANIZATION REPORT NUMBER

9. SPONSORING/MONITORING AGENCY NAME(S) AND ADDRESS(ES)	10. SPONSOR/MONITOR'S ACRONYM(S)
	11. SPONSOR/MONITOR'S REPORT NUMBER(S)

12. DISTRIBUTION/AVAILABILITY STATEMENT
Approved for public release; distribution unlimited

13. SUPPLEMENTARY NOTES
The original document contains color images.

14. ABSTRACT
see report

15. SUBJECT TERMS

16. SECURITY CLASSIFICATION OF:			17. LIMITATION OF ABSTRACT	18. NUMBER OF PAGES **102**	19a. NAME OF RESPONSIBLE PERSON
a. REPORT **unclassified**	b. ABSTRACT **unclassified**	c. THIS PAGE **unclassified**			

Contents

1. Introduction

Stabilized methods were originally developed about 25 years ago and reported on in a series of conference papers and book chapters. The first archival journal article appeared in 1982 (Brooks and Hughes, 1982). This work summarized developments up to 1982 and brought to prominence the SUPG formulation (i.e., Streamline Upwind Petrov-Galerkin). It was argued that stability and accuracy were combined in this approach, and thus it represented an improvement over classical upwind, artificial viscosity, central-difference, and Galerkin finite element methods. Mathematical corroboration came shortly thereafter in the work of Johnson, Nävert and Pitkäranta (1984). Subsequently, many works appeared dealing with fundamental mathematical theory and diverse applications. A very large literature on stabilized methods has accumulated in the process.

In 1995 it was shown by Hughes (1995) that stabilized methods could be derived from a variational multiscale formulation. Subsequently, the multiscale foundations of stabilized methods have become a focal point of research activities and have led to considerable conceptual and practical progress. The view taken in this work is that the basis of residual-based, or consistent, stabilized methods is a variational multiscale analysis of the partial differential equations under consideration. This approach combines ideas of physical modeling with numerical approximation in a unified way. To provide motivation for the developments which follow a relevant physical example will be described first.

Considerations of environmental acoustics are very important in the design of high-speed trains. In Japan, environmental laws limit the sound pressure levels 50 meters from the tracks. The Shinkansen, or "bullet trains", obtain electric power from pantographs in contact with

Figure 1. Shroud surrounding a pantograph.

overhead lines. In order to reduce aerodynamic loads on pantographs, "shrouds" have been designed to deflect airflow. Photographs of pantographs and shrouds are shown in Figures 1 and 2. The shroud reduces structural loads on the pantograph and, concomitantly, reduces acoustic radiation from the pantograph, but it also generates considerable noise in the audible range. Research studies have been performed to determine the acoustic signatures of a shroud design (see, e.g., Holmes et al., 1997). In Holmes et al. (1997) a Large Eddy Simulation is performed to determine the turbulent fluid flow in the vicinity of a shroud. See Figure 3 for a schematic illustration. There are several important length scales in such a calculation. Among them are L, the characteristic length scale of the domain in which there are strong flow gradients and turbulence; h, the characteristic length scale of the mesh used in the numerical analysis; and l, the characteristic length of the smallest turbulent eddy. These scales are widely separated, that is, $L \gg h \gg l$, emphasizing the importance of multiscale phenomena. The results of a fluid dynamics calculation are presented in Figure 4. Note the smooth, braided vortical structure in the boundary layer, and the turbulence inside and above the shroud. Eddies impinge on the downwind face of the shroud and roof of the train and give rise to significant pressures, and ultimately to considerable noise propagation. A Fourier transform, with respect to time, of the pressure field on the surface of the shroud and roof is shown in Figure 5. Note the spots of intense pressure. These locations fluctuate as functions of frequency. In order to determine the radiated pressure in the far field, the Fourier transformed fluid flow is used to generate the so-
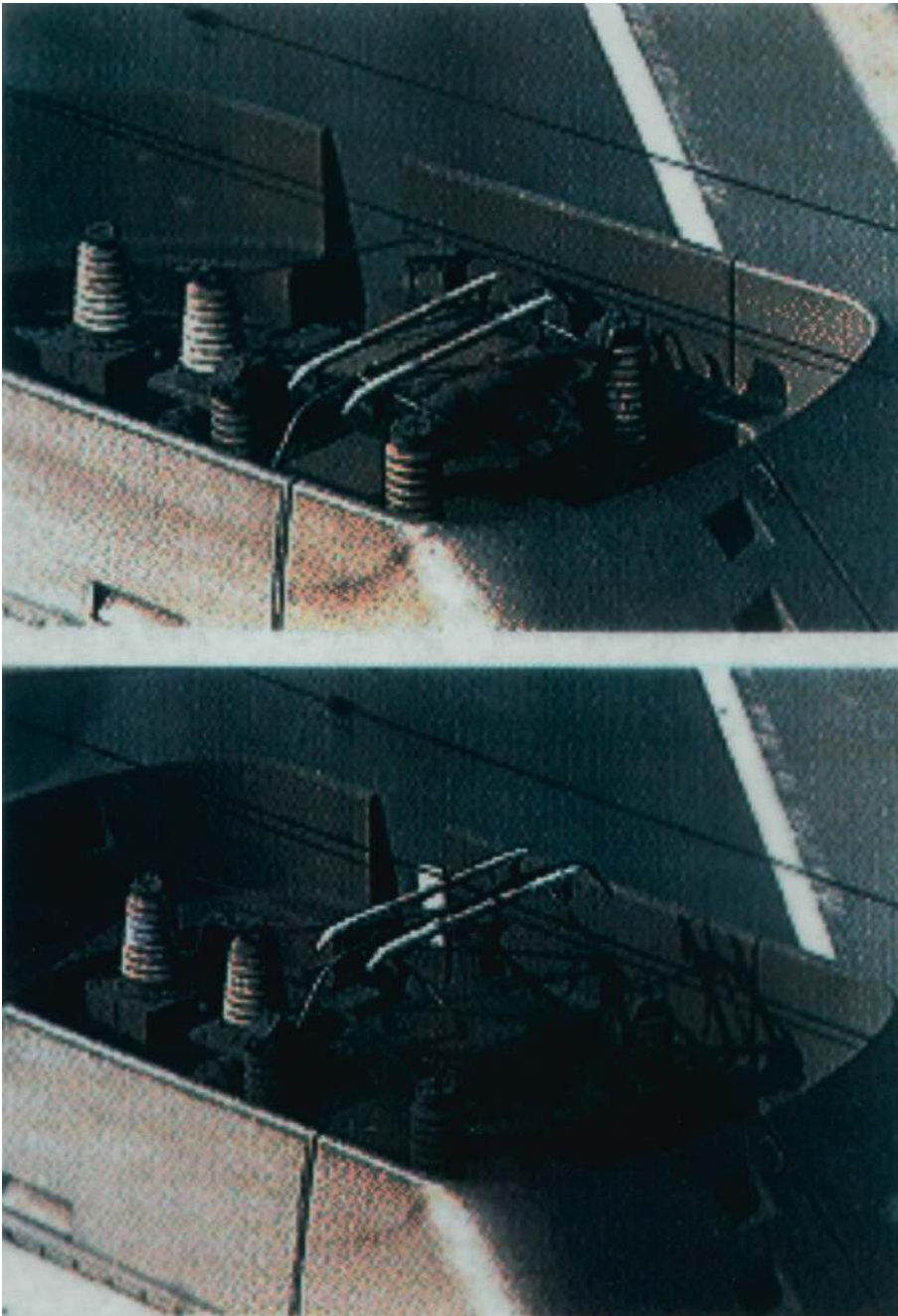
Figure 2. Pantographs in withdrawn and deployed configurations.
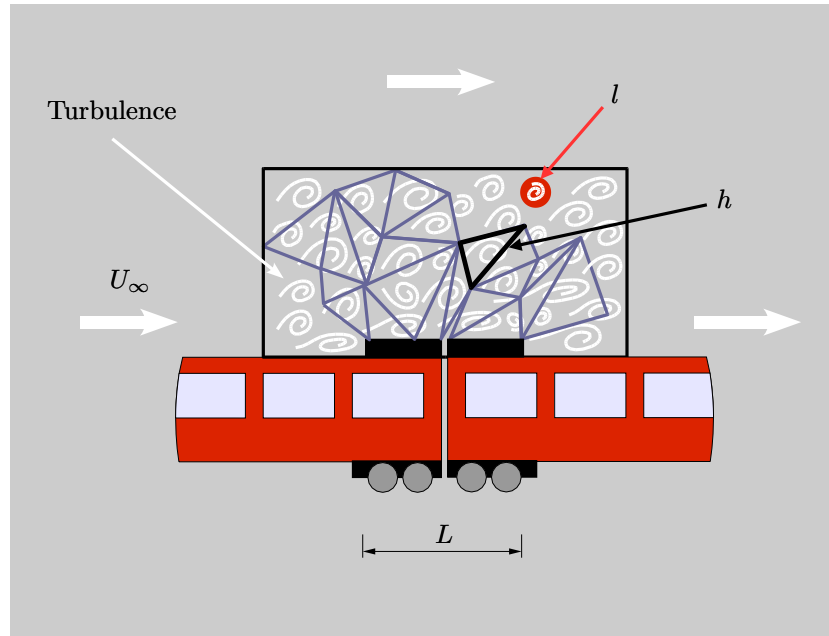
Figure 3. Turbulent flow in a domain surrounding a pantograph shroud on the roof of a high-speed train.

called Lighthill turbulence tensor (Lighthill, 1952,1954), from which sources can be determined. These are used to drive the acoustic field, which is determined by solving the Helmholtz equation (i.e., the time-harmonic wave equation). A boundary-value problem needs to be solved for each frequency of interest in order to construct the sound pressure level spectrum. These problems are classified as "exterior problems," involving domains of infinite extent. In order to use a domain-based numerical procedure, such as finite elements, an artificial boundary is introduced which surrounds the region containing the acoustic sources. See Figure 6 for a schematic illustration. The solution of the problem posed within the artificial boundary needs to approximate the solution of original infinite-domain problem. This necessitates inclusion of a special boundary condition on the artificial boundary, in order to transmit outgoing waves without reflection. Various schemes have been proposed. The characteristic length-scale induced by the artificial boundary, R, is of the order of L in the most effective approaches. The distance to a point of interest in the far-field, D, is usually much larger than R. The solution at D can be determined by the solution on the artificial boundary, which is determined from the near-field numerical solution. The length scales, $R \ll D \ll \infty$, induce additional multiscale considerations. A sound pressure level spectrum at a microphone location (i.e., D) is compared with numerical results in Figure 7. For detailed description of procedures used for aeroacoustic and hydroacoustic applications, see Oberai, Roknaldin and Hughes (2000,2002).

   The multiscale aspects of the fluid flow and acoustic propagation will be discussed in the sequel. The former problem is nonlinear and more complex. It will be described in the last section. In the next section, a multiscale formulation of acoustic radiation is presented.
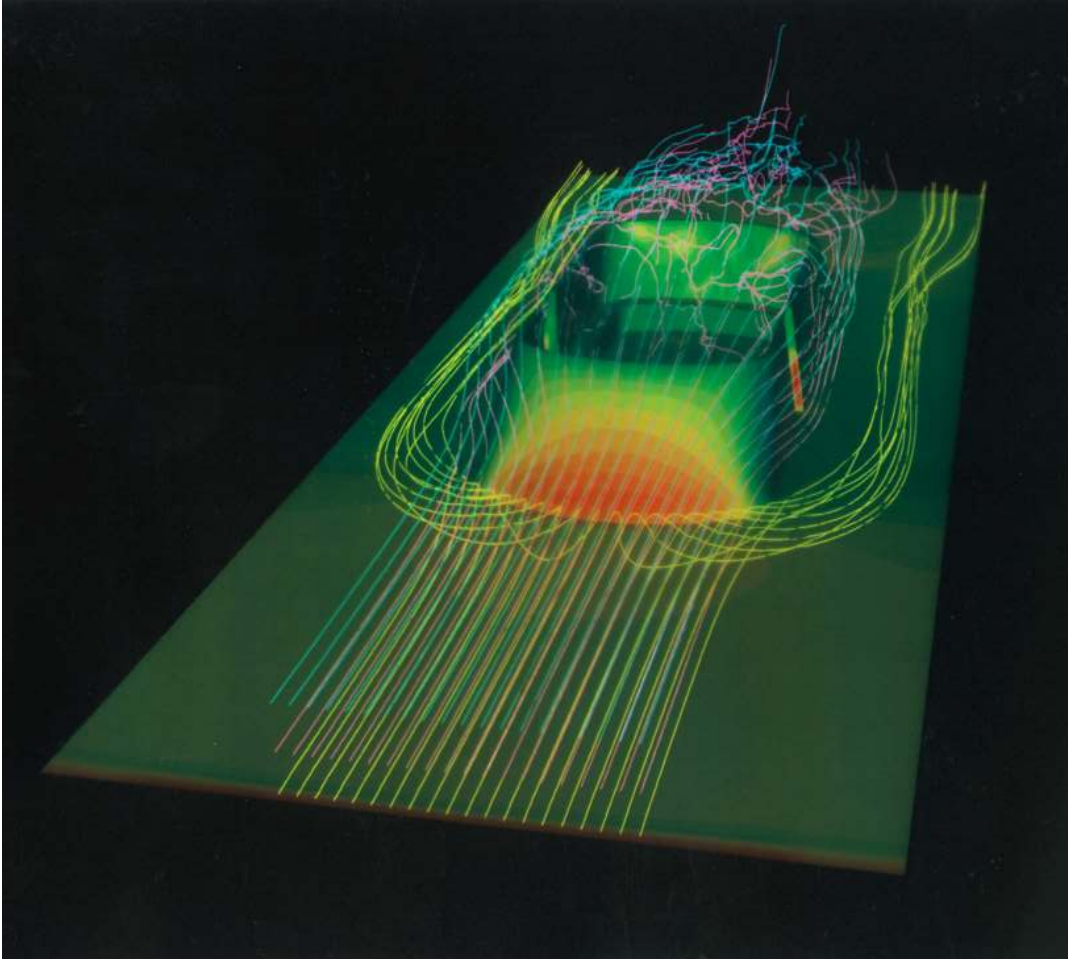
Figure 4. Turbulent flow about a pantograph shroud.

The connections between multiscale formulations and stabilized methods are developed in the intervening sections.

The terminology "multiscale" is used widely for many different things. Other concepts of multiscale analysis are, for example, contained in E and Engquist (2003) and Wagner and Liu (2003).

2. Dirichlet-to-Neumann Formulation

The exterior problem for the Helmholtz equation (i.e., the complex-valued, time-harmonic, wave equation) is considered. The viewpoint adopted is that there are two sets of scales present,
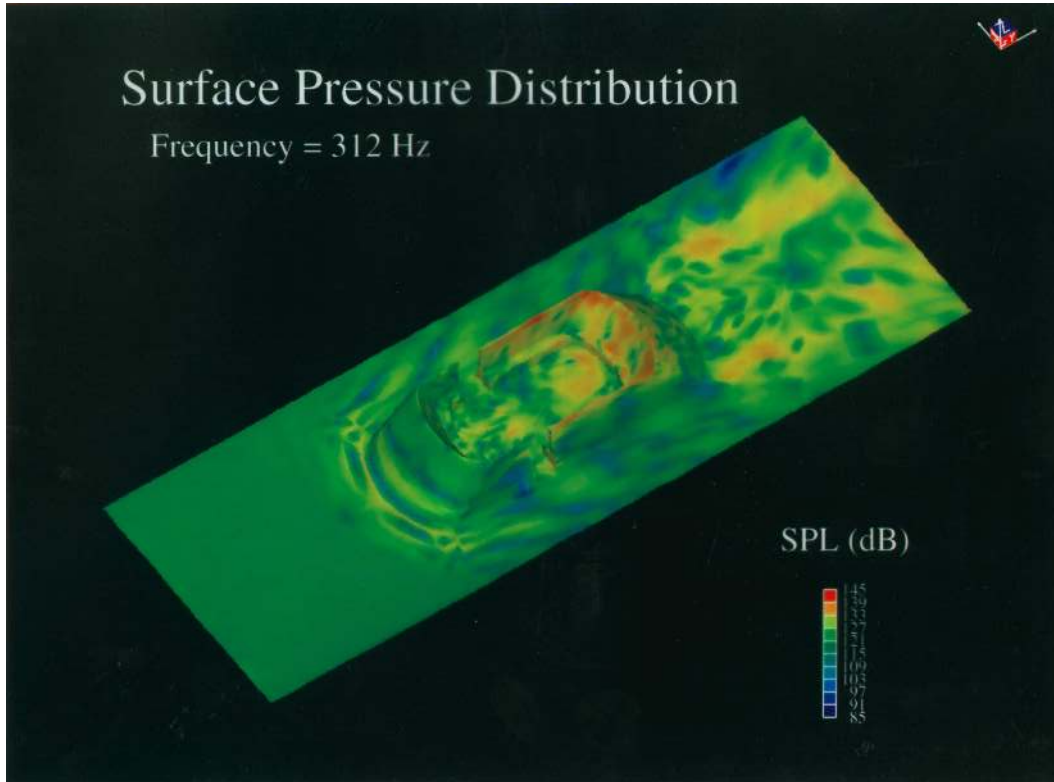
Figure 5.

one associated with the near field and one associated with the far field. The near-field scales are viewed as those of the exact solution exterior to the body, but within an enclosing simple surface, such as, for example, a sphere. The enclosing surface is not part of the specification of the boundary-value problem, but rather it is specified by the analyst. The near-field scales are viewed as numerically "resolvable" in this case. They may also be thought of as local or small scales. The scales associated with the solution exterior to the sphere (far field) are the global or large scales and are viewed as numerically "unresolvable" in the sense that the infinite domain of the far field cannot be dealt with by conventional bounded-domain discretization methods. The solution of the original problem is decomposed into non-overlapping near-field and far-field components, and the far-field component is exactly solved for in terms of the exterior Green's function satisfying homogeneous Dirichlet boundary conditions on the sphere. (Shapes other than a sphere are admissible, and useful in particular cases, but for each shape one must be able to solve the exterior Green's function problem in order to determine the far-field solution.) The far-field component of the solution is then eliminated from the problem for the near field. This results in a well-known variational formulation on a bounded domain which exactly characterizes the near-field component of the original problem. It is referred to as the
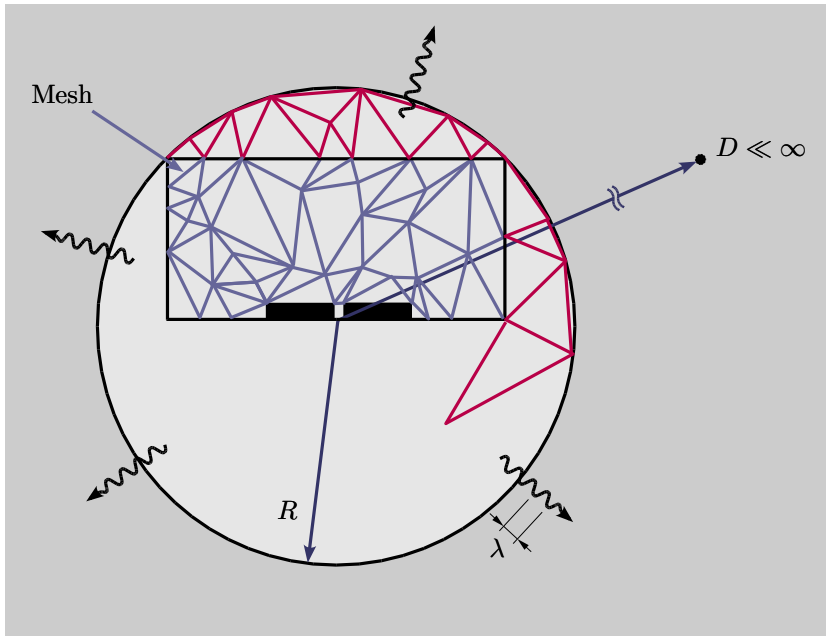
Figure 6. A numerical problem is solved within the artificial boundary at radius R. The point of interest is located at D. The analytical problem involves a domain of infinite extent.
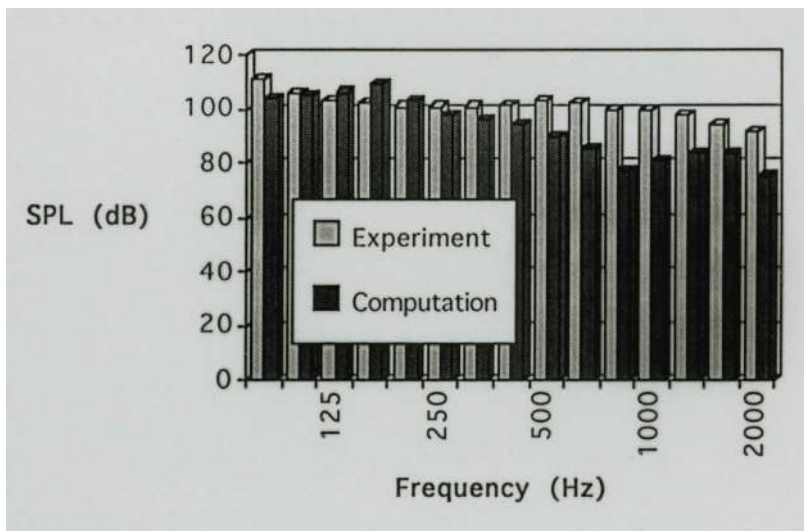
Figure 7. Sound pressure level spectrum.
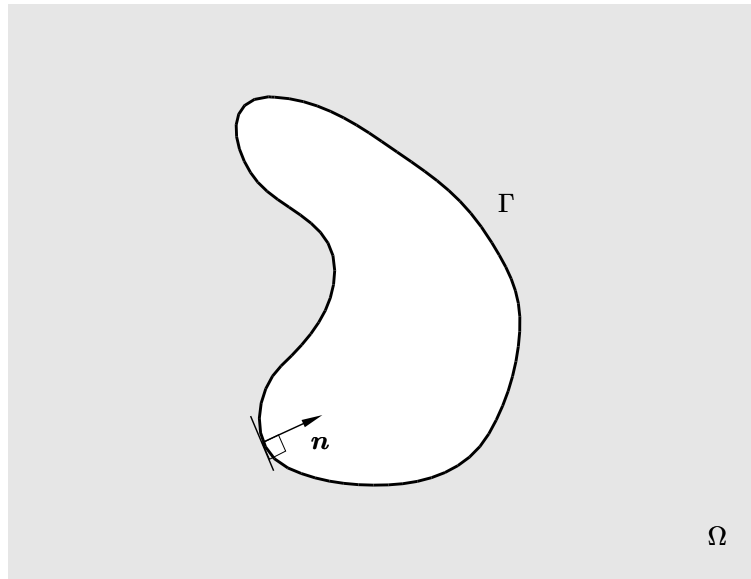
Figure 8. An exterior domain.

Dirichlet-to-Neumann (DtN) formulation because of the form of the boundary condition on the sphere in the problem on the bounded domain (Givoli, 1992; Givoli and Keller, 1988,1989; Harari and Hughes, 1992,1994). The so-called DtN boundary condition is nonlocal in the sense that it involves an integral operator coupling all points on the sphere. Nonlocality is a typical ingredient in formulations of multiscale phenomena.

2.1. Dirichlet-to-Neumann formulation for the Helmholtz operator

Consider the exterior problem for the Helmholtz operator. Let $\Omega \subset \mathbb{R}^d$ be an exterior domain, where d is the number of space dimensions (see Figure 8). The boundary of Ω is denoted by Γ and admits the decomposition

$$\Gamma = \overline{\Gamma_g \bigcup \Gamma_h} \tag{1}$$

$$\emptyset = \overline{\Gamma_g \bigcap \Gamma_h} \tag{2}$$

where Γ_g and Γ_h are subsets of Γ. The unit outward vector to Γ is denoted by $\boldsymbol{n}$. The boundary-value problem consists of finding a function $u : \Omega \to \mathbb{C}$, such that for given functions $f : \Omega \to \mathbb{C}$,
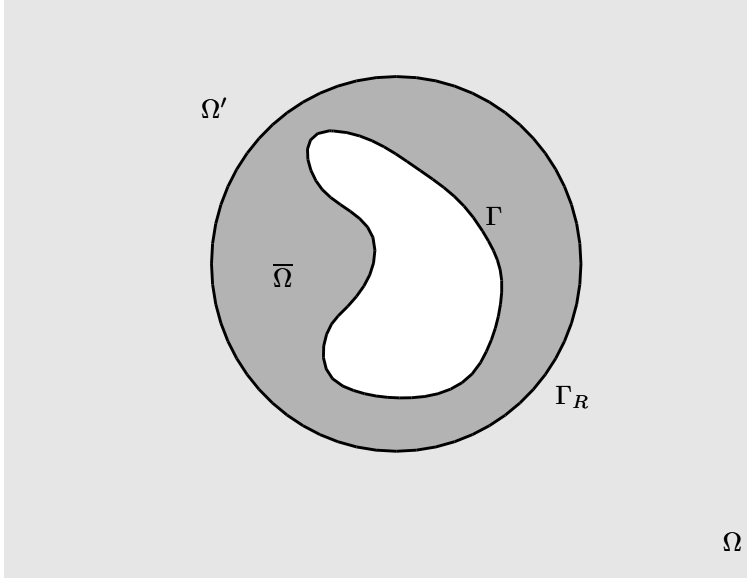
Figure 9. Decomposition of Ω into a bounded domain $\overline{\Omega}$ and an exterior domain Ω'.

$g : \Gamma_g \to \mathbb{C}$ and $h : \Gamma_h \to \mathbb{C}$, the following equations are satisfied:

$$
\begin{aligned}
\mathcal{L}u &= f & &\text{in } \Omega & &(3)\\
u &= g & &\text{on } \Gamma_g & &(4)\\
u_{,n} &= ikh & &\text{on } \Gamma_h & &(5)\\
\lim_{r \to \infty} r^{\frac{d-1}{2}}(u_{,r} - iku) &= 0 & &\text{(Sommerfeld radiation condition)} & &(6)
\end{aligned}
$$

where

$$
-\mathcal{L} = \Delta + k^2 \qquad \text{(Helmholtz operator)} \tag{7}
$$

and $k \in \mathbb{C}$ is the wave number, $i = \sqrt{-1}$, and Δ is the Laplacian operator. The radial coordinate is denoted by r and a comma denotes partial differentiation. The Sommerfeld radiation condition enforces the condition that waves at infinity are outgoing.

Next, consider a decomposition of the domain Ω into a bounded domain $\overline{\Omega}$ and an exterior region Ω'. The boundary which separates $\overline{\Omega}$ and Ω' is denoted Γ_R. It is assumed to have a simple shape (e.g., spherical). See Figure 9. The decomposition of Ω, and a corresponding decomposition of the solution of the boundary-value problem, are expressed analytically as

follows:

$$\Omega \quad = \quad \overline{\overline{\Omega}\bigcup\Omega'} \tag{8}$$

$$\emptyset \quad = \quad \overline{\Omega}\bigcap\Omega' \tag{9}$$

$$u \quad = \quad \overline{u} + u' \qquad \text{(sum decomposition)} \tag{10}$$

$$\left.\begin{array}{rcl} \overline{u}\,|_{\Omega'} & = & 0 \\ u'\,|_{\overline{\Omega}} & = & 0 \end{array}\right\} \qquad \text{(disjoint decomposition)} \tag{11}$$

$$u \quad = \quad \left\{ \begin{array}{ll} \overline{u} & \text{on } \overline{\Omega} \\ u' & \text{on } \Omega' \end{array} \right. \tag{12}$$

Think of $\overline{u}$ as the near-field solution and u' as the far-field solution.

2.2. Exterior Dirichlet problem for $\boldsymbol{u'}$

Attention is now focused on the problem in the domain Ω' exterior to Γ_R. The unit outward normal vector on Γ_R (with respect to Ω') is denoted $\boldsymbol{n'}$ (see Fig. 10). Assume that f vanishes in the far field, that is,

$$f = 0 \qquad \text{on } \Omega' \tag{13}$$

The exterior Dirichlet problem consists of finding a function $u' : \Omega \to \mathbb{C}$ such that

$$\mathcal{L}u' \quad = \quad 0 \qquad \text{in } \Omega' \tag{14}$$

$$u' \quad = \quad \overline{u} \qquad \text{on } \Gamma_R \tag{15}$$

$$\lim_{r\to\infty} r^{\frac{d-1}{2}}(u'_{,r} - iku') \quad = \quad 0 \tag{16}$$

Note that the boundary condition (15) follows from the continuity of u across Γ_R.

2.3. Green's function for the exterior Dirichlet problem

The solution of the exterior Dirichlet problem can be expressed in terms of a Green's function g satisfying

$$\mathcal{L}\text{g} \quad = \quad \delta \qquad \text{in } \Omega' \tag{17}$$

$$\text{g} \quad = \quad 0 \qquad \text{on } \Gamma_R \tag{18}$$

$$\lim_{r\to\infty} r^{\frac{d-1}{2}}(\text{g}_{,r} - ik\text{g}) \quad = \quad 0 \tag{19}$$

From Green's identity,

$$u'(y) = -\int_{\Gamma_R} \text{g}_{,n'_x}(x,y)u'(x)d\Gamma_x \tag{20}$$

The so-called DtN map is obtained from (20) by differentiation with respect to $\boldsymbol{n'}$,

$$u'_{,n'}(y) = -\int_{\Gamma_R} \text{g}_{,n'_x n'_y}(x,y)u'(x)d\Gamma_x \quad \Leftrightarrow \quad u'_{,n'}(y) = Mu' \tag{21}$$
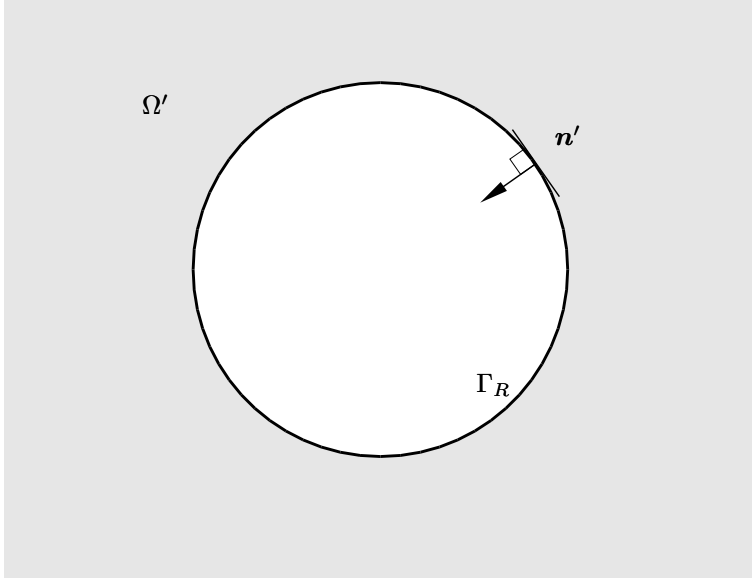
Figure 10. Domain for the far-field problem.

The DtN map is used to develop a formulation for $\overline{u}$ on the bounded domain $\overline{\Omega}$. In this way the far-field phenomena are incorporated in the problem for the near field. The Dirichlet-to-Neumann formulation for $\overline{u}$ will be developed by way of a variational argument.

Let Π denote the potential energy for the original boundary-value problem, namely

$$
\begin{aligned}
\Pi(u) &= \Pi(\overline{u} + u') \\
&= \frac{1}{2}a(\overline{u},\overline{u}) + \frac{1}{2}a(u',u') - (\overline{u},f) - (\overline{u},ikh)_\Gamma
\end{aligned}
\tag{22}
$$

where

$$
a(w,u) = \int_\Omega (\nabla w \cdot \nabla u - k^2 wu)d\Omega
\tag{23}
$$

$$
(w,f) = \int_\Omega wf d\Omega
\tag{24}
$$

$$
(w,ikh)_\Gamma = \int_{\Gamma_h} w\, ikh\, d\Gamma
\tag{25}
$$

Consider a one-parameter family of variations of u, that is,

$$
(\overline{u} + u') + \varepsilon(\overline{w} + w')
\tag{26}
$$

subject to the following **continuity** constraints

$$
\overline{u} = u' \qquad \text{on } \Gamma_R
\tag{27}
$$

$$
\overline{w} = w' \qquad \text{on } \Gamma_R
\tag{28}
$$

where $\varepsilon \in \mathbb{R}$ is a parameter. Taking the Fréchet derivative, the first variation of Π is calculated as follows:

$$
\begin{aligned}
0 &= D\Pi(\overline{u} + u') \cdot (\overline{w} + w') \\
&= a(\overline{w}, \overline{u}) + a(w', u') - (\overline{w}, f) - (\overline{w}, ikh)_\Gamma \\
&= a(\overline{w}, \overline{u}) + (w', \mathcal{L}u') + (w', u'_{,n'})_{\Gamma_R} - (\overline{w}, f) - (\overline{w}, ikh)_\Gamma \\
&= a(\overline{w}, \overline{u}) + 0 + (\overline{w}, M\overline{u})_{\Gamma_R} - (\overline{w}, f) - (\overline{w}, ikh)_\Gamma
\end{aligned}
\tag{29}
$$

where

$$
(\overline{w}, M\overline{u})_{\Gamma_R} = \int_{\Gamma_R} \int_{\Gamma_R} \overline{w}(y) g_{,\overline{n}_x \overline{n}_y}(x, y) \, \overline{u}(x) d\Gamma_x d\Gamma_y
\tag{30}
$$

In obtaining (29), (21) and the continuity conditions, (27) and (28), have been used. Note that in (30) differentiation with respect to $\overline{\boldsymbol{n}} = -\boldsymbol{n}'$ has been employed. Equation (29) can be written concisely as

$$
\boxed{B(\overline{w}, \overline{u}; g) = L(\overline{w})}
\tag{31}
$$

where

$$
\begin{aligned}
B(\overline{w}, \overline{u}; g) &= a(\overline{w}, \overline{u}) + (\overline{w}, M\overline{u})_{\Gamma_R} \tag{32} \\
L(\overline{w}) &= (\overline{w}, f) + (\overline{w}, ikh)_\Gamma \tag{33}
\end{aligned}
$$

Remarks

1. (31) is an **exact** characterization of $\overline{u}$.
2. The effect of u' on the problem for $\overline{u}$ is **nonlocal**. The additional term, (30), is referred to as the DtN boundary condition. It represents a perfect interface that transmits outgoing waves without reflection.
3. (31) is the basis of **numerical** approximations, viz.

$$
B(\overline{w}^h, \overline{u}^h; g) = L(\overline{w}^h)
\tag{34}
$$

   where $\overline{w}^h$ and $\overline{u}^h$ are finite-dimensional approximations of $\overline{w}$ and $\overline{u}$, respectively.
4. In practice, M (or equivalently g) is also **approximated** by way of truncated series, differential operators, etc. Thus, in practice, we work with

$$
B(\overline{w}^h, \overline{u}^h; \tilde{g}) = L(\overline{w}^h)
\tag{35}
$$

   where

$$
\tilde{g} \approx g
\tag{36}
$$

2.4. Bounded domain problem for $\overline{\boldsymbol{u}}$

The **Euler-Lagrange equations** of the variational formulation give rise to the boundary-value problem for $\overline{u}$ on the bounded domain $\overline{\Omega}$ (see Fig. 11), that is,

$$
\begin{aligned}
\mathcal{L}\overline{u} &= f & &\text{in } \overline{\Omega} \tag{37} \\
\overline{u} &= g & &\text{on } \Gamma_g \tag{38} \\
\overline{u}_{,\overline{n}} &= ikh & &\text{on } \Gamma_h \tag{39} \\
\overline{u}_{,\overline{n}} &= -M\overline{u} & &\text{on } \Gamma_R \tag{40}
\end{aligned}
$$
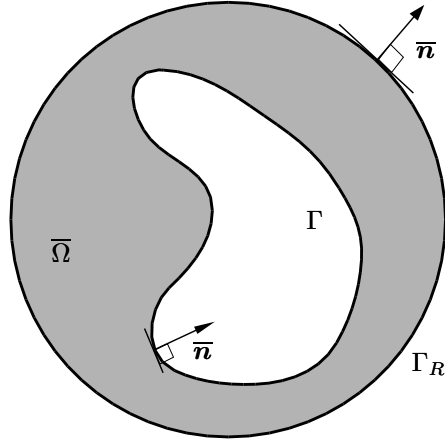
Figure 11. Bounded domain for the near-field problem.

The preceding developments may be summarized in the following statements:

1. $u = \bar{u} + u'$ (***disjoint*** sum decomposition).
2. u' is determined ***analytically***.
3. u' is eliminated, resulting in a formulation for $\bar{u}$ which is the basis of ***numerical*** approximations.
4. The effect of u' is ***nonlocal*** in the problem for $\bar{u}$.
5. Interpreted as a ***multiscale*** problem, u' represents the large scales of the far field, whereas $\bar{u}$ represents the small scales of the near field.

3. Variational Multiscale Method

The variational multiscale method is a procedure for deriving models and numerical methods capable of dealing with multiscale phenomena ubiquitous in science and engineering. It is motivated by the simple fact that straightforward application of Galerkin's method employing standard bases, such as Fourier series and finite elements, is ***not*** a robust approach in the presence of multiscale phenomena. The variational multiscale method seeks to rectify this situation. The anatomy of the method is simple: ***sum decompositions*** of the solution, $u = \bar{u} + u'$, are considered where $\bar{u}$ is solved for ***numerically***. An attempt is made to determine u' ***analytically***, eliminating it from the problem for $\bar{u}$. $\bar{u}$ and u' may ***overlap*** or be ***disjoint***, and u' may be ***globally*** or ***locally*** defined. The effect of u' on the problem for $\bar{u}$ will always be ***nonlocal***. In the previous section, the variational multiscale method was used to derive

15

the Dirichlet-to-Neumann formulation of the Helmholtz equation in an unbounded domain. In this section, attention is confined to cases on bounded domains in which $\bar{u}$ represents "coarse scales" and u' "fine scales".

An attempt is made to present the big picture in the context of an abstract Dirichlet problem involving a second-order differential operator which is assumed nonsymmetric and/or indefinite. This allows consideration of equations of practical interest, such as the advection-diffusion equation, a model for fluid mechanics phenomena, and the Helmholtz equation, of importance in acoustics and electromagnetics. After introducing the variational formulation of the Dirichlet problem, its multiscale version is described.

First the "smooth case" is considered, in which it is assumed that all functions are sufficiently smooth so that distributional effects (e.g., Dirac layers) may be ignored. This enables a simple derivation of the exact equation governing the coarse scales. It is helpful to think of this case as pertaining to the situation in which both the coarse and fine scales are represented by Fourier series.

Next, a case of greater practical interest is considered in which standard finite elements are employed to represent the coarse scales. Due to lack of continuity of derivatives at element interfaces, it is necessary to explicitly account for the distributional effects omitted in the smooth case. This is referred to as the "rough case". Again, an exact equation is derived governing the behavior of coarse scales. It is this equation that is proposed as a paradigm for developing subgrid-scale models. Two distinguishing features characterize this result. The first is that the method may be viewed as the classical Galerkin method plus an additional term driven by the ***distributional*** residual of the coarse scales. This involves residuals of the partial differential equation under consideration on element interiors (this is the smooth part of the residual), and jump terms involving the boundary operator on element interfaces (this is the rough part deriving from Dirac layers in the distributional form of the operator). The appearance of element residuals and jump terms are suggestive of the relationship between the multiscale formulation and various ***stabilized methods*** proposed previously. The second distinguishing feature is the appearance of the fine-scale Green's function. In general, this is ***not*** the classical Green's function, but one that emanates from the fine-scale subspace. It is important to note that the fine-scale subspace, $\mathcal{V}'$, is infinite-dimensional, but a proper subspace of the space, $\mathcal{V}$, in which it is attempted to solve the problem. The direct sum relationship $\mathcal{V} = \bar{\mathcal{V}} \oplus \mathcal{V}'$ where $\bar{\mathcal{V}}$ is the coarse-scale, finite element subspace is satisfied. A problem that arises in developing practical approximations is that the fine-scale Green's function is ***nonlocal***.

Before addressing this issue, the relationship between the fine-scale solution and *a posteriori* error estimation is discussed. It is noted first that by virtue of the formulation being exact, the fine-scale solution is precisely the error in the coarse-scale solution. Consequently, the representation obtained of the fine-scale solution in terms of the distributional coarse-scale residual and the fine-scale Green's function is a paradigm for *a posteriori* error estimation. It is then noted that it is typical in *a posteriori* error estimation procedures to involve the element residuals and/or interface jump terms as driving mechanisms. The mode of distributing these sources of error may thus be inferred to be approximations of the fine-scale Green's function. As a result, it is clear that in *a posteriori* error estimation, the proper distribution of residual errors strongly depends on the operator under consideration. In other words, there is no universally appropriate scheme independent of the operator. (A similar observation may be made for subgrid-scale models by virtue of the form of the coarse-scale equation.) The implications of
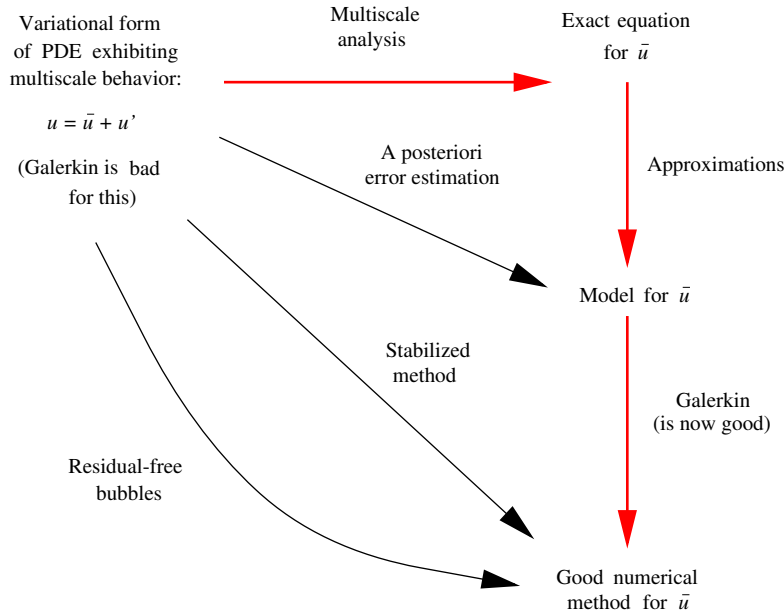
Figure 12. The variational multiscale method is a framework for the construction of subgrid-scale models and effective numerical methods for partial differential equations exhibiting multiscale phenomena. It provides a physical context for understanding methods based on residual-free bubbles and stabilized methods.

the formula for the fine-scale solution with respect to *a posteriori* error estimation for finite element approximations of the advection-diffusion and Helmholtz equations are discussed.

Next, hierarchical p-refinement and bubbles are examined in an effort to better understand the nature of the fine-scale Green's function and to deduce appropriate forms. $\bar{\mathcal{V}}$ is identified with standard, low-order finite elements, and $\mathcal{V}'$ with the hierarchical basis. An explicit formula for the fine-scale Green's function in terms of the hierarchical basis is derived. It is concluded that, despite the nonlocal character of the fine-scale Green's function, it can always be represented in terms of a finite basis of functions possessing local support. In one-dimension, this basis consists solely of bubbles, in two dimensions, bubbles and edge functions; etc. This reduces the problem of approximating the Green's function to one of obtaining a good-quality, finite-dimensional fine-scale basis. This becomes a fundamental problem in the construction of practical methods. Once solved, a subgrid-scale model governing the coarse-scales, **and** an approximate representation of the fine-scale solution which does double duty as an *a posteriori* error estimator for the coarse-scale solution, are obtained.

What constitutes a good-quality, but practical, fine-scale basis is described by reviewing the concept of residual-free bubbles (see Baiocchi, Brezzi and Franca, 1993). The use of fine-scale Green's functions supported by individual elements is then reviewed. Residual-free bubbles and element Green's functions are intimately related as shown in Brezzi et al. (1997). These concepts may be used to derive stabilized methods and identify optimal parameters which appear in their definition. The ideas are illustrated with one-dimensional examples.
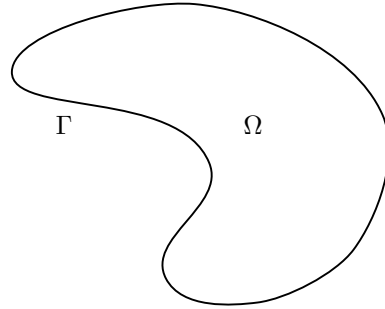
Figure 13. Domain and boundary for the abstract Dirichlet problem.

This section is concluded with a summary of results and identification of some outstanding issues. The overall flow of the main relationships is presented in Figure 12.

An alternative approach for constructing a fine-scale basis can be found in the literature describing the Discontinuous Enrichment Method (DEM) with Lagrange multipliers, Farhat, Harari and Franca (2001), Farhat, Harari and Hetmaniuk (2003a, 2003b), and Harari, Farhat and Hetmaniuk (2003). In this hybrid variational multiscale approach, the fine-scales are based on the free-space solutions of the homogeneous differential equation to be solved. For example, for the Helmholtz equation, these scales are represented analytically by plane waves. This approach leads to fine-scales that, unlike bubbles, do not vanish but are discontinuous on the element boundaries. This allows circumventing both the difficulty in attempting to approximate the global fine-scale Green's function, and the loss of some global effects due to the restriction of residual-free bubbles to a vanishing trace on the element boundaries. However, the DEM approach for constructing a fine-scale basis introduces additional unknowns at the element interfaces in the form of Lagrange multipliers to enforce a weak continuity of the solution.

3.1. Abstract Dirichlet problem

Let $\Omega \subset \mathbb{R}^d$, where $d \geq 1$ is the number of space dimensions, be an open bounded domain with smooth boundary Γ (see Fig. 13). Consider the following boundary-value problem: find $u : \Omega \to \mathbb{R}$ such that

$$\mathcal{L}u = f \quad \text{in } \Omega \tag{41}$$

$$u = g \quad \text{on } \Gamma \tag{42}$$

where $f : \Omega \to \mathbb{R}$ and $g : \Gamma \to \mathbb{R}$ are given functions. Think of $\mathcal{L}$ as a second-order and, in general, **nonsymmetric** differential operator.

3.1.1. Variational formulation Let $\mathcal{S} \subset H^1(\Omega)$ denote the **trial solution space** and $\mathcal{V} \subset H^1(\Omega)$ denote the **weighting function space**, where $H^1(\Omega)$ is the Sobolev space of square-integrable functions with square-integrable derivatives. Assume that $\mathcal{S}$ and $\mathcal{V}$ possess
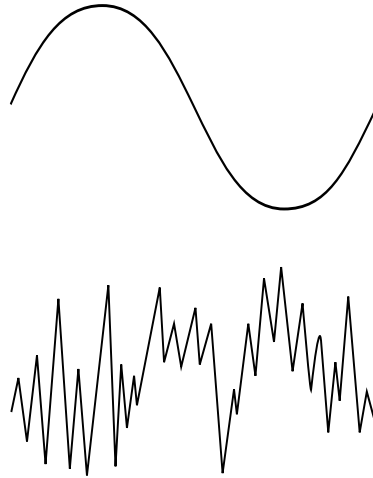
Figure 14. Coarse and fine scale components.

the following properties:

$$u \; = \; g \qquad \text{on } \Gamma \qquad \forall u \in \mathcal{S} \tag{43}$$

$$w \; = \; 0 \qquad \text{on } \Gamma \qquad \forall w \in \mathcal{V} \tag{44}$$

The variational counterpart of the boundary-value problem (41)–(42) is given as follows: find $u \in \mathcal{S}$ such that $\forall w \in \mathcal{V}$

$$a(w, u) = (w, f) \tag{45}$$

where $(\cdot, \cdot)$ is the $L_2(\Omega)$ inner product, and $a(\cdot, \cdot)$ is a bilinear form satisfying

$$a(w, u) = (w, \mathcal{L}u) \tag{46}$$

for all **sufficiently smooth** $w \in \mathcal{V}$ and $u \in \mathcal{S}$.

3.2. Variational multiscale method

Let

$$u = \bar{u} + u' \qquad (\textbf{\textit{overlapping}} \text{ sum decomposition}) \tag{47}$$

where $\bar{u}$ represents **coarse scales** and u' represents **fine scales** (see Fig. 14). Likewise, let

$$w = \bar{w} + w'. \tag{48}$$

Let $\mathcal{S} = \bar{\mathcal{S}} \oplus \mathcal{S}'$ and $\mathcal{V} = \bar{\mathcal{V}} \oplus \mathcal{V}'$ where $\bar{\mathcal{S}}$ (resp., $\mathcal{S}'$) is the trial solution space for **coarse** (resp., **fine**) scales and $\bar{\mathcal{V}}$ (resp., $\mathcal{V}'$) is the weighting function space for **coarse** (resp., **fine**)

scales. Assume

$$
\begin{array}{llll}
\bar{u} & = & g & \text{on } \Gamma \qquad \forall \bar{u} \in \bar{\mathcal{S}} & (49)\\
u' & = & 0 & \text{on } \Gamma \qquad \forall u' \in \mathcal{S}' & (50)\\
\bar{w} & = & 0 & \text{on } \Gamma \qquad \forall \bar{w} \in \bar{\mathcal{V}} & (51)\\
w' & = & 0 & \text{on } \Gamma \qquad \forall w' \in \mathcal{V}' & (52)
\end{array}
$$

We assume $\mathcal{S}' = \mathcal{V}'$. The objective is to derive an equation governing $\bar{u}$.

Remarks

1. It is helpful to think of $\bar{\mathcal{S}}$ and $\bar{\mathcal{V}}$ as finite-dimensional, whereas $\mathcal{S}'$ and $\mathcal{V}'$ are necessarily infinite-dimensional.
2. In order to make the notion of the direct sums precise, one needs to introduce **projectors** $\overline{\Pi}_{\mathcal{S}} : \mathcal{S} \to \bar{\mathcal{S}}$ and $\overline{\Pi}_{\mathcal{V}} : \mathcal{V} \to \bar{\mathcal{V}}$, such that $\overline{\boldsymbol{u}} = \overline{\Pi}_{\mathcal{S}} \boldsymbol{u}$, $\overline{\boldsymbol{w}} = \overline{\Pi}_{\mathcal{V}} \boldsymbol{w}$, $\Pi'_{\mathcal{S}} = \boldsymbol{id} - \overline{\Pi}_{\mathcal{S}}$, $\Pi'_{\mathcal{V}} = \boldsymbol{id} - \overline{\Pi}_{\mathcal{V}}$, and, in particular, $\Pi'_{\mathcal{S}} = \Pi'_{\mathcal{V}} := \Pi'$.

3.2.1. Smooth case The developments are begun by considering the case in which all functions are smooth. The idea for $u = \bar{u} + u'$ is illustrated in Figure 15. The situation for $w = \bar{w} + w'$ is similar. Assume the following integration-by-parts formulas hold:

$$
\begin{array}{llll}
a(\bar{w}, u') & = & (\mathcal{L}^* \bar{w}, u') & \forall \bar{w} \in \bar{\mathcal{V}}, u' \in \mathcal{S}' & (53)\\
a(w', \bar{u}) & = & (w', \mathcal{L}\bar{u}) & \forall w' \in \mathcal{V}', \bar{u} \in \bar{\mathcal{S}} & (54)\\
a(w', u') & = & (w', \mathcal{L}u') & \forall w' \in \mathcal{V}', u' \in \mathcal{S}' & (55)
\end{array}
$$

Exact variational equation for $\bar{u}$ (smooth case) Substitute (47) and (48) into (45):

$$
a(\bar{w} + w', \bar{u} + u') = (\bar{w} + w', f) \qquad \forall \bar{w} \in \bar{\mathcal{V}}, \ \forall w' \in \mathcal{V}' \tag{56}
$$

By virtue of the linear independence of $\bar{w}$ and w', (56) splits into two problems:

$$
\begin{array}{lll}
\text{Problem (1)} & a(\bar{w}, \bar{u}) + a(\bar{w}, u') = (\bar{w}, f) \qquad \forall \bar{w} \in \bar{\mathcal{V}} & (57)\\
& a(\bar{w}, \bar{u}) + (\mathcal{L}^* \bar{w}, u') = (\bar{w}, f) & (58)\\
\text{Problem (2)} & a(w', \bar{u}) + a(w', u') = (w', f) \qquad \forall w' \in \mathcal{V}' & (59)\\
& (w', \mathcal{L}\bar{u}) + (w', \mathcal{L}u') = (w', f) & (60)
\end{array}
$$

In arriving at (58) and (60), the integration-by-parts formulas (53)–(55) have been employed. Rewrite (60) as

$$
\begin{array}{llll}
(\Pi')^* \mathcal{L}u' & = & -(\Pi')^* (\mathcal{L}\bar{u} - f) & \text{in } \Omega & (61)\\
u' & = & 0 & \text{on } \Gamma & (62)
\end{array}
$$

where $(\Pi')^*$ denotes projection onto $(\mathcal{V}')^*$, the dual space of $\mathcal{V}'$. Endeavor to solve this problem for u' and eliminate u' from the equation for $\bar{u}$, namely (58). This can be accomplished with the aid of a Green's function.
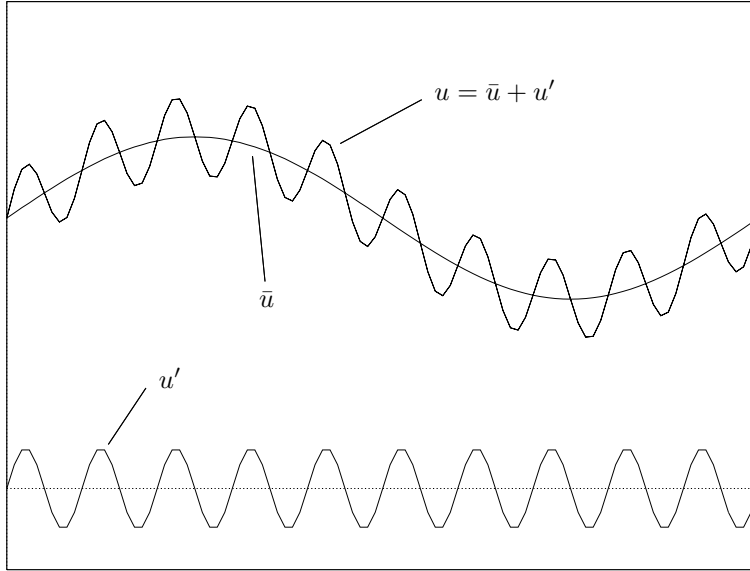
Figure 15. The case in which $\bar{u}$ and u' are smooth.

Green's function for the "dual problem" Consider the following Green's function problem for the adjoint operator:

$$(\Pi')^* \mathcal{L}^* \Pi' \text{g}(x,y) = (\Pi')^* \delta(x-y) \quad \forall x \in \Omega \quad (63)$$

$$\text{g}(x,y) = 0 \quad \forall x \in \Gamma \quad (64)$$

we seek a g $\perp$ ker($(\Pi')^* \mathcal{L}^* \Pi'$). Let g$' = \Pi' \text{g}(\Pi')^*$. In terms of the solution of this problem, u' can be expressed as follows:

$$u'(y) = -\int_\Omega \text{g}'(x,y) \left(\mathcal{L}\bar{u} - f \right)(x) \, d\Omega_x \quad (65)$$

Equivalently, (65) can be written in terms of an integral operator M' as

$$u' = M' \left(\mathcal{L}\bar{u} - f \right) \quad (66)$$

Remarks

1. $\mathcal{L}\bar{u} - f$ is the **residual** of the coarse scales.
2. The fine scales, u', are **driven** by the residual of the coarse scales.
3. It is very important to observe that g$'$ is **not** the usual Green's function associated with the corresponding strong form of (63). Rather, g$'$ is defined entirely in terms of the space of fine scales, namely $\mathcal{V}'$. Later on, an explicit formula for g$'$ will be derived in terms of a basis for $\mathcal{V}'$.

Substituting (66) into (58) yields

$$a(\bar{w}, \bar{u}) + (\mathcal{L}^* \bar{w}, M'(\mathcal{L}\bar{u} - f)) = (\bar{w}, f) \qquad \forall \bar{w} \in \mathcal{V}' \tag{67}$$

where, from (65),

$$(\mathcal{L}^* \bar{w}, M'(\mathcal{L}\bar{u} - f)) = -\int_\Omega \int_\Omega (\mathcal{L}^* \bar{w})(y) g'(x, y)(\mathcal{L}\bar{u} - f)(x) \, d\Omega_x \, d\Omega_y \tag{68}$$

Remarks

1. This is an **exact** equation for the coarse scales.
2. The effect of the fine scales on the coarse scales is **nonlocal**.
3. By virtue of the smoothness assumptions, this result is appropriate for spectral methods, or methods based on Fourier series, but it is not sufficiently general as a basis for finite element methods. In what follows, the smoothness assumption is relaxed and the form of the coarse-scale equation appropriate for finite elements is considered.

3.2.2. Rough case (FEM) Consider a discretization of Ω into finite elements. The domain and boundary of element e, where $e \in \{1, 2, \cdots, n_{\mathrm{el}}\}$, in which n_{el} is the number of elements, are denoted Ω^e and Γ^e, respectively (see Fig. 16). The union of element interiors is denoted Ω' and the union of element boundaries modulo Γ (also referred to as the **element interfaces** or **skeleton**) is denoted Γ', viz.

$$\Omega' = \bigcup_{e=1}^{n_{\mathrm{el}}} \Omega^e \tag{69}$$

$$\Gamma' = \left(\bigcup_{e=1}^{n_{\mathrm{el}}} \Gamma^e \right) \setminus \Gamma \tag{70}$$

$$\bar{\Omega} = \mathrm{closure}(\Omega') \tag{71}$$

Let $\bar{\mathcal{S}}, \bar{\mathcal{V}} \subset C^0(\bar{\Omega}) \cap H^1(\Omega)$ be classical finite element spaces. Note that $\mathcal{S}' = \mathcal{V}' \subset H^1(\Omega)$, but is otherwise arbitrary. In this case $\bar{u}$ and $\bar{w}$ are smooth on element interiors but have slope discontinuities across element boundaries (see, e.g., Fig. 17).

It is necessary to introduce some terminology used in the developments which follow. Let $(\cdot, \cdot)_\omega$ be the $L_2(\omega)$ inner product where $\omega = \Omega, \Omega^e, \Gamma^e, \Omega', \Gamma'$, etc. Recall, $(\cdot, \cdot) = (\cdot, \cdot)_\Omega$. Let $[\![\cdot]\!]$ denote the **jump operator**, viz., if $\boldsymbol{v}$ is a vector field experiencing a discontinuity across an element boundary (e.g., $\boldsymbol{v} = \nabla \bar{w}, \bar{w} \in \bar{\mathcal{V}}$), then

$$\begin{aligned} [\![\boldsymbol{n} \cdot \boldsymbol{v}]\!] &= \boldsymbol{n}^+ \cdot \boldsymbol{v}^+ + \boldsymbol{n}^- \cdot \boldsymbol{v}^- \\ &= \boldsymbol{n}^+ \cdot \boldsymbol{v}^+ - \boldsymbol{n}^+ \cdot \boldsymbol{v}^- \\ &= \boldsymbol{n} \cdot (\boldsymbol{v}^+ - \boldsymbol{v}^-), \end{aligned} \tag{72}$$

where

$$\boldsymbol{n} = \boldsymbol{n}^+ = -\boldsymbol{n}^- \tag{73}$$
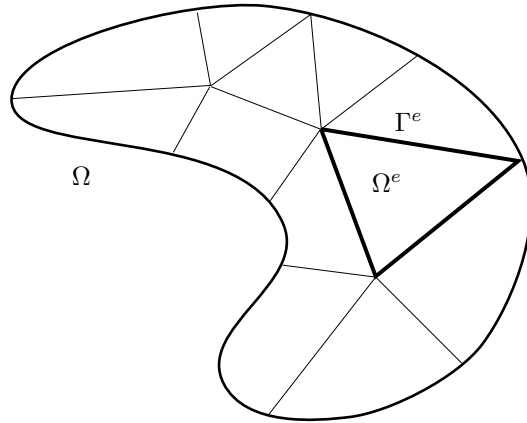
Figure 16. Discretization of Ω into element subdomains.
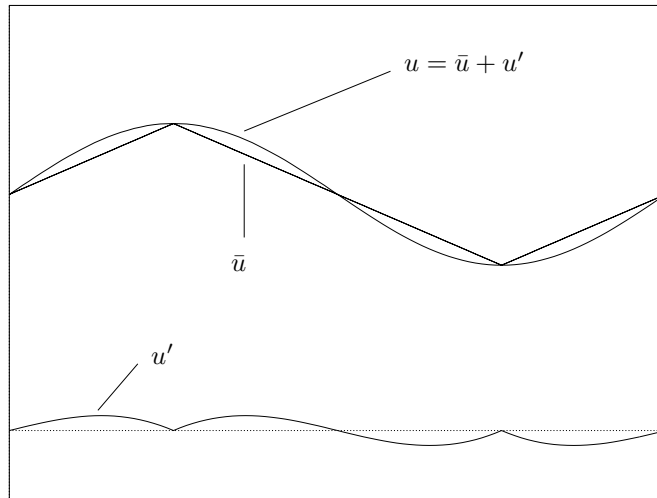
Figure 17. $\bar{u}$ is the piecewise linear interpolate of u.

is a unit normal vector on the element boundary and the $\pm$ designations are defined as illustrated in Figure 18. Note that (72) is invariant with respect to interchange of $\pm$ designations.

In the present case there is smoothness only on element interiors. Consequently, integration-by-parts gives rise to nonvanishing element boundary terms. For example, if $\bar{w} \in \bar{\mathcal{V}}$ and $u' \in \mathcal{S}'$,
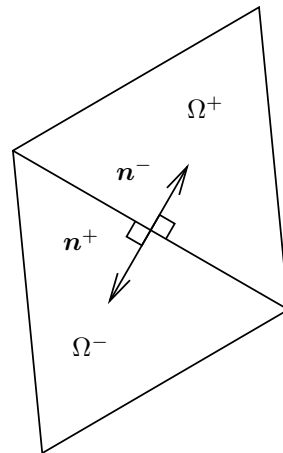
Figure 18. Definition of unit normals on an element boundary.
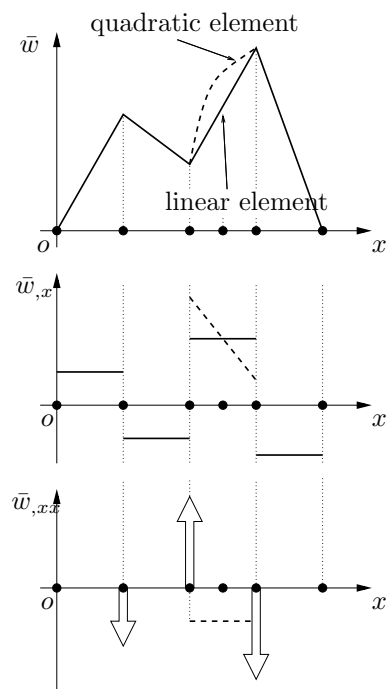
Figure 19. Generalized derivatives of piecewise linear and quadratic finite elements.

the following integration-by-parts formula holds

$$
\begin{aligned}
a(\bar{w}, u') &= \sum_{e=1}^{n_{\text{el}}} \left((\mathcal{L}^*\bar{w}, u')_{\Omega^e} + (b^*\bar{w}, u')_{\Gamma^e} \right) \\
&= (\mathcal{L}^*\bar{w}, u')_{\Omega'} + (\llbracket b^*\bar{w} \rrbracket, u')_{\Gamma'} \\
&= (\mathcal{L}^*\bar{w}, u')_{\Omega}
\end{aligned}
\tag{74}
$$

where b^* is the **boundary operator** corresponding to $\mathcal{L}^*$ (e.g., if $\mathcal{L}^* = \mathcal{L} = -\Delta$, then $b^* = b = \boldsymbol{n} \cdot \nabla = \partial/\partial n$). Note, from (74), there are three different ways to express the integration-by-parts formula. The first line of (74) amounts to performing integration-by-parts on an element-by-element basis. In the second line, the sum over element interiors has been represented by integration over Ω' and the element boundary terms have been combined in pairs, the result being a jump term integrated over element interfaces. Finally, in the third line, $\mathcal{L}^*\bar{w}$ is viewed as a **Dirac distribution** defined on the entire domain Ω. To understand this interpretation, consider the following example:

Let

$$
\mathcal{L}^*\bar{w} = \bar{w}_{,xx}
\tag{75}
$$

and assume $\bar{w}$ consists of piecewise linear, or quadratic, finite elements in one dimension. The set-up is illustrated in Figure 19. Note that $\bar{w}_{,xx}$ consists of Dirac delta functions at element boundaries and smooth functions on element interiors. This amounts to the distributional interpretation of $\mathcal{L}^*\bar{w}$ in the general case. It is smooth on element interiors but contains Dirac layers on the element interfaces, which give rise to the jump terms in the second line of (74).

Likewise, there are additional integration-by-parts formulas: $\forall w' \in \mathcal{V}'$, $\bar{u} \in \bar{\mathcal{S}}$ and $u' \in \mathcal{S}'$,

$$
\begin{aligned}
a(w', \bar{u}) &= \sum_{e=1}^{n_{\text{el}}} \left((w', \mathcal{L}\bar{u})_{\Omega^e} + (w', b\bar{u})_{\Gamma^e} \right) \\
&= (w', \mathcal{L}\bar{u})_{\Omega'} + (w', \llbracket b\bar{u} \rrbracket)_{\Gamma'} \\
&= (w', \mathcal{L}\bar{u})_{\Omega}
\end{aligned}
\tag{76}
$$

$$
\begin{aligned}
a(w', u') &= \sum_{e=1}^{n_{\text{el}}} \left((w', \mathcal{L}u')_{\Omega^e} + (w', bu')_{\Gamma^e} \right) \\
&= (w', \mathcal{L}u')_{\Omega'} + (w', \llbracket bu' \rrbracket)_{\Gamma'} \\
&= (w', \mathcal{L}u')_{\Omega}
\end{aligned}
\tag{77}
$$

where, again, $\mathcal{L}\bar{u}$ and $\mathcal{L}u'$ are **Dirac distributions** on Ω.

Exact variational equation for $\bar{u}$ (rough case) The distributional interpretation of $\mathcal{L}\bar{u}$, $\mathcal{L}u'$ and $\mathcal{L}^*\bar{w}$ allows one to follow the developments of the smooth case (see Section 3.2.1). Thus, the formula for u' can be expressed in three alternative forms analogous to those of the

integration-by-parts formulas, viz.,

$$
\begin{aligned}
u'(y) &= -\int_\Omega g'(x,y)(\mathcal{L}\bar{u}-f)(x)\,d\Omega_x \\
&= -\int_{\Omega'} g'(x,y)(\mathcal{L}\bar{u}-f)(x)\,d\Omega_x - \int_{\Gamma'} g'(x,y)[\![b\bar{u}]\!](x)\,d\Gamma_x \\
&= -\sum_{e=1}^{n_{\text{el}}}\left(\int_{\Omega^e} g'(x,y)\,(\mathcal{L}\bar{u}-f)\,(x)\,d\Omega_x + \int_{\Gamma^e} g'(x,y)(b\bar{u})(x)\,d\Gamma_x\right) \quad (78)
\end{aligned}
$$

which again may be written as $u' = M'(\mathcal{L}\bar{u}-f)$. Note, this is an **exact** formula for u'.

Remarks

1. When a mesh-based method, such as finite elements, is employed, the coarse scales, $\bar{u}$, are referred to as the **resolved scales**, and the fine scales, u', are referred to as the **subgrid scales**. The coarse-scale equation is often referred to as a **subgrid-scale model**.
2. $\mathcal{L}\bar{u} - f$ is the **residual** of the resolved scales. It consists of a **smooth part** on element interiors (i.e., Ω') and a **jump term** $[\![b\bar{u}]\!]$ across element interfaces (i.e., Γ').
3. The subgrid scales u' are **driven** by the residual of the resolved scales.

Upon substituting (78) into the equation for the coarse scales, (67) is arrived at, where

$$
\begin{aligned}
(\mathcal{L}^*\bar{w}, M'(\mathcal{L}\bar{u}-f)) &= -\int_\Omega\int_\Omega (\mathcal{L}^*\bar{w})(y)g'(x,y)(\mathcal{L}\bar{u}-f)(x)\,d\Omega_x\,d\Omega_y \\
&= -\int_{\Omega'}\int_{\Omega'} (\mathcal{L}^*\bar{w})(y)g'(x,y)(\mathcal{L}\bar{u}-f)(x)\,d\Omega_x\,d\Omega_y \\
&\quad - \int_{\Omega'}\int_{\Gamma'} (\mathcal{L}^*\bar{w})(y)g'(x,y)[\![b\bar{u}]\!](x)\,d\Gamma_x\,d\Omega_y \\
&\quad - \int_{\Gamma'}\int_{\Omega'} [\![b^*\bar{w}]\!](y)g'(x,y)(\mathcal{L}\bar{u}-f)(x)\,d\Omega_x\,d\Gamma_y \\
&\quad - \int_{\Gamma'}\int_{\Gamma'} [\![b^*\bar{w}]\!](y)g'(x,y)[\![b\bar{u}]\!](x)\,d\Gamma_x\,d\Gamma_y \\
&= -\sum_{e=1}^{n_{\text{el}}}\sum_{l=1}^{n_{\text{el}}}\left(\int_{\Omega^e}\int_{\Omega^l} (\mathcal{L}^*\bar{w})(y)g'(x,y)(\mathcal{L}\bar{u}-f)(x)\,d\Omega_x\,d\Omega_y\right. \\
&\quad - \int_{\Omega^e}\int_{\Gamma^l} (\mathcal{L}^*\bar{w})(y)g'(x,y)(b\bar{u})(x)\,d\Gamma_x\,d\Omega_y \\
&\quad - \int_{\Gamma^e}\int_{\Omega^l} (b^*\bar{w})(y)g'(x,y)(\mathcal{L}\bar{u}-f)(x)\,d\Omega_x\,d\Gamma_y \\
&\quad \left. - \int_{\Gamma^e}\int_{\Gamma^l} (b^*\bar{w})(y)g'(x,y)(b\bar{u})(x)\,d\Gamma_x\,d\Gamma_y\right) \quad (79)
\end{aligned}
$$

Note, once again, there are three alternative forms due to the distributional nature of $\mathcal{L}^*\bar{w}$ and $\mathcal{L}\bar{u}$.

Remarks

1. Equation (67) along with (79) is an ***exact*** equation for the resolved scales. It can serve as a ***paradigm*** for finite element methods when unresolved scales are present.
2. The effect of the unresolved scales on the resolved scales is ***nonlocal***.
3. The necessity of including jump operator terms to attain stable discretizations for certain problems has been observed previously (see Douglas Jr. and Wang, 1989; Franca, Hughes and Stenberg, 1993; Hughes and Franca, 1987; Hughes and Hulbert, 1988; Hulbert and Hughes, 1990; Silvester and Kechkar, 1990). The present result demonstrates that the jump operator terms may be ***derived*** directly from the governing equations.
4. Equation (79) illustrates that the distributional part of $\mathcal{L}^*\bar{w}$ and $\mathcal{L}\bar{u}$ needs to be included in a consistent stabilized method. Classically, these terms have been omitted, which has led to some problems. Jansen et al. (1999) first observed the need to include the effect of the distributional term. In their approach, rather than explicitly including the jump terms, a variational reconstruction of second-derivative terms is employed. Jansen et al. (1999) showed that ***significant*** increases in accuracy are attained thereby. The method presented by Jansen et al. (1999) is similar to one presented by Bochev and Gunzburger (2003), who refer to procedures of this kind as ***weakly consistent***.

Equation (67) can be concisely written as

$$\boxed{B(\bar{w}, \bar{u}; g') = L(\bar{w}; g') \qquad \forall \bar{w} \in \bar{\mathcal{V}}} \qquad (80)$$

where

$$B(\bar{w}, \bar{u}; g') \quad = \quad a(\bar{w}, \bar{u}) + (\mathcal{L}^*\bar{w}, M'(\mathcal{L}\bar{u})) \qquad (81)$$
$$L(\bar{w}; g') \quad = \quad (\bar{w}, f) + (\mathcal{L}^*\bar{w}, M'f) \qquad (82)$$

Note that $B(\cdot, \cdot; \cdot)$ is bilinear with respect to the first two arguments and affine with respect to the third argument; $L(\cdot; \cdot)$ is linear with respect to the first argument and affine with respect to the second. Equations (80)–(82) are valid in both the smooth and rough cases, with the distributional interpretation appropriate in the latter case.

Numerical method   An ***approximation***, $\tilde{g}' \approx g'$, is the key ingredient in developing a practical numerical method. It necessarily entails some form of ***localization***. The numerical method is written as follows:

$$\boxed{B(\bar{w}^h, \bar{u}^h; \tilde{g}') = L(\bar{w}^h; \tilde{g}') \qquad \forall \bar{w} \in \bar{\mathcal{V}}} \qquad (83)$$

u' **and *a posteriori* error estimation**   Note that $u' = u - \bar{u}$ is the **error** in the coarse scales. The formula $u' = M'(\mathcal{L}\bar{u}^h - f)$ is a **paradigm** for *a posteriori* error estimation. Thus, it is plausible that

$$u' \approx \tilde{M}'(\mathcal{L}\bar{u}^h - f) \tag{84}$$

where $\tilde{M}' \approx M'$, is an *a posteriori error estimator*, which can be used to estimate coarse-scale error in any suitable norm, for example, the W_p^s-norm, $0 \leq p \leq \infty, 0 \leq s < \infty$. (Keep in mind, $\mathcal{L}\bar{u}$ is a Dirac distribution.) An approximation of the fine-scale Green's function, $\tilde{g}' \approx g'$, induces an approximation $\tilde{M}' \approx M'$; see (78). Conversely, an *a posteriori* error estimator of the form (84) may be used to infer an approximation of the Green's function and to develop a numerical method of the form (83).

A particularly insightful form of the estimator is given by

$$u'(y) \approx - \int_{\Omega'} \tilde{g}'(x,y)(\mathcal{L}\bar{u}^h - f)(x)\, d\Omega_x - \int_{\Gamma'} \tilde{g}'(x,y)[\![b\bar{u}^h]\!](x)\, d\Gamma_x \tag{85}$$

Note that the residuals of the computed coarse-scale solution, that is $\mathcal{L}\bar{u}^h - f$ and $[\![b\bar{u}^h]\!]$, are the **sources** of error, and the fine-scale Green's function acts as the **distributor** of error.

There seems to be agreement in the literature on *a posteriori* estimators that either one, or both, the residuals are the sources of error. Where there seems to be considerable disagreement is in how these sources are distributed. From (85), we see that there is no universal solution to the question of what constitutes an appropriate distribution scheme. It is strongly dependent on the particular operator $\mathcal{L}$ through the fine-scale Green's function. This result may serve as a context for understanding differences of opinion which have occurred over procedures of *a posteriori* error estimation.

Remark
An advantage of the variational multiscale method is that it comes **equipped** with a fine-scale solution which may be viewed as an *a posteriori* estimate of the coarse-scale solution error.

Discussion
It is interesting to examine the behavior of the exact counterpart of (85) for different operators of interest. Assume that u^h is piecewise linear in all cases, and that $f = 0$.

First consider the Laplace operator, $\mathcal{L} = -\Delta$, $b = \partial/\partial n$. In this case, $\mathcal{L}\bar{u}^h = 0$, and the interface residual, $[\![b\bar{u}^h]\!]$, is the entire source of error. Keeping in mind the highly local nature of the Green's function for the Laplacian, a local distribution of $[\![b\bar{u}^h]\!]$ would seem to be a reasonable approximation. The same could be said for linear elasticity, assuming there are no constraints, such as, for example, incompressibility, or unidirectional inextensibility.

Next consider the advection-diffusion operator, $\mathcal{L} = \boldsymbol{a} \cdot \nabla - \kappa\Delta$, $[\![b\bar{u}^h]\!] = [\![\kappa\partial\bar{u}^h/\partial n]\!]^*$, where $\boldsymbol{a}$ is a given solenoidal velocity field, and $\kappa > 0$, the diffusivity, is a positive constant. In the case of diffusion domination (i.e., advective effects are negligible), $\mathcal{L} \approx -\kappa\Delta$, and the situation is the same as for the Laplacian. On the other hand, when advection dominates, $\mathcal{L}\bar{u}^h \approx \boldsymbol{a}\cdot\nabla\bar{u}^h$,

---

*This follows from the continuity of advective flux.

and $[\![b\bar{u}^h]\!] = [\![\kappa \partial \bar{u}^h / \partial n]\!]$ may be ignored. This time, the element residual, $\mathcal{L}\bar{u}^h$, is the primary source of error. A local distribution scheme would seem less than optimal because the Green's function propagates information along the integral curves of $-\boldsymbol{a}$ (keep in mind that the Green's function is for the adjoint operator, $\mathcal{L}^*$), with little amplitude decay. This means that there is an approximately constant trajectory of error corresponding to the residual error $\mathcal{L}\bar{u}^h$, in the element in question.

Finally, consider the Helmholtz operator, $\mathcal{L} = -\Delta - k^2$, $b = \partial/\partial n$, where k is the **wave number**. If k is real, we have **propagating waves**, whereas if k is imaginary, we have **evanescent** (decaying) **waves**. In the latter case, the Green's function is highly localized; as $|k| \to 0$ the Green's function approaches that for the Laplacian, as $|k| \to \infty$ the Green's function approaches $-k^{-2}\delta$, a delta function. In the case of propagating waves, the Green's function is oscillatory. In general, for $|k|$ large, the dominant source of error is the element residual, $\mathcal{L}\bar{u}^h = -k^2\bar{u}^h$. As $|k| \to 0$, the interface residual, $[\![b\bar{u}^h]\!] = [\![\partial \bar{u}^h / \partial n]\!]$, dominates.

3.3. Hierarchical p-refinement and bubbles

Hierarchical p-refinement plays an important role in clarifying the nature of the fine-scale Green's function, g′, and provides a framework for its approximation. Some notations are required. Let

$$\bar{u}^h = \sum_{A=1}^{\bar{n}_{\text{nodes}}} \bar{N}_A \bar{u}_A \qquad (\text{likewise } \bar{w}^h) \tag{86}$$

where $\bar{N}_A$ is a finite element shape function associated with the primary nodes, $A = 1, 2, \cdots, \bar{n}_{\text{nodes}}$, and $\bar{u}_A$ is the corresponding nodal value; and let

$$u' = \sum_{A=1}^{n'_{\text{nodes}}} N'_A u'_A \qquad (\text{likewise } w') \tag{87}$$

where N'_A is a hierarchical finite element shape function associated with the additional nodes, $A = 1, 2, \cdots, n'_{\text{nodes}}$, and u'_A are the corresponding hierarchical degrees of freedom. For example, let $\bar{u}^h$ be expanded in piecewise linear basis functions and u' in hierarchical cubics (see Fig. 20). Note, bubble functions are **zero** on element boundaries. An illustration in one dimension is presented in Figure 21.

Substituting (86) and (87) into (57)–(60), and eliminating u'_A by **static condensation** results in

$$B(\bar{w}^h, \bar{u}^h; \tilde{\text{g}}') = L(\bar{w}^h; \tilde{\text{g}}') \qquad \forall \bar{w}^h \in \bar{\mathcal{V}} \tag{88}$$

where

$$B(\bar{w}^h, \bar{u}^h; \tilde{\text{g}}') = a(\bar{w}^h, \bar{u}^h) + (\mathcal{L}^* \bar{w}^h, \tilde{M}'(\mathcal{L}\bar{u}^h)) \tag{89}$$
$$L(\bar{w}^h; \tilde{\text{g}}') = (\bar{w}^h, f) + (\mathcal{L}^* \bar{w}^h, \tilde{M}'f) \tag{90}$$

and

$$(\mathcal{L}^* \bar{w}^h, \tilde{M}'(\mathcal{L}\bar{u}^h)) = -\int_\Omega \int_\Omega (\mathcal{L}^* \bar{w}^h)(y)\tilde{\text{g}}'(x,y)(\mathcal{L}\bar{u}^h)(x)\, d\Omega_x\, d\Omega_y \tag{91}$$

$\bar{u}^h = \text{standard linears } (\bullet)$

$u' = \text{hierarchical cubics } (\circ)$

typical linear

function

typical cubic

edge function

typical cubic

bubble function

Figure 20. Hierarchical cubics in two dimensions.
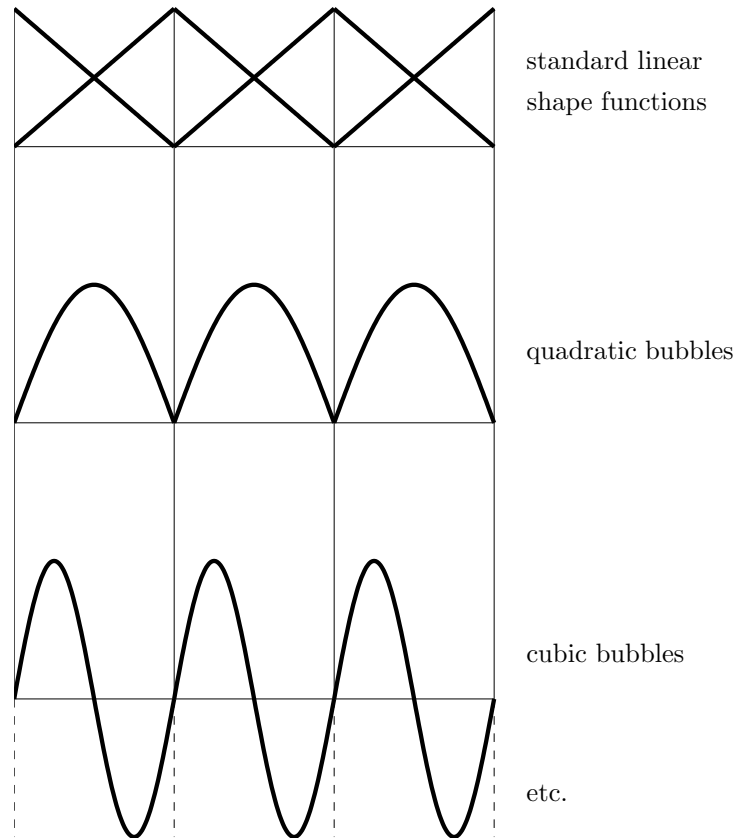
Figure 21. Finite element shape functions and polynomial "bubbles".

$$\tilde{g}'(x,y) = \sum_{A,B=1}^{n'_{\text{nodes}}} N'_A(y) \left[(\boldsymbol{K}'')^{-1} \right]_{AB} N'_B(x) \tag{92}$$

where

$$\boldsymbol{K}'' = [K''_{AB}] \tag{93}$$
$$K''_{AB} = a(N'_A, N'_B) \tag{94}$$

Remarks

1. Recall, $\mathcal{L}\bar{u}^h$ and $\mathcal{L}^*\bar{w}^h$ are **Dirac distributions** in the finite element case (cf. (91) and (79)).
2. Hierarchical p-refinement generates an **approximate** fine-scale Green's function, $\tilde{g}' \approx g'$.

3. For ***implementational purposes***, it is more convenient to rewrite (89)–(91) in forms avoiding Dirac distributions. This can be accomplished by using the integration-by-parts formulas, viz.,

$$(\mathcal{L}^* \bar{w}^h, \tilde{M}'(\mathcal{L}\bar{u}^h - f)) = - \sum_{A,B=1}^{n'_{\text{nodes}}} a(\bar{w}^h, N'_A) \left[(\boldsymbol{K}'')^{-1} \right]_{AB} (a(N'_B, \bar{u}^h) - (N'_B, f)) \quad (95)$$

which amounts to the usual ***static condensation*** algorithm.

4. *A posteriori* error estimation for the coarse-scale solution, $\bar{u}^h$, is provided by the fine-scale solution (see (78) and (84)):

$$
\begin{aligned}
u'(y) \quad &= \quad - \int_\Omega \tilde{g}(x,y)(\mathcal{L}\bar{u}^h - f)(x)\, d\Omega_x \\
&= \quad - \int_{\Omega'} \tilde{g}'(x,y)(\mathcal{L}\bar{u}^h - f)(x)\, d\Omega_x \\
&\quad - \int_{\Gamma'} \tilde{g}'(x,y)[\![b\bar{u}^h]\!](x)\, d\Gamma_x \\
&= \quad - \sum_{e=1}^{n_{\text{el}}} \left(\int_{\Omega^e} \tilde{g}'(x,y)(\mathcal{L}\bar{u}^h - f)(x)\, d\Omega_x \right. \\
&\qquad\qquad \left. + \int_{\Gamma^e} \tilde{g}'(x,y)(b\bar{u}^h)(x)\, d\Gamma_x \right)
\end{aligned}
\quad (96)
$$

or, in analogy with (95), by

$$u'(y) = - \sum_{A,B=1}^{n'_{\text{nodes}}} N'_A(y) \left[(\boldsymbol{K}'')^{-1} \right]_{AB} \left(a(N'_B, \bar{u}^h) - (N'_B, f) \right) \quad (97)$$

The quality of this estimator depends on the ability of $\{N'_A\}_{A=1}^{n'_{\text{nodes}}}$ to approximate the fine scales, or equivalently, the quality of the approximation $\tilde{g}' \approx g'$.

5. Note that the fine-scale Green's function ***only*** depends on the hierarchical basis (see (92)–(94)). The ***exact*** fine-scale Green's function corresponds to the limit $p \to \infty$.

6. The fine-scale Green's function is ***nonlocal***, but it is computed from a basis of functions having ***compact support***. For example, in the two-dimensional case, the basis consists of bubbles, supported by individual elements, and edge functions, supported by pairs of elements sharing an edge. The three-dimensional case is similar, but somewhat more complicated; the basis consists of bubbles, face and edge functions. In three dimensions, pairs of elements support face functions whereas the number of elements supporting edge functions depends on the topology of the mesh.

7. In two dimensions, by virtue of the convergence of hierarchical p-refinement, the exact fine-scale solution may be decomposed into a finite number of ***limit*** functions – one bubble for each element and one edge function for each pair of elements sharing an edge. In one dimension the situation is simpler in that only bubbles are required. The three-dimensional case is more complex in that bubbles, face and edge functions are required.

8. Polynomial bubbles are typically ineffective, but so-called **residual-free bubbles** (Brezzi et al. (1997)) are equivalent to exactly calculating element Green's functions. This approximation works exceptionally well in some important cases and will be discussed in more detail later on.

9. If **only** bubble functions are considered in the refinement, coupling between different elements and all jump terms is **eliminated**. In this case,

$$(\mathcal{L}^*\bar{w}^h, \tilde{M}'(\mathcal{L}\bar{u}^h)) = -\int_{\Omega'}\int_{\Omega'} (\mathcal{L}^*\bar{w}^h)(y)\tilde{g}'(x,y)(\mathcal{L}\bar{u}^h)(x)\,d\Omega_x\,d\Omega_y \qquad (98)$$
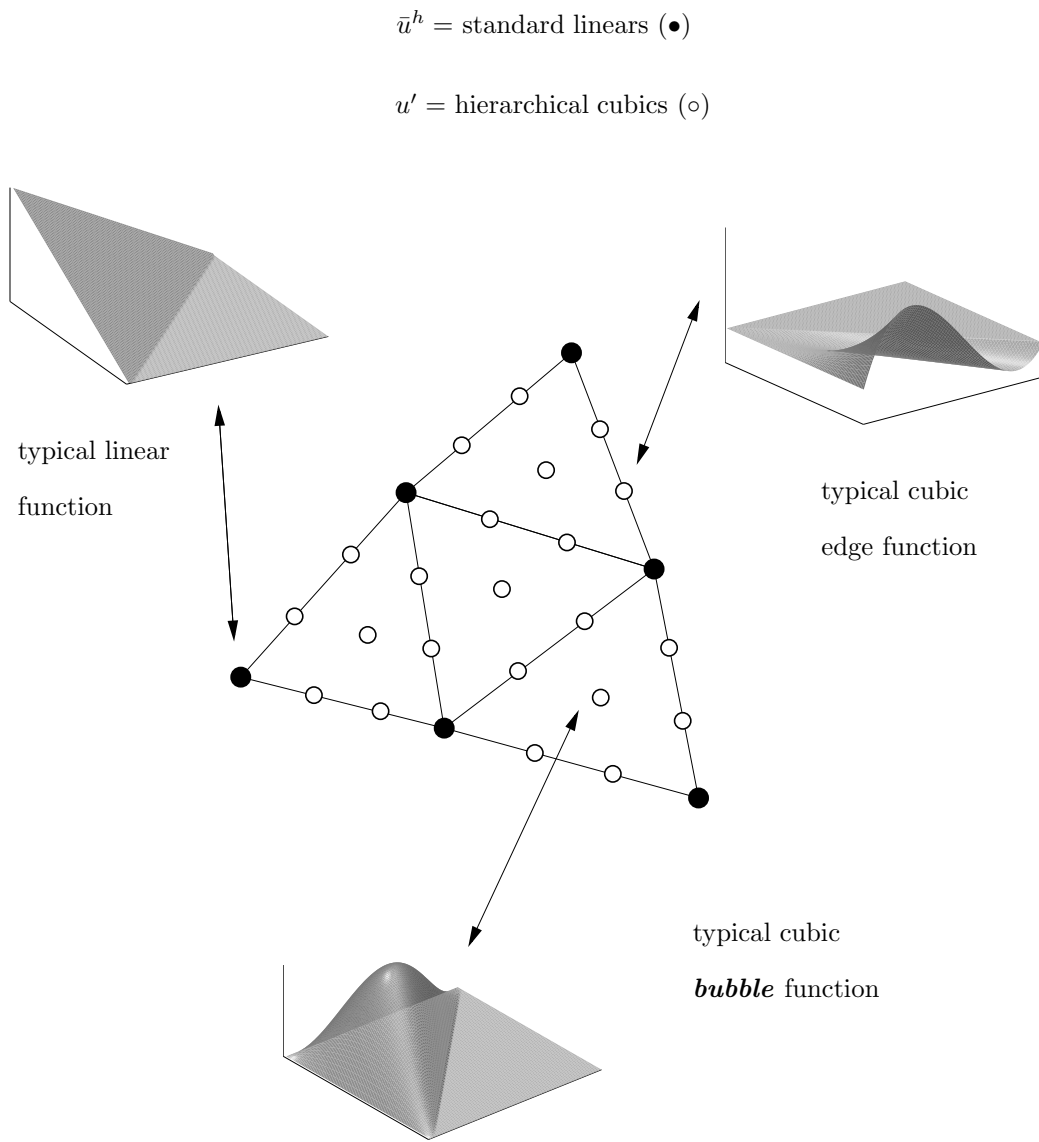
where Ω' has replaced Ω, and now the effect of u' is **nonlocal** only within each element. The approximate Green's function $\tilde{g}'$, is defined **element-wise** and takes on **zero** values on element boundaries.

10. It may be observed that the fine-Green's function formula has an interpretation analogous to projection methods in linear algebraic systems, such as, for example, multigrid methods. To explicate this analogy, the notation of Saad (1995), Chapter 5, is adopted. Let $\mathcal{K}$ be an m-dimensional subspace of $\mathbb{R}^n$, and let A be an $n \times n$ real matrix. The objective is to solve $Ax = b$ for $x \in \mathbb{R}^n$, where $b \in \mathbb{R}^n$ is a given vector. Assume an initial guess, $x_0 \in \mathbb{R}^n$, and determine an approximate solution $\tilde{x} \in x_0 + \mathcal{K}$, such that the residual $\tilde{r} = b - A\tilde{x} \perp \mathcal{K}$. If $\tilde{x}$ is written as $\tilde{x} = x_0 + \delta$, where $\delta \in \mathcal{K}$, and $r_0 = b - Ax_0$, then $b - A(x_0 + \delta) \perp \mathcal{K}$, or equivalently, $r_0 - A\delta \perp \mathcal{K}$. In terms of a basis $\{v_1, v_2, \ldots, v_m\}$ of $\mathcal{K}$, the approximate solution becomes $\tilde{x} = x_0 + Vy$, where $V = [v_1, v_2, \ldots, v_m]$, an $n \times m$ matrix. The orthogonality condition becomes $V^T A V y = V^T r_0$, and thus $\delta = \tilde{x} - x_0 = V(V^T A V)^{-1} V^T r_0$, assuming nonsingularity of $V^T A V$. Note the similarity of this result to that of (92) and (97): $\delta \sim u'$, $\tilde{x} \sim u$, $x_0 \sim \overline{u}^h$, $V \sim [N'_1, N'_2, \ldots, N'_{n'_{\text{nodes}}}]$, $V^T A V \sim \boldsymbol{K}''$, $V^T r_0 \sim [a(N'_1, \overline{u}^h) - (N'_1, f), \ldots, a(N'_{n'_{\text{nodes}}}, \overline{u}^h) - (N'_{n'_{\text{nodes}}}, f)]^T$, and $V(V^T A V)^{-1} V^T \sim \tilde{g}'$. In multilevel solution strategies, the fine-scale space here may be analogized to the "coarse grid", and δ is obtained by restriction to the coarse-grid subspace (i.e., $V^T r_0$), a coarse-grid correction (i.e., $V^T A V y = V^T r_0$), and prolongation, or interpolation (i.e., Vy).

11. **Defect-correction** techniques have become popular in the multigrid community to obtain stable second-order accurate solutions of the convection-diffusion equation. These methods use upwind schemes for relaxation (stability) and central difference schemes for residual evaluation (accuracy). A standard reference is Hemker (1981); see also Trottenberg, Oosterlee and Schüller (2001). More generally, defect-correction is a powerful abstraction for various iterative methods, including Newton, multigrid, and domain decomposition. It can also be extended to multiscale problems. See Lai (1981) for an example of how defect-correction is used in the treatment of small-scale fluctuations in aeroacoustics.

3.4. Residual-free bubbles

The concept of **residual-free bubbles** has been developed and explored in Baiocchi, Brezzi and Franca (1993), Brezzi et al. (1997), Brezzi and Russo (1994), Franca and Russo (1996), Russo (1996a,1996b). The basic idea is to solve the fine-scale equation on individual elements with zero Dirichlet boundary conditions. For example, the objective is to find $u' \in \mathcal{V}'$, such

that $\forall \bar{u} \in \bar{\mathcal{V}}$,

$$\left.\begin{aligned} (\Pi')^* \mathcal{L} u' &= -(\Pi')^*(\mathcal{L}\bar{u} - f) & \text{on } \Omega^e \\ u' &= 0 & \text{on } \Gamma^e \end{aligned}\right\} \qquad e = 1, 2, \cdots, n_{\text{el}} \qquad (99)$$

Noting that $\bar{u}$ can be expressed in terms of the coarse-scale basis having support in the element in question, a fine-scale basis of residual-free bubbles can be constructed for each element, i.e.

$$\left.\begin{aligned} (\Pi')^* \mathcal{L} N'_a &= -(\Pi')^*(\mathcal{L}\bar{N}_a - f) & \text{on } \Omega^e \\ N'_a &= 0 & \text{on } \Gamma^e \end{aligned}\right\} \qquad e = 1, 2, \cdots, n_{\text{el}} \qquad (100)$$

where $a = 1, 2, \cdots, n_{\text{en}}$ is the local numbering of the primary nodes of element e. Thus, to each coarse-scale basis function $\bar{N}_a$, solve (100) for a corresponding residual-free bubble N'_a. Consequently, the maximal dimension of the space of residual-free bubbles for element e is n_{en}. It is typical, however, that the dimension is less than n_{en}.

Brezzi and Russo (1994) have constructed residual-free bubbles for the homogeneous advection-diffusion equation assuming the coarse-scale basis consists of continuous, piecewise linears on triangles. For this case $n_{\text{en}} = 3$, but the dimension of the space of residual-free bubbles is only one. Let B_e denote the residual-free bubble basis solution of the following problem:

$$\left.\begin{aligned} \mathcal{L} B_e &= 1 & \text{on } \Omega^e \\ B_e &= 0 & \text{on } \Gamma^e \end{aligned}\right\} \qquad (101)$$

Note that, due to the fact the coarse-scale space consist only of piecewise linears, combined with the fact that the fine-scale space satisfies zero Dirichlet boundary conditions, the projection operator, Π', present in the general case, namely (100), can be omitted and (101) can be solved in the strong sense. However, in order to avoid potential linear dependencies, in general, (100) needs to be respected.

In principle, the computation of the residual-free bubble should involve the solution of one or more partial differential equations in each element. This, however, can be done in an approximate way, using a suitable subgrid in each element, as in Brezzi, Marini and Russo (1998) and Franca, Neslinturk and Stynes (1998). This leads to the idea of the stabilizing subgrid: if one does not eliminate the discrete bubbles, one can think of solving the Galerkin method on the enriched subgrid, having the beneficial effects of the bubble stabilization. See Brezzi and Marini (2002), Brezzi et al. (2003), and Brezzi, Marini and Russo (2004) for further development of this idea.

3.5. Element Green's functions

The idea of employing an **element Green's function** was proposed in the initial work on the variational multiscale method (Hughes (1995)). In place of (63)–(64), the Green's function problem for each element is solved:

$$\left.\begin{aligned} (\Pi')^* \mathcal{L}^* \mathrm{g}'_e(x, y) &= (\Pi')^* \delta(x - y) & \forall x \in \Omega^e \\ \mathrm{g}'_e(x, y) &= 0 & \forall x \in \Gamma^e \end{aligned}\right\} \qquad e = 1, 2, \cdots, n_{\text{el}} \qquad (102)$$

Use of element Green's functions in place of the global Green's function amounts to a **local approximation**,

$$\tilde{\mathrm{g}}'(x, y) = \mathrm{g}'_e(x, y) \qquad \forall x, y \in \Omega^e, \quad e = 1, 2, \cdots, n_{\text{el}} \qquad (103)$$

The upshot is that the subgrid scales **vanish** on element boundaries, i.e.,

$$u' = 0 \qquad \text{on } \Gamma^e, \qquad e = 1, 2, \cdots, n_{\text{el}} \tag{104}$$

This means the subgrid scales are completely confined within element interiors.

There is an intimate link between element Green's functions and residual-free bubbles. This idea was first explored in Brezzi et al. (1997), in which it was shown that, for the case governed by (101),

$$\boxed{B_e(y) = \int_{\Omega^e} \text{g}'_e(x, y) \, d\Omega_x} \tag{105}$$

This result can be easily derived as follows:

$$
\begin{aligned}
\int_{\Omega^e} \text{g}'_e(x, y) \, d\Omega_x &= (\text{g}'_e, 1)_{\Omega^e_x} \\
&= (\text{g}'_e, \mathcal{L} B_e)_{\Omega^e_x} \\
&= a(\text{g}'_e, B_e)_{\Omega^e_x} \\
&= (\mathcal{L}^* \text{g}'_e, B_e)_{\Omega^e_x} \\
&= (\delta, B_e)_{\Omega^e_x} \\
&= B_e(y)
\end{aligned}
\tag{106}
$$

Another way to derive (105) is to appeal to the general formula for the Green's function in terms of a fine-scale basis, namely (92). Specialized to the present case, (92) becomes

$$\tilde{\text{g}}'_e(x, y) = B_e(x) \left(a(B_e, B_e)_{\Omega^e} \right)^{-1} B_e(y) \tag{107}$$

Note that

$$
\begin{aligned}
a(B_e, B_e)_{\Omega^e} &= (B_e, \mathcal{L} B_e)_{\Omega^e} \\
&= (B_e, 1)_{\Omega^e} \\
&= \int_{\Omega^e} B_e \, d\Omega
\end{aligned}
\tag{108}
$$

The result follows by integrating (107) and using (108),

$$
\begin{aligned}
\int_{\Omega^e} \tilde{\text{g}}'_e(x, y) \, d\Omega_x &= \int_{\Omega^e} B_e(x) \, d\Omega_x \left(a(B_e, B_e)_{\Omega^e} \right)^{-1} B_e(y) \\
&= B_e(y)
\end{aligned}
\tag{109}
$$

Remarks

1. In general, the relationship between a fine-scale basis and a Green's function is given by (92). The result (105) is special to a residual-free bubble governed by (101).
2. In general, the coarse-scale residual will not be constant within an element. For example, suppose the residual is a linear polynomial in x. Then there are two residual-free bubbles, one corresponding to 1 and one corresponding to x, say $B_e^{(0)}$ and $B_e^{(1)}$, respectively. $B_e^{(0)}$

is the same as B_e, and is given by (105). $B_e^{(1)}$ may be determined in the same way as (106):

$$
\begin{aligned}
\int_{\Omega^e} \mathrm{g}_e'(x,y)x\,d\Omega_x &= (\mathrm{g}_e',x)_{\Omega_x^e} \\
&= (\mathrm{g}_e',\mathcal{L}B_e^{(1)})_{\Omega_x^e} \\
&= a(\mathrm{g}_e',B_e^{(1)})_{\Omega_x^e} \\
&= (\mathcal{L}^*\mathrm{g}_e',B_e^{(1)})_{\Omega_x^e} \\
&= (\delta,B_e^{(1)})_{\Omega_x^e} \\
&= B_e^{(1)}(y)
\end{aligned}
\tag{110}
$$

As may be seen, $B_e^{(1)}$ is the first moment of g_e'. This is the general case: If the coarse-scale residual is expanded in terms of a basis of functions, then the residual-free bubbles are the moments of g_e' with respect to the elements of that basis.

3.6. Stabilized methods

Classical **stabilized methods** are generalized Galerkin methods of the form

$$
a(\bar{w}^h,\bar{u}^h) + (\mathbf{L}\bar{w}^h,\tau(\mathcal{L}\bar{u}^h - f))_{\Omega'} = (\bar{w}^h,f)
\tag{111}
$$

where $\mathbf{L}$ is typically a **differential operator**, such as

$$
\begin{aligned}
\mathbf{L} &= +\mathcal{L} && \text{Galerkin/least-squares (GLS)} && (112) \\
\mathbf{L} &= +\mathcal{L}_{\mathrm{adv}} && \text{SUPG} && (113) \\
\mathbf{L} &= -\mathcal{L}^* && \text{Multiscale} && (114)
\end{aligned}
$$

and τ is typically an **algebraic operator**. SUPG is a method defined for advective-diffusive operators, that is, ones decomposable into advective ($\mathcal{L}_{\mathrm{adv}}$) and diffusive ($\mathcal{L}_{\mathrm{diff}}$) parts. A stabilized method of the form (114) is referred to as a "multiscale" stabilized method for reasons that will become apparent shortly.

3.6.1. Relationship of stabilized methods with subgrid-scale models
It was shown in Hughes (1995) that a stabilized method of **multiscale** type is an approximate subgrid-scale model in which the algebraic operator τ approximates the integral operator M' based on **element Green's functions**,

$$
\tau = -\tilde{M}' \approx -M'
\tag{115}
$$

Equivalently,

$$
\tau \cdot \delta(y-x) = \tilde{\mathrm{g}}_e'(x,y) \approx \mathrm{g}'(x,y)
\tag{116}
$$

The result follows from the calculation

$$
\begin{aligned}
\int_{\Omega'}\int_{\Omega'} (-\mathcal{L}^*\bar{w}^h)(y)\tilde{\mathrm{g}}_e'(x,y)(\mathcal{L}\bar{u}^h - f)(x)\,d\Omega_x\,d\Omega_y & \\
= \int_{\Omega'}\int_{\Omega'} (-\mathcal{L}^*\bar{w}^h)(y)\tau \cdot \delta(y-x)(\mathcal{L}\bar{u}^h - f)(x)\,d\Omega_x\,d\Omega_y & \\
= \int_{\Omega'} (-\mathcal{L}^*\bar{w}^h)(x)\tau \cdot (\mathcal{L}\bar{u}^h - f)(x)\,d\Omega_x &
\end{aligned}
\tag{117}
$$

3.6.2. Formula for τ based on the element Green's function   The approximation

$$\tau \cdot \delta(y - x) \approx \tilde{\mathrm{g}}'_e(x, y) \tag{118}$$

suggests defining τ by

$$\int_{\Omega^e} \int_{\Omega^e} \tau \cdot \delta(y - x) \, d\Omega_x \, d\Omega_y = \int_{\Omega^e} \int_{\Omega^e} \mathrm{g}'_e(x, u) \, d\Omega_x \, d\Omega_y \tag{119}$$

$$\boxed{\tau = \frac{1}{\mathrm{meas}(\Omega^e)} \int_{\Omega^e} \int_{\Omega^e} \mathrm{g}'_e(x, y) \, d\Omega_x \, d\Omega_y} \tag{120}$$

Remarks

1. The element **mean value** of the Green's function provides the simplest definition of τ.
2. This formula is adequate for low-order methods (h-adaptivity). For higher-order methods (p-adaptivity), accounting for variation of τ over an element may be required. In this case, it may be assumed, for example, that $\tau = \tau(x, y)$ is a polynomial of sufficiently high degree. Given an element Green's function g'_e, an equivalent function τ can, in principle, always be calculated. Consequently, there is a **generalized stabilized method**, that is, a method of the form,

$$a(\bar{w}^h, \bar{u}^h) - \sum_e \int_{\Omega^e} \int_{\Omega^e} \mathcal{L}^* \bar{w}^h(y) \tau(x, y)(\mathcal{L}\bar{u}^h - f)(x) \, d\Omega_x \, d\Omega_y = (\bar{w}^h, f) \tag{121}$$

   equivalent to the element Green's function method. The generalized stabilized method involves determining τ such that the following **equivalence condition** is satisfied

$$\int_{\Omega^e} \int_{\Omega^e} \mathcal{L}^* \bar{w}^h(y) \tau(x, y)(\mathcal{L}\bar{u}^h - f)(x) \, d\Omega_x \, d\Omega_y$$

$$= \int_{\Omega^e} \int_{\Omega^e} \mathcal{L}^* \bar{w}^h(y) \mathrm{g}'_e(x, y)(\mathcal{L}\bar{u}^h - f)(x) \, d\Omega_x \, d\Omega_y \qquad \forall \bar{w}^h, \bar{u}^h \in \bar{\mathcal{V}} \tag{122}$$

   Thus a full equivalence exists as indicated in Figure 22. Examples of the calculation of τ by way of this procedure will be presented subsequently.

Examples

   Two one-dimensional examples are considered, the advection-diffusion equation and the Helmholtz equation. In both cases it is assumed that standard piecewise linears are used for the coarse-scale basis. Consequently, determination of the element Green's function may be performed using the strong-form counterpart of (102), namely

$$\left. \begin{array}{rcll} \mathcal{L}^* \mathrm{g}'_e(x, y) & = & \delta(x - y) & \forall x \in \Omega^e \\ \mathrm{g}'_e(x, y) & = & 0 & \forall x \in \Gamma^e \end{array} \right\} \qquad e = 1, 2, \cdots, n_{\mathrm{el}} \tag{123}$$

Remark

In **one dimension**, use of the element Green's function g'_e results in $u = \bar{u} + u'$ being **pointwise exact** for any

$$\bar{u} = \sum_{A=1}^{\bar{n}_{\mathrm{nodes}}} \bar{N}_A \bar{u}_A \tag{124}$$

and $\bar{u}$ being an end-node **interpolant** of u. This result holds for **all** problems.

residual free bubbles $\Longleftrightarrow$ element Green's functions

stabilized methods
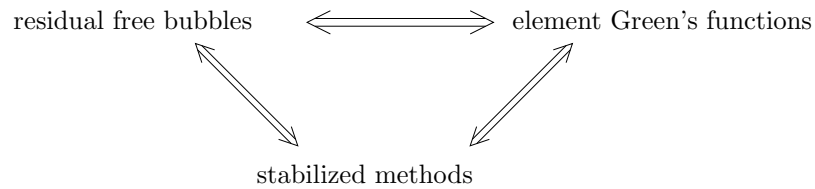
Figure 22. Stabilized methods can be constructed which are equivalent to methods based on element Green's functions, which in turn are equivalent to methods developed from the residual-free bubbles concept. Historically, stabilized methods preceded the residual-free bubbles and element Green's function approaches, and there are certain stabilized methods (e.g., SUPG and GLS) which have been established for some time that are not, strictly speaking, equivalent to these concepts. Nevertheless, they have been justified independently by mathematical analysis and numerical testing, and, in the case of SUPG, may be viewed as a simplified variational multiscale method.

(a) $\alpha = 0.1$ (b) $\alpha = 1$ (c) $\alpha = 2$

(d) $\alpha = 5$ (e) $\alpha = 10$ (f) $\alpha = 100$
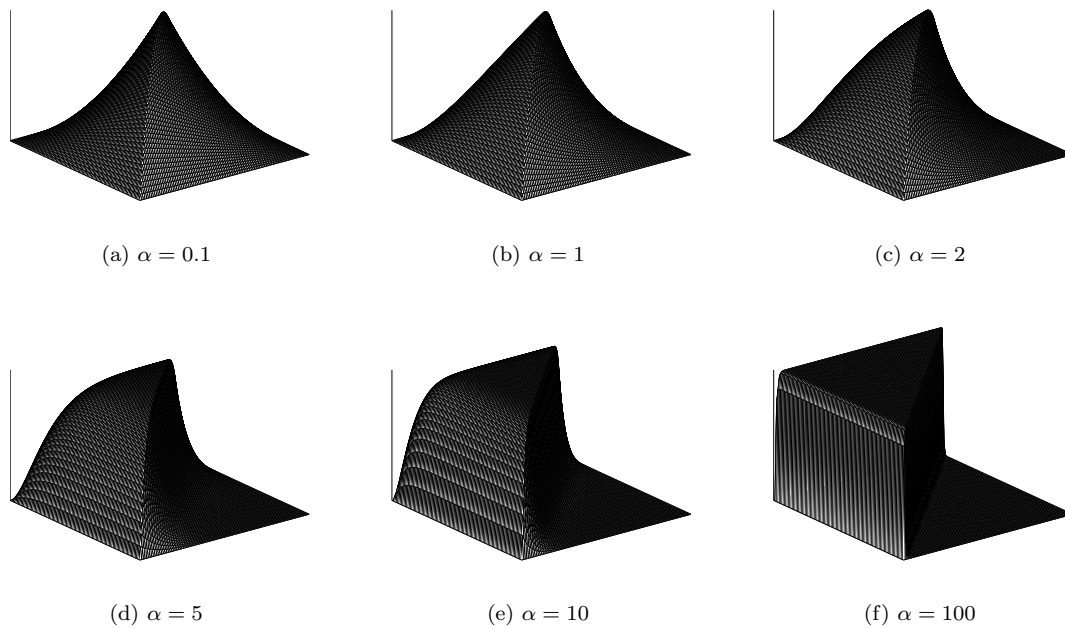
Figure 23. Element Green's function for the one-dimensional advection-diffusion equation as a function of element Péclet number (α).
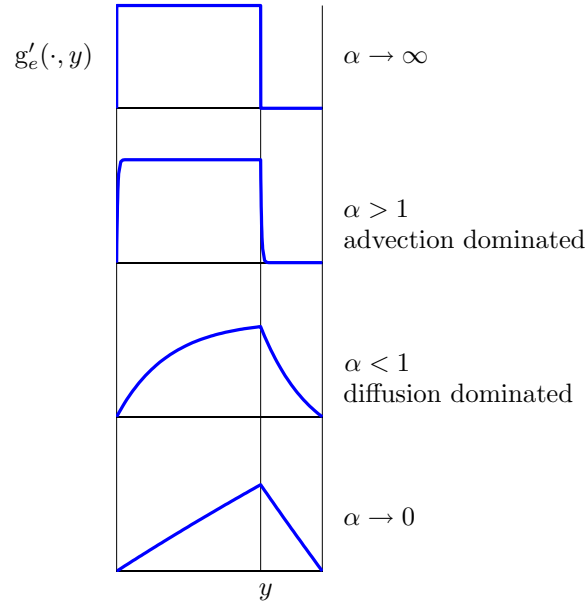
Figure 24. Schematic behavior of the element Green's function for the advection-diffusion operator, for y fixed.

Advection-diffusion equation   Let

$$\mathcal{L} = \mathcal{L}_{\text{adv}} + \mathcal{L}_{\text{diff}} \tag{125}$$

where

$$\mathcal{L}_{\text{adv}} = a\frac{d}{dx} \tag{126}$$

$$\mathcal{L}_{\text{diff}} = -\kappa\frac{d^2}{dx^2} \tag{127}$$

and a and κ are assumed to be positive constants. Consider the **homogeneous Dirichlet problem**

$$\mathcal{L}u = f \qquad \text{in } \Omega = [0, L] \tag{128}$$

$$u = 0 \qquad \text{on } \Gamma = \{0, L\} \tag{129}$$

Note that

$$\mathcal{L}^* = \mathcal{L}^*_{\text{adv}} + \mathcal{L}^*_{\text{diff}} \tag{130}$$

$$= -\mathcal{L}_{\text{adv}} + \mathcal{L}_{\text{diff}} \tag{131}$$

The solution of (123) is given by

$$g'_e(x, y) = \begin{cases} C_1(y)(1 - e^{-2\alpha\frac{x}{h}}) & x \leq y \\ C_2(y)(e^{-2\alpha\frac{x}{h}} - e^{-2\alpha}) & x \geq y \end{cases} \tag{132}$$

where

$$C_1(y) \quad = \quad \frac{1 - e^{-2\alpha\left(1 - \frac{y}{h}\right)}}{a\left(1 - e^{-2\alpha}\right)} \tag{133}$$

$$C_2(y) \quad = \quad \frac{e^{2\alpha\frac{y}{h}} - 1}{a\left(1 - e^{-2\alpha}\right)} \tag{134}$$

$$\alpha \quad = \quad \frac{ah}{2\kappa} \qquad \text{(element Péclet number)} \tag{135}$$

and $h = \text{meas}(\Omega^e)$ is the element length. This element Green's function is shown in Figure 23 for various element Péclet numbers. For fixed y it behaves as shown in Figure 24.

By virtue of the fact that the coarse scales are piecewise linear and $\mathcal{L}\bar{u}^h$ and $\mathcal{L}^*\bar{w}^h$ are therefore constants on each element, the simple formula (120) suffices to define a constant τ satisfying (122), that is, one equivalent to use of the element Green's function, viz.,

$$\begin{aligned}
\tau \quad &= \quad \frac{1}{\text{meas}(\Omega^e)} \int_{\Omega^e} \int_{\Omega^e} \text{g}'_e(x, y)\, d\Omega_x\, d\Omega_y \\
&= \quad \frac{h}{2a}\left(\coth\alpha - \frac{1}{\alpha}\right)
\end{aligned} \tag{136}$$

Remarks

1. This is a well known formula from the theory of stabilized methods. It was originally derived using Fourier methods on regular meshes and assuming constant coefficients.
2. This τ results in a ***nodally exact*** stabilized method for piecewise linear $\bar{N}_A$'s and element-wise constant a, κ and f. Remarkably, element lengths need ***not*** be uniform.
3. By virtue of (105) and (135), the same optimal τ is obtained from the residual-free bubble, namely,

$$\begin{aligned}
\tau \quad &= \quad \frac{1}{\text{meas}(\Omega^e)} \int_{\Omega^e} B_e(x)\, d\Omega \\
&= \quad \frac{h}{2a}(\coth\alpha - \frac{1}{\alpha})
\end{aligned} \tag{137}$$

4. If the fine-scales are modeled by a single quadratic polynomial bubble in each element, the approximate element Green's function is given by

$$\tilde{\text{g}}'_e(x, y) = \frac{N'(x)N'(y)}{a(N', N')} \tag{138}$$

Employing (120) results in

$$\tilde{\tau} = \frac{h^2}{12\kappa} = \frac{h}{2a}\frac{\alpha}{3} \tag{139}$$

Comparing (139) with (137) reveals that $\tilde{\tau}$ is much larger than τ in advection dominated cases. See Figure 25. This results in a method for the coarse scales which is overly diffusive.

Although the addition of the quadratic polynomial bubble produces an overly diffuse method, it is a curious fact that in conjunction with the addition of an appropriately
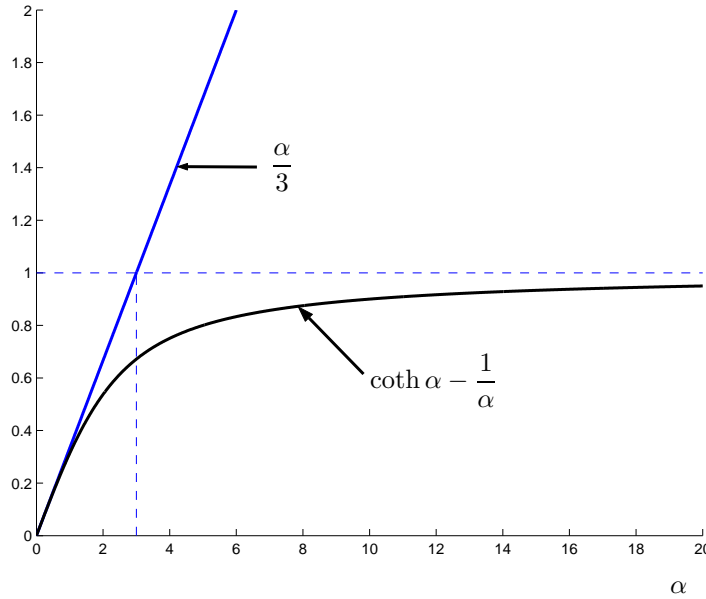
Figure 25. Behavior $\tilde{\tau}$ and τ as $\alpha \to \infty$.

defined artificial diffusivity in the fine-scale equation, the modified method is capable of generating the optimal value of τ given by (137). This may be seen as follows: in the fine-scale equation, (59), replace the term $a(w', u')$ by $a(w', u') + a'(w', u')$ where

$$a'(w', u') = (\nabla w', \kappa' \nabla u') \tag{140}$$

in which κ' is the ***fine-scale artificial diffusivity***. In the present, one-dimensional case, this term is simply $(\frac{dw'}{dx}, \kappa' \frac{du'}{dx})$ and reduces to element integrals of the derivatives of the quadratic polynomial bubbles. From the previous development it is clear that this will produce a τ of the same form as (139) but with κ replaced by $\kappa + \kappa'$, namely

$$\tau' = \frac{h^2}{12(\kappa + \kappa')} \tag{141}$$

Equating τ' with τ leads to the following definition for κ':

$$\kappa' = \kappa\left(\frac{\alpha}{3} - 1\right) = \frac{ah}{6} - \kappa \tag{142}$$

The "effective diffusivity" in the fine scales is

$$\kappa + \kappa' = \frac{ah}{6} = O(h) \tag{143}$$

This method is identical to the one produced by the exact element Green's function and thus is superconvergent with respect to the nodal values (i.e., it is exact at the nodes),

and attains optimal coarse-scale convergence rates in the L_2 and H^1 norms (i.e., $O(h^2)$ and $O(h)$, resp.). It is a somewhat remarkable fact that adding artificial diffusivity to the fine-scale equation actually *reduces* the diffusive effect in the coarse-scale equation. If an $O(h)$ effective diffusivity of the form (143) was added to *all* scales (i.e., to (56)), then the method would amount to the classical artificial diffusivity method which is overly diffusive and limited to $O(h)$ in L_2 and $O(h^{1/2})$ in H^1, *independent* of the polynomial order of the elements employed. It may be concluded that fine-scale artificial diffusivity is a viable modeling tool in multiscale analysis and one that is very different than, and superior to, classical artificial diffusivity in all scales. Of course, to obtain (142), the optimal value of τ, given by (137), needed to be known. (The idea of a fine-scale artificial diffusivity is due to Guermond (2001), and has been further analysed in Brezzi et al. (2000).)

5. The approximate fine-scale solution is given by

$$u'(y) \quad \approx \quad -\int_{\Omega'} \tilde{g}'(x,y)(\mathcal{L}\bar{u}^h - f)(x)\, d\Omega_x - \int_{\Gamma'} \tilde{g}'(x,y)[\![b\bar{u}^h]\!](x)\, d\Gamma_x \qquad (144)$$

where $\tilde{g}'$ is an approximation to the fine-scale Green's function, g'. For the multidimensional advection-dominated case, the jump term can be neglected and the approximation $\mathcal{L}\bar{u}^h \approx \boldsymbol{a} \cdot \nabla \bar{u}^h$ can be used. Furthermore, employing the approximation (116) results in

$$u' \approx -\tau(\boldsymbol{a} \cdot \nabla \bar{u}^h - f) \qquad (145)$$

Assuming τ has the form $h/(2|\boldsymbol{a}|)$ in the advection-dominated case, (145) becomes

$$u' \approx -\frac{h}{2|\boldsymbol{a}|}(\boldsymbol{a} \cdot \nabla \bar{u}^h - f) \qquad (146)$$

This may be used as a simple, local, error estimator for the advection-dominated case.

Helmholtz equation   The set-up is identical to the previous example. Consider the Dirichlet problem, (128)–(129), for the Helmholtz equation in which

$$\mathcal{L} \quad = \quad -\frac{d^2}{dx^2} - k^2 \qquad (147)$$

is the Helmholtz operator and k is the **wave number**. Assume $k \in \mathbb{R}$, corresponding to the case of **propagating waves**. Note $\mathcal{L}^* = \mathcal{L}$. The Green's function for an element of length h is given by

$$g'_e(\xi, \eta) \quad = \quad \begin{cases} \dfrac{\sin(kh(1+\xi)/2)\sin(kh(1-\eta)/2)}{k\sin(kh)}, & \xi < \eta \\ \dfrac{\sin(kh(1-\xi)/2)\sin(kh(1+\eta)/2)}{k\sin(kh)}, & \xi \geq \eta \end{cases} \qquad (148)$$

where ξ and η are normalized, bi-unit coordinates,

$$-1 \leq \xi, \eta \leq +1 \qquad (149)$$

The element Green's function is depicted in Figure 26 for various **element wave numbers**.
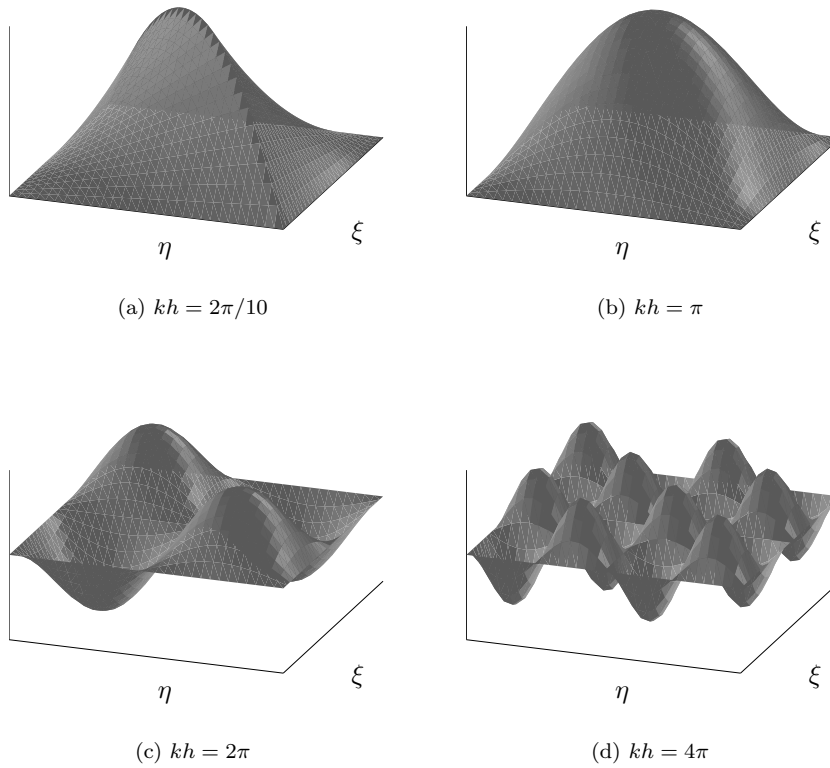
Figure 26. Element Green's function (kg'_e) for the one-dimensional Helmholtz equation as a function of wave number (kh).

This time $\mathcal{L}\bar{u}^h$ and $\mathcal{L}^*\bar{w}^h$ vary linearly over each element and satisfaction of the equivalence condition, (122), entails a non-constant τ, as follows:

$$\tau(\xi,\eta) = \tau_{00} + \tau_{11}\xi\eta \approx g'_e(\xi,\eta) \tag{150}$$

where

$$\tau_{ij} = \frac{\displaystyle\int_{-1}^{+1}\int_{-1}^{+1} \xi^i\eta^j g'_e(\xi,\eta)\,d\xi\,d\eta}{\displaystyle\int_{-1}^{+1}\int_{-1}^{+1} \xi^{2i}\eta^{2j}\,d\xi\,d\eta} \tag{151}$$

Remarks

1. Oberai and Pinsky (1998) have also derived an element Green's function in two dimensions for a bilinear rectangle and an equivalent τ. Similar results for three dimensions are also easily derived.

2. As in the previous example, this τ results in a **nodally exact** stabilized method for piecewise linear $\bar{N}_A$'s and element-wise constant k and f, for an arbitrary non-uniform mesh.

3.7. Summary

In this section, the variational multiscale formulation for an abstract Dirichlet problem was described. The case in which finite elements are used to represent the coarse scales was considered and an exact equation governing the coarse scales was derived. This equation amounts to the Galerkin formulation plus an additional term which depends on the distributional form of the residual (i.e., element interior and interface jump terms) and a fine-scale Green's function. A representation was also derived for the fine-scale solution, which amounts to the error in the coarse scales. The results serve as paradigms for subgrid-scale models and *a posteriori* error estimators.

To understand the nature of the fine-scale Green's function, hierarchical p-refinement and bubbles were considered. An explicit formula for the fine-scale Green's function was obtained in terms of the hierarchical (i.e., fine-scale) basis. This formula suggests that the fine-scale Green's function can be represented in terms of a basis of functions having local support. Subsequent discussion dealt with developing practical approximations.

The concepts of residual-free bubbles, element Green's functions, and stabilized methods were reviewed, and relationships among them were summarized.

4. Space-time Formulations

In Sections 2 and 3, a methodology was described to address problems in which scales are present that are viewed as numerically unresolvable, and accurate computation of the resolvable scales necessitates incorporating the effects of the unresolvable scales. The analysis of Section 3 was restricted to steady phenomena. In this section the study of the variational multiscale method is continued, generalizing the development of the subgrid-scale models to the time-dependent case. A first-order in time, second-order in space, non-symmetric, linear partial differential equation is considered. Creation of the subgrid-scale model of the initial/boundary-value problem requires solution of an element problem for the unresolved scales which is overspecified. This theoretical impediment is overcome by way of an elliptic regularization procedure, giving rise to an element Green's function problem. In the limiting case of the regularization parameter, the desired causal Green's function of the adjoint operator is derived. This enables the subgrid scales to be determined analytically and represented in terms of the residual of the resolved scales.

The variational setting for the developments is space-time. That is, a fully-discrete method is developed entirely from finite element concepts. It is believed this provides the most theoretically coherent framework for the derivations.

As in Section 3, the subgrid-scale model, when numerically approximated by Galerkin's method, provides, on the one hand, a paradigm for bubble function finite element methods, and, on the other hand, an exposé of the theoretical foundations of stabilized methods. Both bubbles and stabilized methods are thus identified as approximate subgrid-scale models. In
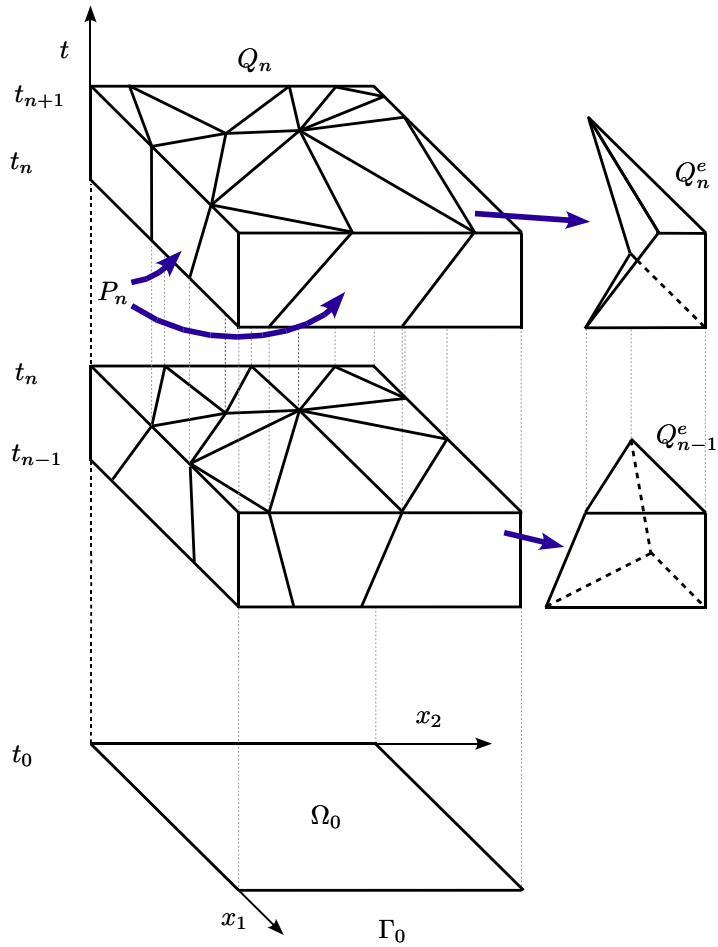
Figure 27. Finite element discretization in space-time.

the case of stabilized methods, this identification leads to formulas enabling the calculation of τ, the parameter present in stabilized methods.

To illustrate the use of the theory in calculating τ, the simple case of an ordinary differential equation in time is considered. The known optimal value is arrived at, complementing the analogous calculation for the advection-diffusion operator in space, presented in Section 3.

4.1. Finite elements in space-time

Consider a discretization of the space-time domain in question into **time slabs** which are in turn discretized into space-time elements. A schematic illustration is presented in Figure 27.

Slab Q_n is the space-time domain bounded by spatial hypersurfaces at times t_n and t_{n+1}. The lateral boundary of Q_n is denoted by P_n. A decomposition of this type is a suitable starting point for the variational formulation of **equations of evolution**. A discrete problem is solved on each slab sequentially, starting with the first. This gives rise to a fully-discrete time-stepping algorithm. For appropriately formulated finite element methods, the space-time approach is amenable to *a priori* and *a posteriori* error estimation, adaptive strategies, and relatively simple moving domain procedures (see, e.g., Aliabadi and Tezduyar (1993), Hughes, Franca and Hulbert (1989), Hughes and Hulbert (1988), Johnson (1986,1987,1992), Johnson and Hansbo (1992), Johnson, Nävert and Pitkäranta (1984), Mittal and Tezduyar (1994), Tezduyar, Behr and Liou (1992), Tezduyar et al. (1992)).

4.2. Subgrid-scale modeling

To simplify subsequent writing, let Q denote a generic space-time slab bounded at $t = 0$ by Ω_0 and at $t = T$ by Ω_T. Thus Q may represent any slab or the entire space-time domain. The following definitions are important for subsequent developments:

$$
\begin{align}
Q' &= \bigcup_{e=1}^{n_{\text{el}}} Q^e \qquad \text{(element interiors)} \tag{152}\\
P' &= \bigcup_{e=1}^{n_{\text{el}}} P^e \qquad \text{(element boundaries)} \tag{153}\\
Q &= \overline{Q} = \text{closure}(Q') \tag{154}\\
P &= \partial Q \setminus (\Omega_0 \cup \Omega_T) \tag{155}
\end{align}
$$

n_{el} is the number of elements in slab Q. Consider an **overlapping** sum decomposition in which $\bar{u}$ represents the **resolvable scales** and u' represents the **unresolvable**, or **subgrid**, **scales**.

4.3. Initial/boundary-value problem

Consider the following initial/boundary-value problem: Given $f : Q \to \mathbb{R}$, $g : P \to \mathbb{R}$, and $u(0^-) : \Omega_0 \to \mathbb{R}$, find $u : Q \to \mathbb{R}$, such that

$$
\begin{align}
\mathcal{L}u &= f \qquad \text{in } Q \tag{156}\\
u &= g \qquad \text{on } P \tag{157}\\
u(0^+) &= u(0^-) \qquad \text{on } \Omega_0 \tag{158}
\end{align}
$$

where, for definiteness, $\mathcal{L}$ is taken to be **time-dependent**, **advection-diffusion operator**, that is,

$$
\mathcal{L} = \frac{\partial}{\partial t} + \boldsymbol{a} \cdot \nabla - \kappa \Delta \tag{159}
$$

in which $\kappa > 0$ is a given constant and $\boldsymbol{a}$ is a given solenoidal vector field, viz.

$$
\nabla \cdot \boldsymbol{a} = 0 \tag{160}
$$

Remark

The results to follow are applicable to a wider class of problems than the one considered here. However, focusing on it simplifies the presentation.

4.4. Variational multiscale formulation

Let

$$a(w, u)_Q = -\left(\frac{\partial w}{\partial t} + \boldsymbol{a} \cdot \nabla w, u\right)_Q - (\nabla w, \kappa \nabla u)_Q \tag{161}$$

where $(u, v)_Q = \int_Q uv\, dQ$. Then

$$a(w, u)_Q = (w, \mathcal{L}u)_Q = (\mathcal{L}^*w, u)_Q \tag{162}$$

for all sufficiently smooth w, u such that

$$u = w = 0 \qquad \text{on } P' \tag{163}$$

where

$$\mathcal{L}^* = -\frac{\partial}{\partial t} - \boldsymbol{a} \cdot \nabla - \kappa \Delta \tag{164}$$

Let

$$u = \bar{u} + u' \tag{165}$$
$$w = \bar{w} + w' \tag{166}$$

where we assume

$$u' = w' = 0 \qquad \text{on } P' \tag{167}$$

The variational equation corresponding to the initial/boundary-value problem is

$$(w(T^-), u(T^-))_{\Omega_T} + a(w, u)_Q = (w, f)_Q + (w(0^+), u(0^-))_{\Omega_0} \tag{168}$$

In (168), $(\cdot, \cdot)_{\Omega_T}$ and $(\cdot, \cdot)_{\Omega_0}$ denote L_2 inner products on Ω_T and Ω_0, respectively. The Euler-Lagrange equations corresponding to (168) are (156) and (157). The Dirichlet boundary condition, (157), is assumed satisfied *ab initio* by the trial solution $\bar{u}$. Likewise, $\bar{w}$ is assumed to satisfy a homogeneous Dirichlet boundary condition. Substituting (165) and (166) into (168) leads to

$$(\bar{w}(T^-), \bar{u}(T^-))_{\Omega_T} + a(\bar{w} + w', \bar{u} + u')_Q = (\bar{w} + w', f)_Q + (\bar{w}(0^+), \bar{u}(0^-))_{\Omega_0} \tag{169}$$

Note that the integrals over Ω_T and Ω_0 are unaffected by u' and w' because of assumption (167). Assuming $\bar{w}$ and w' are linearly independent, gives rise to two subproblems:

$$(\bar{w}(T^-), \bar{u}(T^-))_{\Omega_T} + a(\bar{w}, \bar{u})_Q + a(\bar{w}, u')_Q = (\bar{w}, f)_Q + (\bar{w}(0^+), \bar{u}(0^-))_{\Omega_0} \tag{170}$$
$$(\bar{w}(T^-), \bar{u}(T^-))_{\Omega_T} + a(\bar{w}, \bar{u})_Q + (\mathcal{L}^*\bar{w}, u')_Q = (\bar{w}, f)_Q + (\bar{w}(0^+), \bar{u}(0^-))_{\Omega_0} \tag{171}$$
$$a(w', \bar{u})_Q + a(w', u')_Q = (w', f)_Q \tag{172}$$
$$(w', \mathcal{L}\bar{u})_Q + (w', \mathcal{L}u')_Q = (w', f)_Q \tag{173}$$

In deriving (171) and (173) we used (162).

Equation (173) is equivalent to the following system of element-wise problems for u':

$$\left.\begin{array}{rcll} \mathcal{L}u' & = & -(\mathcal{L}\bar{u} - f) & \text{in } Q^e \\ u' & = & 0 & \text{on } P^e \end{array}\right\} e = 1, 2, \ldots, n_{\text{el}} \tag{174}$$

Unfortunately, these problems are ***ill-posed*** in the sense that they are overspecified. The space-time Dirchlet condition $u' = 0$ on P^e cannot be satisfied due to the causal evolutionary structure of $\mathcal{L}$. To circumvent this difficulty, consider an ***elliptic regularization*** of (174):

$$\left. \begin{array}{rcll} \mathcal{L}_\varepsilon u'_\varepsilon & = & -(\mathcal{L}\bar{u} - f) & \text{in } Q^e \\ u'_\varepsilon & = & 0 & \text{on } P^e \end{array} \right\} e = 1, 2, \ldots, n_{\text{el}} \tag{175}$$

where

$$\mathcal{L}_\varepsilon = \frac{\partial}{\partial t} + \boldsymbol{a} \cdot \nabla - \kappa \Delta - \varepsilon \frac{\partial^2}{\partial t^2} \tag{176}$$

These problems are ***well-posed*** for all $\varepsilon > 0$.

The solution of (175) can be obtained with the aid of the ***corresponding Green's function problems***

$$\left. \begin{array}{rcll} \mathcal{L}_\varepsilon^* \mathrm{g}'_\varepsilon & = & \delta & \text{in } Q^e \\ \mathrm{g}'_\varepsilon & = & 0 & \text{on } P^e \end{array} \right\} e = 1, 2, \ldots, n_{\text{el}} \tag{177}$$

Thus

$$u'_\varepsilon(r_0) = -\int_{Q'} \mathrm{g}'_\varepsilon(r, r_0)(\mathcal{L}\bar{u} - f)(r) dQ_r \tag{178}$$

$$u'_\varepsilon = M'_\varepsilon(\mathcal{L}\bar{u} - f) \tag{179}$$

where

$$r = \{\boldsymbol{x}, t\} \in Q, \qquad r_0 = \{\boldsymbol{x}_0, t_0\} \in Q \tag{180}$$

Remarks

1. $\mathcal{L}\bar{u} - f$ is the ***residual*** of the resolved scales.
2. The subgrid scales are ***driven*** by the residual of the resolved scales.

The desired variational equation is obtained by taking the limit $\varepsilon \to 0$. Let

$$\mathrm{g}' = \lim_{\varepsilon \to 0} \mathrm{g}'_\varepsilon \tag{181}$$

$$M' = \lim_{\varepsilon \to 0} M'_\varepsilon \tag{182}$$

Note that g' is the ***causal Green's function*** (see, e.g., Stakgold (1979)) for the adjoint operator $\mathcal{L}^*$.

Substituting u'_ε into (171) for u' and taking the limit $\varepsilon \to 0$ yields

$$\boxed{(\bar{w}(T^-), \bar{u}(T^-))_{\Omega_T} + a(\bar{w}, \bar{u})_Q + (\mathcal{L}^*\bar{w}, M'(\mathcal{L}\bar{u} - f))_{Q'} = (\bar{w}, f)_Q + (\bar{w}(0^+), \bar{u}(0^-))_{\Omega_0}}$$

$$\tag{183}$$

where

$$(\mathcal{L}^*\bar{w}, M'(\mathcal{L}\bar{u} - f))_{Q'} = -\int_{Q'}\int_{Q'} \mathcal{L}^*\bar{w}(r_0)\mathrm{g}'(r, r_0)(\mathcal{L}\bar{u} - f)(r) dQ_r dQ_{r_0} \tag{184}$$

and

$$\int_{Q'} = \sum_{e=1}^{n_{\text{el}}} \int_{Q^e} \tag{185}$$

Remarks

1. Note that this integration is over **element interiors** Q'
2. The effect of the unresolved scales on the resolved scales is exactly accounted for, up to the assumption $u' = 0$ on P'.
3. The **nonlocal** effect of the unresolved scales on the resolved scales is confined within individual elements.

The variational equation (183) can be written succinctly as

$$B(\bar{w}, \bar{u}; \mathrm{g}') = L(\bar{w}; \mathrm{g}') \tag{186}$$

where:

$$B(\bar{w}, \bar{u}; \mathrm{g}) = (\bar{w}(T^-), \bar{u}(T^-))_{\Omega_T} + a(\bar{w}, \bar{u})_Q + (\mathcal{L}^*\bar{w}, M(\mathcal{L}\bar{u}))_{Q'} \tag{187}$$

$$L(\bar{w}; \mathrm{g}) = (\bar{w}, f)_Q + (\bar{w}(0^+), \bar{u}(0^-))_{\Omega_0} + (\mathcal{L}^*\bar{w}, Mf)_{Q'} \tag{188}$$

The numerical version of (186) can be developed by selecting finite element approximations of the trial solution and weighting functions, $\bar{u}^h \approx \bar{u}$ and $\bar{w}^h \approx \bar{w}$, respectively, and approximating the element Green's function, $\tilde{\mathrm{g}}' \approx \mathrm{g}'$, viz.

$$B(\bar{w}^h, \bar{u}^h; \tilde{\mathrm{g}}') = L(\bar{w}^h; \tilde{\mathrm{g}}') \tag{189}$$

This amounts to applying **Galerkin's method** to the subgrid-scale model obtained from the variational multiscale procedure.

4.5. Bubbles in space-time

Now consider typical finite element shape function expansions plus bubbles (see, e.g. Baiocchi, Brezzi and Franca (1993), Brezzi et al. (1992), Franca and Farhat (1994a,1994b,1995), Franca and Frey (1992)). The set-up is as follows:

$$\bar{u}^h = \sum_{A=1}^{n_{\mathrm{nodes}}} N_A \bar{u}_A \qquad (\text{likewise } \bar{w}^h) \tag{190}$$

$$N_A = \text{standard finite element shape functions} \tag{191}$$

$$\bar{u}_A = \text{nodal values} \tag{192}$$

$$u' = \sum_{A=1}^{n_{\mathrm{bubbles}}} N'_A u'_A \qquad (\text{likewise } w') \tag{193}$$

$$N'_A = \text{bubble functions} \tag{194}$$

$$u'_A = \text{generalized coordinates} \tag{195}$$

The situation for linear finite element shape functions plus typical bubbles is illustrated in Figure 21.

Substituting these functions into (171) and (173), and eliminating u'_A by **static condensation** yields:

$$B(\bar{w}^h, \bar{u}^h; \tilde{g}') = L(\bar{w}^h; \tilde{g}') \qquad (196)$$

where

$$B(\bar{w}^h, \bar{u}^h; \tilde{g}') = (\bar{w}^h(T^-), \bar{u}^h(T^-))_{\Omega_T} + a(\bar{w}^h, \bar{u}^h)_Q + (\mathcal{L}^* \bar{w}^h, \tilde{M}'(\mathcal{L}\bar{u}^h))_{Q'} \qquad (197)$$

$$L(\bar{w}^h; \tilde{g}') = (\bar{w}^h, f)_Q + (\bar{w}(0^+), \bar{u}(0^-))_{\Omega_0} + (\mathcal{L}^* \bar{w}^h, \tilde{M}' f)_{Q'} \qquad (198)$$

and

$$(\mathcal{L}^* \bar{w}^h, \tilde{M}'(\mathcal{L}\bar{u}^h - f))_{Q'} = -\int_{Q'}\int_{Q'}(\mathcal{L}^* \bar{w}^h)(r_0)\tilde{g}'(r, r_0)(\mathcal{L}\bar{u}^h)(r)dQ_r dQ_{r_0} \qquad (199)$$

$$\tilde{g}'(r, r_0) = \sum_{A,B=1}^{n_{\text{bubbles}}} N'_A(r)[a(N'_B, N'_A)]^{-1} N'_B(r_0) \qquad (200)$$

This is an approximate subgrid scale model. Bubbles, according to (200), generate an **approximate** element Green's function, $\tilde{g}' \approx g'$. In practice, the quality of the approximation may be **poor**, because standard polynomial bubbles do not adequately represent the fine-scale structures which characterize u'.

4.6. Stabilized methods

Stabilized methods in the present case are generalized Galerkin methods of the form

$$(\bar{w}^h(T^-), \bar{u}^h(T^-))_{\Omega_T} + a(\bar{w}^h, \bar{u}^h)_Q + (\mathbf{L}\bar{w}^h, \tau(\mathcal{L}\bar{u}^h - f))_{Q'} = (\bar{w}^h, f)_Q + (\bar{w}(0^+), \bar{u}(0^-))_{\Omega_0} \quad (201)$$

where, typically, $\mathbf{L}$ is a **differential operator** and τ is an **algebraic operator**. Examples of $\mathbf{L}$ are

$$\begin{array}{lll} \mathbf{L} = +\mathcal{L} & \text{Galerkin/least-squares (GLS)} \\ \mathbf{L} = +\mathcal{L}_{\text{adv}} = \frac{\partial}{\partial t} + \boldsymbol{a} \cdot \nabla & \text{SUPG} \\ \mathbf{L} = -\mathcal{L}^* & \text{Multiscale} \end{array} \qquad (202)$$

By comparing (200) with (189), a stabilized method of multiscale type is seen to be an approximate subgrid scale model in which the algebraic operator τ approximates the exact **integral operator** M, i.e.,

$$\tau = -\tilde{M}' \approx -M' \qquad (203)$$

Equivalently,

$$\tau \cdot \delta(r_0 - r) = \tilde{g}'(r, r_0) \approx g'(r, r_0) \qquad (204)$$

This assertion is established by the following calculation:

$$\int_{Q'} \int_{Q'} (-\mathcal{L}^* \bar{w}^h)(r_0) \tilde{g}'(r, r_0)(\mathcal{L}\bar{u}^h - f)(r) dQ_r dQ_{r_0}$$

$$= \int_{Q'} \int_{Q'} (-\mathcal{L}^* \bar{w}^h)(r_0) \tau \delta(r_0 - r)(\mathcal{L}\bar{u}^h - f)(r) dQ_r dQ_{r_0}$$

$$= \int_{Q'} (-\mathcal{L}^* \bar{w}^h)(r) \tau (\mathcal{L}\bar{u}^h - f)(r) dQ_r \tag{205}$$

4.6.1. Formulas for τ Formulas for τ may be derived from (204). For example, assume it is sufficient to approximate τ as a constant over each element. Then

$$\int_{Q^e} \int_{Q^e} \tau \delta(r_0 - r) dQ_r dQ_{r_0} = \int_{Q^e} \int_{Q^e} \tilde{g}'(r, r_0) dQ_r dQ_{r_0}$$

$$\approx \int_{Q^e} \int_{Q^e} g'(r, r_0) dQ_r dQ_{r_0} \tag{206}$$

$$\boxed{\tau = \frac{1}{\text{meas}(Q^e)} \int_{Q^e} \int_{Q^e} g'(r, r_0) dQ_r dQ_{r_0}} \tag{207}$$

4.6.2. Example: First-order ordinary differential equation in time To demonstrate the use of formula (207), consider the simple example of a first-order ordinary differential equation in time. (In Section 3 the exact value of τ for the steady advection-diffusion operator in space was determined.) Let

$$\mathcal{L} = \frac{d}{dt} \tag{208}$$

$$\mathcal{L}_\varepsilon = \mathcal{L} - \varepsilon \frac{d^2}{dt^2} \tag{209}$$

The initial-value problem is: Given $f : Q \to \mathbb{R}$, $u(0^-) \in \mathbb{R}$, find $u : Q \to \mathbb{R}$ such that

$$\mathcal{L}u = f \qquad \text{in } Q = [0, T] \tag{210}$$

$$u(0^+) = u(0^-) \tag{211}$$

The element Green's function problems for the regularized equation are

$$\left. \begin{array}{rcll} \mathcal{L}_\varepsilon^* g'_\varepsilon & = & \delta & \text{in } Q^e \\ g'_\varepsilon & = & 0 & \text{on } \partial Q^e \end{array} \right\} \quad e = 1, 2, \ldots, n_{\text{el}} \tag{212}$$

where

$$\mathcal{L}_\varepsilon^* = \left(\frac{d}{dt} - \varepsilon \frac{d^2}{dt^2} \right)^* = -\frac{d}{dt} - \varepsilon \frac{d^2}{dt^2} \tag{213}$$

The element Green's function is sketched in Figure 28 as a function of $\alpha = \Delta t/(2\varepsilon)$, where $\Delta t = \text{meas}(Q^e) = $ element "length". Note that the limit $\alpha \to \infty$ (equivalently $\varepsilon \to 0$), gives rise to the causal Green's function for $\mathcal{L}^*$.
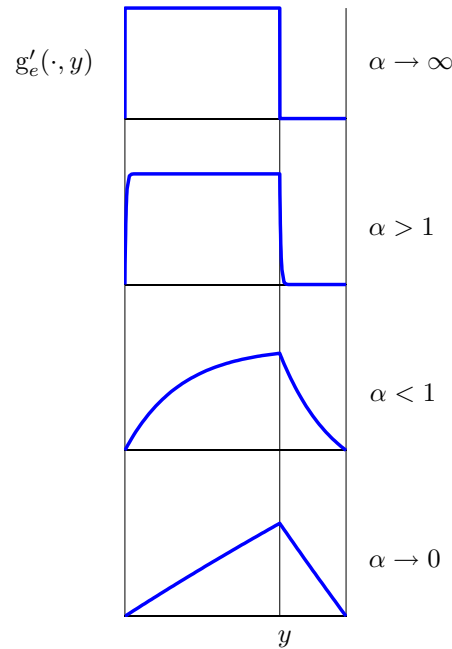
Figure 28. Green's function for $\mathcal{L}_\varepsilon^*$. The limit $\alpha \to \infty$ is the causal Green's function for $\mathcal{L}^*$.

Let

$$\tau_\alpha = \frac{1}{\text{meas}(Q^e)} \int_{Q^e} \int_{Q^e} g(t, t_0) dQ_t dQ_{t_0} = \frac{\Delta t}{2} \left(\coth \alpha - \frac{1}{\alpha} \right) \tag{214}$$

Then

$$\tau = \lim_{\alpha \to \infty} \tau_\alpha = \frac{\Delta t}{2} \tag{215}$$

Remark

This expression for τ is known to be the correct one for the case at hand from the mathematical theory of stabilized methods. It is clear that this value of τ is as good as using the exact Green's function representation as long as the trial functions are piecewise constant with respect to time on element subdomains.

4.7. Summary

The development of a class of subgrid scale models for time-dependent problems was presented. The corresponding steady case was described previously in Section 3. It was shown that bubble functions give rise to approximate element Green's functions in the subgrid-scale models, albeit typically not good approximations. Likewise, stabilized methods were identified as approximate subgrid-scale models. Formulas for τ emerged from this identification and this opens the way to improved representations of τ in stabilized methods for equations of evolution. Stabilized

methods have been shown to be "good" numerical methods for problems in which the classical Galerkin finite element method fails (see, e.g. Barbosa and Hughes (1992), Codina (1998,2000), Franca and Do Carmo (1989), Franca and Farhat (1995), Franca and Frey (1992), Franca, Frey and Hughes (1992), Franca and Hughes (1988), Franca and Hughes (1993), Franca et al. (1988), Franca, Hughes and Stenberg (1993), Franca and Valentin (2000), Hughes and Brezzi (1989), Hughes and Franca (1987), Hughes, Franca and Balestra (1986), Hughes, Franca and Hulbert (1989), Hughes, Hauke and Jansen (1994) in which error estimates, stability results, and verification problems are presented). The results described in this and the previous section provide an alternative perspective of stabilized methods.

Starting with partial differential equation plus boundary and initial conditions, application of the variational multiscale method, then the Galerkin's method, results in a numerical method that has the form of a stabilized method. In addition, it provides detailed expressions that enable one to derive more accurate stabilized methods.

5. Stabilized Methods for Advective-Diffusive Equations

Stabilized methods for steady and unsteady advective-diffusive systems are described. Fairly general boundary conditions, leading to well-posed variational problems, are considered. The boundary-value problems are specialized to the hyperbolic case for completeness. Galerkin, SUPG, Galerkin/least-squares, and multiscale stabilized finite element methods are contrasted. An *a priori* error analysis of Galerkin least-squares is presented. The developments for the steady case are generalized to the unsteady case by way of space-time formulations employing the discontinuous Galerkin method with respect to time. Symmetric advective-diffusive systems are also considered. The set-up so closely follows the scalar case that completely analogous results are obtained. In order to fully comprehend these developments, the reader is urged to first carefully study the scalar case, as the system case is presented in virtually equation-for-equation form with little amplification.

5.1. Scalar steady advection-diffusion equation

5.1.1. Preliminaries   Let Ω be an open, bounded region in $\mathbb{R}^d$, where d is the number of space dimensions. The boundary of Ω is denoted by Γ and is assumed smooth. The unit outward normal vector to Γ is denoted by $\boldsymbol{n} = (n_1, n_2, \ldots, n_d)$. Let $\boldsymbol{a}$ denote the given flow velocity, assumed solenoidal, that is, $\nabla \cdot \boldsymbol{a} = 0$. The following notations prove useful:

$$
\begin{align}
a_n &= \boldsymbol{n} \cdot \boldsymbol{a} \tag{216} \\
a_n^+ &= (a_n + |a_n|)/2 \tag{217} \\
a_n^- &= (a_n - |a_n|)/2 \tag{218}
\end{align}
$$

Let $\{\Gamma^-, \Gamma^+\}$ and $\{\Gamma_g, \Gamma_h\}$ be partitions of Γ, where

$$
\begin{align}
\Gamma^- &= \{\boldsymbol{x} \in \Gamma \mid a_n(\boldsymbol{x}) < 0\} \qquad \text{(inflow boundary)} \tag{219} \\
\Gamma^+ &= \Gamma - \Gamma^- \qquad \text{(outflow boundary)} \tag{220}
\end{align}
$$

The following subsets are also needed (see Figure 29):
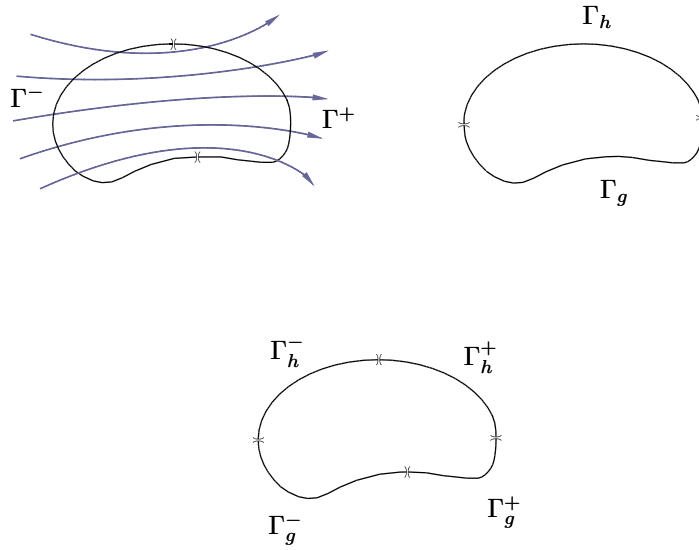
Figure 29. Illustration of boundary partitions.

$$\Gamma_g^\pm = \Gamma_g \bigcap \Gamma^\pm \tag{221}$$

$$\Gamma_h^\pm = \Gamma_h \bigcap \Gamma^\pm \tag{222}$$

Let $\kappa = \text{const.} > 0$ denote the diffusivity. Various fluxes are employed in the sequel:

$$\boldsymbol{\sigma^a}(u) = -\boldsymbol{a}u \qquad \text{(advective flux)} \tag{223}$$

$$\boldsymbol{\sigma^d}(u) = \kappa\nabla u \qquad \text{(diffusive flux)} \tag{224}$$

$$\boldsymbol{\sigma} = \boldsymbol{\sigma^a} + \boldsymbol{\sigma^d} \qquad \text{(total flux)} \tag{225}$$

$$\sigma_n^a = \boldsymbol{n}\cdot\boldsymbol{\sigma^a} \tag{226}$$

$$\sigma_n^d = \boldsymbol{n}\cdot\boldsymbol{\sigma^d} \tag{227}$$

$$\sigma_n = \boldsymbol{n}\cdot\boldsymbol{\sigma} \tag{228}$$

Let D denote a domain (e.g., Ω, Γ, etc.). The $L_2(D)$ inner product and norm are denoted by $(\cdot,\cdot)_D$ and $\|\cdot\|_D$, respectively.

5.1.2. Problem statement   The problem consists of finding $u = u(\boldsymbol{x})\ \forall\boldsymbol{x}\in\overline{\Omega}$, such that

$$\mathcal{L}u \equiv -\nabla\cdot\boldsymbol{\sigma}(u) = f \qquad \text{in } \Omega \tag{229}$$

$$u = g \qquad \text{on } \Gamma_g \tag{230}$$

$$-a_n^- u + \sigma_n^d(u) = h \qquad \text{on } \Gamma_h \tag{231}$$

where $f : \Omega \to \mathbb{R}$, $g : \Gamma_g \to \mathbb{R}$, and $h : \Gamma_h \to \mathbb{R}$ are prescribed data. (229) is an elliptic equation. The boundary condition (231) can be better understood by letting

$$h = \begin{cases} h^- & \text{on } \Gamma_h^- \\ h^+ & \text{on } \Gamma_h^+ \end{cases} \tag{232}$$

Thus, (231) may be written in the equivalent form:

$$\begin{aligned} \sigma_n(u) &= h^- & \text{on } \Gamma_h^- & \qquad \text{(total flux b.c.)} & (233) \\ \sigma_n^d(u) &= h^+ & \text{on } \Gamma_h^+ & \qquad \text{(diffusive flux b.c.)} & (234) \end{aligned}$$

5.1.3. Variational formulation   The variational form of the boundary-value problem is stated in terms of the following function spaces:

$$\begin{aligned} \mathcal{S} &= \{u \in H^1(\Omega) \mid u = g \text{ on } \Gamma_g\} & (235) \\ \mathcal{V} &= \{w \in H^1(\Omega) \mid w = 0 \text{ on } \Gamma_g\} & (236) \end{aligned}$$

The objective is to find $u \in \mathcal{S}$ such that $\forall w \in \mathcal{V}$

$$B(w, u) = L(w) \tag{237}$$

where

$$\begin{aligned} B(w, u) &\equiv (\nabla w, \boldsymbol{\sigma}(u))_\Omega + (w, a_n^+ u)_{\Gamma_h} & (238) \\ L(w) &\equiv (w, f)_\Omega + (w, h)_{\Gamma_h} & (239) \end{aligned}$$

The **formal consistency** of (237) with the strong form of the boundary-value problem, that is, (229)–(231), may be verified as follows:

$$\begin{aligned} 0 &= B(w, u) - L(w) \\ &= -(w, \nabla \cdot \boldsymbol{\sigma}(u))_\Omega + (w, \sigma_n(u))_{\Gamma_h} + (w, a_n^+ u)_{\Gamma_h} - (w, f)_\Omega - (w, h)_{\Gamma_h} \\ &= -(w, \nabla \cdot \boldsymbol{\sigma}(u) + f)_\Omega + (w, -a_n^- u + \sigma_n^d(u) - h)_{\Gamma_h} \end{aligned} \tag{240}$$

Stability, or **coercivity**, is established as follows

$$\begin{aligned} B(w, w) &= (\nabla w, -\boldsymbol{a} w + \kappa \nabla w)_\Omega + (w, a_n^+ w)_{\Gamma_h} \\ &= -\frac{1}{2}(w, a_n w)_{\Gamma_h} + \kappa \|\nabla w\|_\Omega^2 + (w, a_n^+ w)_{\Gamma_h} \\ &= \kappa \|\nabla w\|_\Omega^2 + \frac{1}{2} \left\| |a_n|^{\frac{1}{2}} w \right\|_{\Gamma_h}^2, \qquad \forall w \in \mathcal{V} \end{aligned} \tag{241}$$

For future reference, define:

$$|||w|||^2 = B(w, w) \tag{242}$$

Finally, the **global conservation of flux** is investigated. Consider the case in which $\Gamma_g = \emptyset$. Set $w \equiv 1$ in (237):

$$\begin{aligned} 0 &= B(1, u) - L(1) \\ &= \int_{\Gamma^+} a_n^+ u \, d\Gamma - \int_\Omega f \, d\Omega - \int_\Gamma h \, d\Gamma, \end{aligned} \tag{243}$$

which may be written equivalently as

$$0 \;=\; \int_{\Gamma^-} h^- \, d\Gamma + \int_\Omega f \, d\Omega + \int_{\Gamma^+} \left(-a_n u + h^+ \right) d\Gamma, \tag{244}$$

This confirms the conservation property for the case assumed. If $\Gamma_g \neq \emptyset$, "consistent" fluxes on Γ_g may be defined via a mixed variational formulation which automatically attains global conservation. See Hughes (1987) p. 107, Hughes et al. (2000) and Hughes et al. (1987) for background.

5.1.4. Hyperbolic case In the absence of diffusion, a boundary condition on the outflow boundary cannot be specified. The equations of the boundary-value problem are

$$\mathcal{L}u \;\equiv\; -\nabla \cdot \boldsymbol{\sigma}^a(u) = f \qquad \text{in } \Omega \tag{245}$$

$$u \;=\; g \qquad\qquad\qquad \text{on } \Gamma_g^- \tag{246}$$

$$\sigma_n^a(u) \;=\; h^- \qquad\qquad\quad \text{on } \Gamma_h^- \tag{247}$$

The variational operators are defined as

$$B(w,u) \;\equiv\; (\nabla w, \boldsymbol{\sigma}^a(u))_\Omega + (w, a_n^+ u)_\Gamma \tag{248}$$

$$L(w) \;\equiv\; (w, f)_\Omega + (w, h^-)_{\Gamma_h^-} \tag{249}$$

Consistency, stability and conservation are established as follows:

Consistency

$$\begin{aligned}
0 \;&=\; B(w,u) - L(w) \\
&=\; -(w, \nabla \cdot \boldsymbol{\sigma}^a(u))_\Omega + (w, -a_n u)_\Gamma + (w, a_n^+ u)_\Gamma - (w, f)_\Omega - (w, h^-)_{\Gamma_h^-} \\
&=\; -(w, \nabla \cdot \boldsymbol{\sigma}^a(u) + f)_\Omega + (w, -a_n^- u - h^-)_{\Gamma_h^-}
\end{aligned} \tag{250}$$

Stability

$$\begin{aligned}
B(w,w) \;&=\; (\nabla w, -\boldsymbol{a}w)_\Omega + (w, a_n^+ w)_\Gamma \\
&=\; -\frac{1}{2}(w, a_n w)_\Gamma + (w, a_n^+ w)_\Gamma \\
&=\; \frac{1}{2} \left\| \, |a_n|^{\frac{1}{2}} w \right\|_\Gamma^2, \qquad \forall w \in \mathcal{V}
\end{aligned} \tag{251}$$

Conservation $(\Gamma_g^- = \emptyset)$

$$\begin{aligned}
0 \;&=\; B(1,u) - L(1) \\
&=\; \int_\Gamma a_n^+ \, d\Gamma - \int_\Omega f \, d\Omega - \int_{\Gamma_h^-} h \, d\Gamma
\end{aligned} \tag{252}$$

Equivalently,

$$0 = \int_\Gamma h^- \, d\Gamma + \int_\Omega f \, d\Omega + \int_{\Gamma^+} -a_n u \, d\Gamma \tag{253}$$

5.1.5. Finite element formulations Consider a partition of Ω into finite elements. Let Ω^e be the interior of the eth element, let Γ^e be its boundary, and

$$\Omega' = \bigcup_e \Omega^e \qquad \text{(element interiors)} \qquad (254)$$

$$\Gamma' = \bigcup_e \Gamma^e \setminus \Gamma \qquad \text{(element interfaces)} \qquad (255)$$

Let $\mathcal{S}^h \subset \mathcal{S}$, $\mathcal{V}^h \subset \mathcal{V}$ be finite element spaces consisting of **continuous** piecewise polynomials of order k. As a point of departure, consider the classical **Galerkin method**:

Find $u^h \in \mathcal{S}^h$ such that $\forall w^h \in \mathcal{V}^h$

$$B(w^h, u^h) = L(w_h) \qquad (256)$$

Remark

The element Peclet number is defined by $\alpha = h|\boldsymbol{a}|/(2\kappa)$. The entire range of α, that is, $0 < \alpha < \infty$, is important. The advection dominated case (i.e., α large) is viewed as "hard". The Galerkin method possesses poor stability properties for this case. Spurious oscillations are generated by unresolved internal and boundary layers. The reason $B(w, u)$ is not capable of suppressing the spurious oscillations can also be easily inferred from its stability bound (251). This bound indicates that the bilinear form of the Galerkin method does not exercise any control over the first derivatives of the solution. As a result, the norm of the gradient of the solution can grow.

Methods with improved stability properties are given below:

SUPG

$$B_{SUPG}(w^h, u^h) = L_{SUPG}(w^h) \qquad (257)$$
$$B_{SUPG}(w^h, u^h) \equiv B(w^h, u^h) + (\tau \boldsymbol{a} \cdot \nabla w^h, \mathcal{L}u^h)_{\Omega'} \qquad (258)$$
$$L_{SUPG}(w^h) \equiv L(w^h) + (\tau \boldsymbol{a} \cdot \nabla w^h, f)_{\Omega'} \qquad (259)$$

Galerkin/least-squares

$$B_{GLS}(w^h, u^h) = L_{GLS}(w^h) \qquad (260)$$
$$B_{GLS}(w^h, u^h) \equiv B(w^h, u^h) + (\tau \mathcal{L}w^h, \mathcal{L}u^h)_{\Omega'} \qquad (261)$$
$$L_{GLS}(w^h) \equiv L(w^h) + (\tau \mathcal{L}w^h, f)_{\Omega'} \qquad (262)$$

Multiscale

$$B_{MS}(w^h, u^h) = L_{MS}(w^h) \qquad (263)$$
$$B_{MS}(w^h, u^h) \equiv B(w^h, u^h) - (\tau \mathcal{L}^* w^h, \mathcal{L}u^h)_{\Omega'} \qquad (264)$$
$$L_{MS}(w^h) \equiv L(w^h) - (\tau \mathcal{L}^* w^h, f)_{\Omega'} \qquad (265)$$
$$\mathcal{L}^*(w^h) \equiv -\boldsymbol{a} \cdot \nabla w^h - \kappa \Delta w^h \qquad (\Delta \text{ is the Laplace operator}) \qquad (266)$$

Remarks

1. In the hyperbolic case, or for piecewise linear elements in the general case, SUPG, Galerkin/least-squares, and multiscale become identical.
2. SUPG, Galerkin/least-squares, and multiscale stabilized methods are **residual methods**. That is, (257), (260), and (263) are satisfied if u^h is replaced by u, the exact solution of the boundary-value problem.
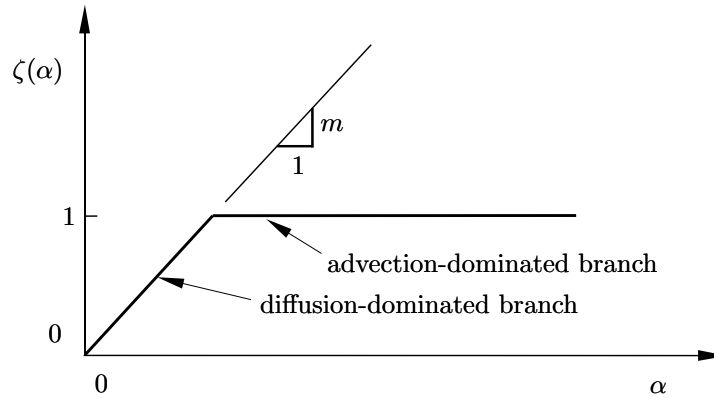
Figure 30. Definition of $\zeta(\alpha)$.

5.1.6. Error analysis The SUPG method was originally analyzed in Johnson, Nävert and Pitkäranta (1984) and Nävert (1982). In this section an *a priori* error analysis of Galerkin/least-squares is performed. The multiscale method may be analyzed using similar techniques.

Let $e = u^h - u$ denote the error in the finite element solution. By Remark 2, above,

$$B_{GLS}(w^h, e) \;=\; 0, \quad \forall w^h \in \mathcal{V}^h \tag{267}$$

This is referred to as the ***consistency condition*** for Galerkin/least-squares.

Let

$$\left|\left|\left|w^h\right|\right|\right|^2_{GLS} = \left|\left|\left|w^h\right|\right|\right|^2 + \left\|\tau^{\frac{1}{2}} \mathcal{L} w^h\right\|^2_{\tilde{\omega}} \tag{268}$$

By (261) and (268),

$$B_{GLS}(w^h, w^h) = \left|\left|\left|w^h\right|\right|\right|^2_{GLS}, \qquad \forall w^h \in \mathcal{V}^h \tag{269}$$

This is the ***stability condition*** for Galerkin/least-squares.

Remarks

1. Stability is less straightforward for SUPG and multiscale. One needs to invoke an "inverse estimate" and specific properties of τ. These assumptions are seen to be unnecessary for establishing the stability of Galerkin/least-squares. However, they resurface in the convergence analysis.

2. A term of the form $\|w^h\|_\Omega^2$ can be added to (268) by employing a change of variables. See Johnson, Nävert and Pitkäranta (1984) and Nävert (1982) for further discussion.

3. For the related residual-free bubble approach (that coincides with SUPG, with a specific choice of τ for linear elements, but is slightly different for quadratic and higher-order elements) error estimates were proved in Brezzi et al. (1999) and Brezzi, Marini and Süli (2000). Additional results, including local error bounds were proved in Sangalli (2000). See also Asensio, Russo, and Sangalli (2004) for additional comments on residual-free bubbles for quadratic elements.

4. The quasi-optimality of SUPG methods with respect to the suitable problem-dependent "ideal" norms was analyzed in depth by Sangalli (2004).

5. SUPG and the related residual-free bubble methods were also analyzed from the point of view of *a posteriori* error estimates in Russo (1996b), Verfürth (1998), Papastavrou and Verfürth (2000), Sangalli (2001), and references therein.

Let $\tilde{u}^h \in \mathcal{V}^h$ denote an interpolant of u. The interpolation error is denoted by $\eta = \tilde{u}^h - u$. Thus, $e = e^h + \eta$, where $e^h \in \mathcal{V}^h$.

It is assumed that τ possesses the following properties:

$$\tau = O\left(\frac{h}{|\boldsymbol{a}|}\right), \qquad \alpha \text{ large} \tag{270}$$

$$\tau = O\left(\frac{h^2}{\kappa}\right), \qquad \alpha \text{ small} \tag{271}$$

A specific choice of τ satisfying these properties is given by

$$\tau = \frac{1}{2}\frac{h}{|\boldsymbol{a}|}\zeta(\alpha) \tag{272}$$

where $\zeta(\alpha)$ is illustrated in Figure 30. (See Hughes, Mallet and Mizukami (1986), Appendix I, for some other possibilities.)

For sufficiently smooth u, standard interpolation theory (see, e.g., Ciarlet (1978)) and the above asymptotic properties of τ lead to the following ***interpolation estimate***:

$$2\left\|\tau^{-\frac{1}{2}}\eta\right\|_\Omega^2 + \kappa\|\nabla\eta\|_\Omega^2 + \left\||a_n|^{\frac{1}{2}}\eta\right\|_{\Gamma^h}^2 + \left\|\tau^{\frac{1}{2}}\mathcal{L}\eta\right\|_{\Omega'}^2 \leq c_u h^{2l} \tag{273}$$

$$2l = \begin{cases} 2k+1, & \alpha \text{ large} \\ 2k, & \alpha \text{ small} \end{cases} \tag{274}$$

where c_u is a function of u. The notation c_u is used subsequently, it being understood that in each instance its value may change by a multiplicative constant.

An ***inverse estimate*** also needs to be introduced. The appropriate form in the present circumstances is

$$\left\|\Delta w^h\right\|_{\Omega'} \leq ch^{-1}\left\|\nabla w^h\right\|_\Omega \qquad \forall w^h \in \mathcal{V}^h \tag{275}$$

where c is a nondimensional constant. (See Ciarlet (1978), pp. 140–146, for results of this kind.)

Theorem 5.1. *Assume the consistency condition (267), stability condition (269), and interpolation estimate (273) hold. Assume the slope m in the definition of $\zeta(\alpha)$ satisfies $m \leq 4/c^2$, where c is the constant in the inverse estimate (275). Then the error for the Galerkin/least-squares method is*

$$|||e|||^2_{GLS} \leq c_u h^{2l} \tag{276}$$

PROOF.

First, estimate e^h:

$$
\begin{aligned}
|||e^h|||^2_{GLS} &= B_{GLS}(e^h, e^h) \qquad \text{(stability)} \\
&= B_{GLS}(e^h, e - \eta) \\
&= -B_{GLS}(e^h, \eta) \qquad \text{(consistency)} \\
&\leq |B_{GLS}(e^h, \eta)| \\
&= \Big| -(\boldsymbol{a} \cdot \nabla e^h, \eta)_\Omega + \kappa(\nabla e^h, \nabla \eta)_\Omega \\
&\quad + (e^h, a_n^+ \eta)_{\Gamma_h} + (\tau \mathcal{L} e^h, \mathcal{L} \eta)_{\Omega'} \Big| \qquad \text{(definition of } B_{GLS}(\cdot, \cdot)) \\
&= \Big| -(\mathcal{L} e^h, \eta)_{\Omega'} - \kappa(\Delta e^h, \eta)_{\Omega'} \\
&\quad + \kappa(\nabla e^h, \nabla \eta)_\Omega + (e^h, a_n^+ \eta)_{\Gamma_h} \\
&\quad + (\tau \mathcal{L} e^h, \mathcal{L} \eta)_{\Omega'} \Big| \\
&\leq \frac{1}{4} \left\| \tau^{\frac{1}{2}} \mathcal{L} e^h \right\|^2_{\Omega'} + \left\| \tau^{-\frac{1}{2}} \eta \right\|^2_\Omega \\
&\quad + \frac{\kappa^2}{4} \left\| \tau^{\frac{1}{2}} \Delta e^h \right\|^2_{\Omega'} + \left\| \tau^{-\frac{1}{2}} \eta \right\|^2_\Omega \\
&\quad + \frac{\kappa}{4} \left\| \nabla e^h \right\|^2_\Omega + \kappa \left\| \nabla \eta \right\|^2_\Omega \\
&\quad + \frac{1}{4} \left\| |a_n|^{\frac{1}{2}} e^h \right\|^2_{\Gamma_h} + \left\| |a_n|^{\frac{1}{2}} \eta \right\|^2_{\Gamma_h} \\
&\quad + \frac{1}{4} \left\| \tau^{\frac{1}{2}} \mathcal{L} e^h \right\|^2_{\Omega'} + \left\| \tau^{\frac{1}{2}} \mathcal{L} \eta \right\|^2_{\Omega'}
\end{aligned}
\tag{277}
$$

To proceed further, invoke the bound on m;

$$
\begin{aligned}
\kappa\tau &= \frac{\kappa h}{2|\boldsymbol{a}|} \zeta(\alpha) \\
&= \frac{h^2}{4\alpha} \zeta(\alpha) \\
&\leq \frac{h^2}{c^2}
\end{aligned}
\tag{278}
$$

Combining (278) with the inverse estimate yields

$$\kappa^2 \left\| \tau^{\frac{1}{2}} \Delta e^h \right\|^2_{\Omega'} \leq \kappa \left\| \nabla e^h \right\|^2_\Omega \tag{279}$$

Employing the result in (277) leads to

$$\frac{1}{2} |||e^h|||^2_{GLS} \leq 2 \left\| \tau^{-\frac{1}{2}} \eta \right\|^2_\Omega + \kappa \left\| \nabla \eta \right\|^2_\Omega + \left\| |a_n|^{\frac{1}{2}} \eta \right\|^2_{\Gamma^h} + \left\| \tau^{\frac{1}{2}} \mathcal{L} \eta \right\|^2_{\Omega'} \tag{280}$$

Therefore, by the interpolation estimate,

$$|||e^h|||^2_{GLS} \leq c_u h^{2l} \tag{281}$$

Likewise,

$$|||\eta|||^2_{GLS} \leq c_u h^{2l}, \tag{282}$$

and so, by the triangle inequality,

$$|||e|||^2_{GLS} \leq c_u h^{2l} \tag{283}$$

This completes the proof of the theorem. $\square$

Remark

The same rates of convergence can be proved for SUPG and multiscale stabilized methods.

5.2. Scalar unsteady advection-diffusion equation: Space-time formulation

The initial/boundary-value problem consists of finding $u(\boldsymbol{x}, t)$, $\forall \boldsymbol{x} \in \overline{\Omega}, \forall t \in [0, T]$, such that

$$
\begin{align}
\mathcal{L}_t u &\equiv \dot{u} + \mathcal{L}u = f & \text{in } \Omega \times]0, T[\tag{284}\\
u(\boldsymbol{x}, 0) &= u_0(\boldsymbol{x}) & \forall \boldsymbol{x} \in \Omega \tag{285}\\
u &= g & \text{on } \Gamma_g \times]0, T[\tag{286}\\
-a_n^- u + \sigma_n^d(u) &= h & \text{on } \Gamma_h \times]0, T[\tag{287}
\end{align}
$$

where $\dot{u} = \partial u / \partial t$, and $u_0 : \Omega \to \mathbb{R}$, $f : \Omega \times]0, T[\to \mathbb{R}$, $g : \Gamma_g \times]0, T[\to \mathbb{R}$, and $h : \Gamma_h \times]0, T[\to \mathbb{R}$ are prescribed data.

The procedures to be described are based upon the **discontinuous Galerkin method in time**. (See Johnson (1987), and references therein, for a description of the discontinuous Galerkin method.) Space-time (i.e. $\Omega \times]0, T[$) is divided into *time slabs* $\Omega \times]t_n, t_{n+1}[$, where $0 = t_0 < t_1 < \ldots < t_N = T$. Each time slab is discretized by space-time finite elements. The finite element spaces consist of piecewise polynomials of order k in $\boldsymbol{x}$ and t, continuous within each slab, but *discontinuous* across time slabs. Again, as a point of departure, the **Galerkin method** will be presented first:

$$
\begin{align}
B(w^h, u^h)_n &= L(w^h)_n , & n = 0, 1, \ldots, N-1 \tag{288}\\
B(w^h, u^h)_n &\equiv \int_{t_n}^{t_{n+1}} \left(-\dot{w}^h, u^h \right)_\Omega + B(w^h, u^h) \, \mathrm{d}t + (w^h(t_{n+1}^-), u^h(t_{n+1}^-))_\Omega \tag{289}\\
L(w^h)_n &\equiv \int_{t_n}^{t_{n+1}} L(w^h) \mathrm{d}t + (w^h(t_n^+), u^h(t_n^-))_\Omega \tag{290}
\end{align}
$$

$$\tag{291}$$

where

$$
\begin{align}
u^h(t_n^\pm) &= u^h(\boldsymbol{x}, t_n^\pm) \tag{292}\\
u^h(t_0^-) &\equiv u_0(\boldsymbol{x}) \tag{293}
\end{align}
$$

Remark

Continuity of the solution across time slabs is seen to be *weakly* enforced.

Generalization of SUPG, Galerkin/least-squares and multiscale proceeds analogously to the steady case:

SUPG

$$B_{SUPG}(w^h, u^h)_n = L_{SUPG}(w^h)_n , \qquad n = 0, 1, \dots, N-1 \tag{294}$$

$$B_{SUPG}(w^h, u^h)_n \equiv B(w^h, u^h)_n + \int_{t_n}^{t_{n+1}} \left(\tau \left(\dot{w}^h + \boldsymbol{a} \cdot \nabla w^h \right), \mathcal{L}_t u^h \right)_{\Omega'} dt \tag{295}$$

$$L_{SUPG}(w^h)_n \equiv L(w^h)_n + \int_{t_n}^{t_{n+1}} \left(\tau \left(\dot{w}^h + \boldsymbol{a} \cdot \nabla w^h \right), f \right)_{\Omega'} dt \tag{296}$$

Galerkin/least-squares

$$B_{GLS}(w^h, u^h)_n = L_{GLS}(w^h)_n , \qquad n = 0, 1, \dots, N-1 \tag{297}$$

$$B_{GLS}(w^h, u^h)_n \equiv B(w^h, u^h)_n + \int_{t_n}^{t_{n+1}} \left(\tau \mathcal{L}_t w^h, \mathcal{L}_t u^h \right)_{\Omega'} dt \tag{298}$$

$$L_{GLS}(w^h)_n \equiv L(w^h)_n + \int_{t_n}^{t_{n+1}} \left(\tau \mathcal{L}_t w^h, f \right)_{\Omega'} dt \tag{299}$$

Multiscale

$$B_{MS}(w^h, u^h)_n = L_{MS}(w^h)_n , \qquad n = 0, 1, \dots, N-1 \tag{300}$$

$$B_{MS}(w^h, u^h)_n \equiv B(w^h, u^h)_n - \int_{t_n}^{t_{n+1}} \left(\tau \mathcal{L}_t^* w^h, \mathcal{L}_t u^h \right)_{\Omega'} dt \tag{301}$$

$$L_{MS}(w^h)_n \equiv L(w^h)_n - \int_{t_n}^{t_{n+1}} \left(\tau \mathcal{L}_t^* w^h, f \right)_{\Omega'} dt \tag{302}$$

$$\mathcal{L}_t^* = -\dot{w}^h + \mathcal{L}^* w^h \tag{303}$$

Remarks

1. In the unsteady case, h represents a space-time mesh parameter.
2. The issue of the time integration method is obviated by the choice of space-time interpolation. Unconditional stability (i.e., stability for all time steps, $\Delta t = t_{n+1} - t_n > 0$) is achieved in all cases. On each time slab a system of linear algebraic equations needs to be solved.

Let

$$\begin{aligned} \left| w^h \right|^2 \equiv\ & \frac{1}{2} \sum_{n=1}^{N-1} \left\| \llbracket w^h(t_n) \rrbracket \right\|_\Omega^2 + \frac{1}{2} \left(\left\| w^h(T^-) \right\|_\Omega^2 + \left\| w^h(0^+) \right\|_\Omega^2 \right) \\ & + \int_0^T \left| \left| \left| w^h \right| \right| \right|^2 dt \end{aligned} \tag{304}$$

where $\llbracket w^h(t_n) \rrbracket = w^h(t_n^+) - w^h(t_n^-)$. It is a simple exercise to show that

$$\sum_{n=0}^{N-1} B(w^h, w^h)_n - \sum_{n=1}^{N-1} (w^h(t_n^+), w^h(t_n^-))_\Omega = \left| w^h \right|^2 \tag{305}$$

where the constraint $w^h(t_0^-) = w^h(0^-) = 0$ has been used.
Likewise,

$$\sum_{n=0}^{N-1} B_{GLS}(w^h, w^h)_n - \sum_{n=1}^{N-1} (w^h(t_n^+), w^h(t_n^-))_\Omega = \big| w^h \big|_{GLS}^2 \tag{306}$$

where

$$\big| w^h \big|_{GLS}^2 \equiv \big| w^h \big|^2 + \sum_{n=0}^{N-1} \int_{t_n}^{t_{n+1}} \left\| \tau^{\frac{1}{2}} \mathcal{L}_t w^h \right\|_{\tilde\Omega}^2 \mathrm{d}t \tag{307}$$

The following error estimate, analogous to the steady case, can be established for the space-time Galerkin/least-squares method:

$$\big| e \big|_{GLS}^2 \le c_u h^{2l} \tag{308}$$

Remark

The hypotheses necessary to prove (308) are virtually identical to those for the steady case.

5.3. Symmetric advective-diffusive systems

The previous developments for the scalar advection-diffusion equation may be generalized to *symmetric* advective-diffusive systems. The equations are (see also Hughes, Franca and Mallet (1987), Hughes and Mallet (1986)):

$$\mathcal{L}_t V \equiv A_0 V_{,t} + \mathcal{L}V = \mathcal{F} \tag{309}$$
$$\mathcal{L}V \equiv \tilde A \cdot \nabla V - \nabla \cdot \tilde K \nabla V \tag{310}$$
$$V = (V_1, V_2, \ldots, V_n)^T \tag{311}$$
$$\tilde A^T = \left[\tilde A_1, \tilde A_2, \ldots, \tilde A_d \right] \tag{312}$$
$$\tilde K = \begin{bmatrix} \tilde K_{11} & \ldots & \tilde K_{1d} \\ \vdots & \ddots & \vdots \\ \tilde K_{d1} & \ldots & \tilde K_{dd} \end{bmatrix} \tag{313}$$
$$\tilde A \cdot \nabla V = \tilde A^T \nabla V = \tilde A_i \nabla V_{,i} = \tilde A_1 \frac{\partial \tilde V}{\partial x_1} + \ldots + \tilde A_d \frac{\partial \tilde V}{\partial x_d} \tag{314}$$

in which A_0 is an $m \times m$ symmetric, positive-definite matrix; $\tilde A_i$ is an $m \times m$ symmetric, matrix, $1 \le i \le d$, $\tilde A$ is a solenoidal matrix, that is, $\tilde A_{i,i} = 0$; and $\tilde K$ is an $(m \cdot d) \times (m \cdot d)$ constant, symmetric, positive-definite matrix. (The case in which $\tilde K$ is positive-*semidefinite* is more important in practice, but complicates the specification of boundary conditions.)

Corresponding to the developments for the scalar case, the following results are obtained:

$$\tilde{\boldsymbol{A}}_n = n_i \tilde{\boldsymbol{A}}_i \tag{315}$$

$$\tilde{\boldsymbol{A}}_n^+ = \frac{1}{2}\left(\tilde{\boldsymbol{A}}_n + \left|\tilde{\boldsymbol{A}}_n\right|\right) \tag{316}$$

$$\tilde{\boldsymbol{A}}_n^- = \frac{1}{2}\left(\tilde{\boldsymbol{A}}_n - \left|\tilde{\boldsymbol{A}}_n\right|\right) \tag{317}$$

$$\boldsymbol{U}(\boldsymbol{V}) = \boldsymbol{A}_0 \boldsymbol{V} \qquad \text{(temporal flux)} \tag{318}$$

$$\boldsymbol{F}_i^a(\boldsymbol{V}) = -\tilde{\boldsymbol{A}}_i \boldsymbol{V} \qquad \text{(advective flux)} \tag{319}$$

$$\boldsymbol{F}_i^d(\boldsymbol{V}) = -\tilde{\boldsymbol{K}}_{ij} \boldsymbol{V}_{,j} \qquad \text{(diffusive flux)} \tag{320}$$

$$\boldsymbol{F}_i = \boldsymbol{F}_i^a(\boldsymbol{V}) + \boldsymbol{F}_i^d(\boldsymbol{V}) \qquad \text{(total flux)} \tag{321}$$

$$\boldsymbol{F}_n^a = n_i \boldsymbol{F}_i^a \tag{322}$$

$$\boldsymbol{F}_n^d = n_i \boldsymbol{F}_i^d \tag{323}$$

$$\boldsymbol{F}_n = n_i \boldsymbol{F}_i \tag{324}$$

For simplicity, assume that for $\boldsymbol{x} \in \Gamma$, $\tilde{\boldsymbol{A}}_n(\boldsymbol{x})$ is either positive- or negative-definite. This will allow a concise statement of boundary conditions analogous to the scalar case. For situations in which $\tilde{\boldsymbol{A}}_n$ is indefinite, boundary condition specification is more complex, necessitating component by component specification. Let

$$\Gamma^- = \left\{\boldsymbol{x} \in \Gamma \left| \tilde{\boldsymbol{A}}_n(\boldsymbol{x}) < 0 \right.\right\} \tag{325}$$

$$\Gamma^+ = \Gamma - \Gamma^- \tag{326}$$

$$\Gamma_{\mathcal{G}}^\pm = \Gamma_{\mathcal{G}} \bigcap \Gamma^\pm \tag{327}$$

$$\Gamma_{\mathcal{H}}^\pm = \Gamma_{\mathcal{H}} \bigcap \Gamma^\pm \tag{328}$$

5.3.1. Boundary-value problem

$$\mathcal{L}\boldsymbol{V} = -\nabla \cdot \boldsymbol{F} = -\boldsymbol{F}_{i,i} = \mathcal{F} \qquad \text{on } \Omega \tag{329}$$

$$\boldsymbol{V} = \mathcal{G} \qquad \text{on } \Gamma_{\mathcal{G}} \tag{330}$$

$$-\tilde{\boldsymbol{A}}_n^- \boldsymbol{V} + \boldsymbol{F}_n^d(\boldsymbol{V}) = \mathcal{H} \qquad \text{on } \Gamma_{\mathcal{H}} \tag{331}$$

(331) is equivalent to

$$\boldsymbol{F}_n(\boldsymbol{V}) = \mathcal{H}^- \qquad \text{on } \Gamma_{\mathcal{H}}^- \text{ (total flux b.c.)} \tag{332}$$

$$\boldsymbol{F}_n^d(\boldsymbol{V}) = \mathcal{H}^+ \qquad \text{on } \Gamma_{\mathcal{H}}^+ \text{ (diffusive flux b.c.)} \tag{333}$$

variational formulation

$$\mathcal{S} = \left\{\boldsymbol{V} \in H^1(\Omega)^m \left| \boldsymbol{V} = \mathcal{G} \quad \text{on } \Gamma_{\mathcal{G}} \right.\right\} \tag{334}$$

$$\mathcal{V} = \left\{\boldsymbol{W} \in H^1(\Omega)^m \left| \boldsymbol{W} = \boldsymbol{0} \quad \text{on } \Gamma_{\mathcal{H}} \right.\right\} \tag{335}$$

$$B(\boldsymbol{W}, \boldsymbol{V}) \equiv (\nabla \boldsymbol{W}, \boldsymbol{F}(\boldsymbol{V}))_\Omega + (\boldsymbol{W}, \tilde{\boldsymbol{A}}_n^+ \boldsymbol{V})_{\Gamma_{\mathcal{H}}} \tag{336}$$

$$L(\boldsymbol{W}) \equiv (\boldsymbol{W}, \mathcal{F})_\Omega + (\boldsymbol{W}, \mathcal{H})_{\Gamma_{\mathcal{H}}} \tag{337}$$

$$
\begin{aligned}
0 &= B(\boldsymbol{W}, \boldsymbol{V}) - L(\boldsymbol{W}) \\
&= -(\boldsymbol{W}, \nabla \cdot \boldsymbol{F}(\boldsymbol{V}) + \mathcal{F})_{\Omega} + (\boldsymbol{W}, -\tilde{\boldsymbol{A}}_n^- \boldsymbol{V} + \boldsymbol{F}_n^d(\boldsymbol{V}) - \mathcal{H})_{\Gamma_{\mathcal{H}}}
\end{aligned}
$$
$$\text{(formal consistency)} \tag{338}$$

$$
B(\boldsymbol{W}, \boldsymbol{W}) = \left\| \left| \tilde{\boldsymbol{K}} \right|^{\frac{1}{2}} \nabla \boldsymbol{W} \right\|_{\Omega}^2 + \frac{1}{2} \left\| \left| \tilde{\boldsymbol{A}}_n \right|^{\frac{1}{2}} \boldsymbol{W} \right\|_{\Gamma_{\mathcal{H}}}^2 \quad \forall \boldsymbol{W} \in \mathcal{V}
$$
$$\text{(stability)} \tag{339}$$

$$
\||\boldsymbol{W}\||^2 \equiv B(\boldsymbol{W}, \boldsymbol{W}) \tag{340}
$$

$$
\begin{aligned}
0 &= B(\mathbf{1}, \boldsymbol{V}) - L(\mathbf{1}) \\
&= -\left(\int_{\Gamma^-} \mathcal{H}^- \mathrm{d}\Gamma + \int_{\Omega} \mathcal{F} \mathrm{d}\Omega + \int_{\Gamma^+} (-\tilde{\boldsymbol{A}}_n \boldsymbol{V} + \mathcal{H}^+) \, \mathrm{d}\Gamma \right)
\end{aligned}
$$
$$\text{(conservation for } \Gamma_{\mathcal{G}} = \emptyset) \tag{341}$$

hyperbolic case

$$
\begin{aligned}
-\nabla \cdot \boldsymbol{F}^a(\boldsymbol{V}) &= \mathcal{F} & &\text{on } \Omega & (342) \\
\boldsymbol{V} &= \mathcal{G}^- & &\text{on } \Gamma_{\mathcal{G}^-} & (343) \\
\boldsymbol{F}_n^a(\boldsymbol{V}) &= \mathcal{H}^- & &\text{on } \Gamma_{\mathcal{H}^-} & (344)
\end{aligned}
$$

$$
\begin{aligned}
B(\boldsymbol{W}, \boldsymbol{V}) &\equiv (\nabla \boldsymbol{W}, \boldsymbol{F}^a(\boldsymbol{V}))_{\Omega} + (\boldsymbol{W}, \tilde{\boldsymbol{A}}_n^+ \boldsymbol{V})_{\Gamma^+} & (345) \\
L(\boldsymbol{W}) &\equiv (\boldsymbol{W}, \mathcal{F})_{\Omega} + (\boldsymbol{W}, \mathcal{H}^-)_{\Gamma_{\mathcal{H}^-}} & (346)
\end{aligned}
$$

$$
\begin{aligned}
0 &= B(\boldsymbol{W}, \boldsymbol{V}) - L(\boldsymbol{W}) \\
&= -(\boldsymbol{W}, \nabla \cdot \boldsymbol{F}^a(\boldsymbol{V}) + \mathcal{F})_{\Omega} + (\boldsymbol{W}, -\tilde{\boldsymbol{A}}_n^- \boldsymbol{V} - \mathcal{H}^-)_{\Gamma_{\mathcal{H}^-}}
\end{aligned}
$$
$$\text{(formal consistency)} \tag{347}$$

$$
B(\boldsymbol{W}, \boldsymbol{W}) = \frac{1}{2} \left\| \left| \tilde{\boldsymbol{A}}_n \right|^{\frac{1}{2}} \boldsymbol{W} \right\|_{\Gamma_{\mathcal{H}}}^2 \quad \forall \boldsymbol{W} \in \mathcal{V}
$$
$$\text{(stability)} \tag{348}$$

$$
0 = \int_{\Gamma^-} \mathcal{H}^- \mathrm{d}\Gamma + \int_{\Omega} \mathcal{F} \mathrm{d}\Omega + \int_{\Gamma^+} -\tilde{\boldsymbol{A}}_n \boldsymbol{V} \, \mathrm{d}\Gamma
$$
$$\text{(conservation for } \Gamma_{\mathcal{G}^-} = \emptyset) \tag{349}$$

finite element formulations

$$B_{SUPG}(\boldsymbol{W}^h, \boldsymbol{V}^h) = L_{SUPG}(\boldsymbol{W}^h) \tag{350}$$

$$B_{SUPG}(\boldsymbol{W}^h, \boldsymbol{V}^h) \equiv B(\boldsymbol{W}^h, \boldsymbol{V}^h) + \left(\tau\tilde{\boldsymbol{A}}\cdot\nabla\boldsymbol{W}^h, \mathcal{L}\boldsymbol{V}^h\right)_{\Omega'} \tag{351}$$

$$L_{SUPG}(\boldsymbol{W}^h) \equiv L(\boldsymbol{W}^h) + \left(\tau\tilde{\boldsymbol{A}}\cdot\nabla\boldsymbol{W}^h, \mathcal{F}\right)_{\Omega'} \tag{352}$$

$$B_{GLS}(\boldsymbol{W}^h, \boldsymbol{V}^h) = L_{GLS}(\boldsymbol{W}^h) \tag{353}$$

$$B_{GLS}(\boldsymbol{W}^h, \boldsymbol{V}^h) \equiv B(\boldsymbol{W}^h, \boldsymbol{V}^h) + \left(\tau\mathcal{L}\boldsymbol{W}^h, \mathcal{L}\boldsymbol{V}^h\right)_{\Omega'} \tag{354}$$

$$L_{GLS}(\boldsymbol{W}^h) \equiv L(\boldsymbol{W}^h) + \left(\tau\mathcal{L}\boldsymbol{W}^h, \mathcal{F}\right)_{\Omega'} \tag{355}$$

$$B_{MS}(\boldsymbol{W}^h, \boldsymbol{V}^h) = L_{MS}(\boldsymbol{W}^h) \tag{356}$$

$$B_{MS}(\boldsymbol{W}^h, \boldsymbol{V}^h) \equiv B(\boldsymbol{W}^h, \boldsymbol{V}^h) - \left(\tau\mathcal{L}^*\boldsymbol{W}^h, \mathcal{L}\boldsymbol{V}^h\right)_{\Omega'} \tag{357}$$

$$L_{MS}(\boldsymbol{W}^h) \equiv L(\boldsymbol{W}^h) - \left(\tau\mathcal{L}^*\boldsymbol{W}^h, \mathcal{F}\right)_{\Omega'} \tag{358}$$

$$\mathcal{L}^*\boldsymbol{W}^h = -\tilde{\boldsymbol{A}}_i\boldsymbol{W}^h_{,i} - \tilde{\boldsymbol{K}}_{ij}\boldsymbol{W}^h_{,ij} \tag{359}$$

GLS-norm and error estimate

$$\left|\left|\left|\boldsymbol{W}^h\right|\right|\right|^2_{GLS} \equiv B_{GLS}(\boldsymbol{W}^h, \boldsymbol{W}^h)$$

$$= \left|\left|\left|\boldsymbol{W}^h\right|\right|\right|^2 + \left\|\tau^{\frac{1}{2}}\mathcal{L}\boldsymbol{W}^h\right\|^2_{\Omega'} \tag{360}$$

$$|||\boldsymbol{E}|||^2_{GLS} \leq C_{\boldsymbol{V}}h^{2l} \tag{361}$$

5.3.2. Initial/boundary-value problem

$$\mathcal{L}_t\boldsymbol{V} \equiv \dot{\boldsymbol{U}}(\boldsymbol{V}) + \mathcal{L}\boldsymbol{V} = \mathcal{F} \qquad \text{in } \Omega\times]0,T[\tag{362}$$

$$\boldsymbol{U}(\boldsymbol{V}(\boldsymbol{x},0)) = \boldsymbol{U}(\boldsymbol{V}_0(\boldsymbol{x})) \qquad \forall\boldsymbol{x}\in\Omega \tag{363}$$

$$\boldsymbol{V} = \mathcal{G} \qquad \text{on } \Gamma_{\mathcal{G}}\times]0,T[\tag{364}$$

$$-\tilde{\boldsymbol{A}}^-_n\boldsymbol{V} + \boldsymbol{F}^d_n(\boldsymbol{V}) = \mathcal{H} \qquad \text{on } \Gamma_{\mathcal{H}} \tag{365}$$

finite element formulations

$$B(\boldsymbol{W}^h, \boldsymbol{V}^h)_n \equiv \int_{t_n}^{t_{n+1}} \left(\left(-\dot{\boldsymbol{W}}^h, \boldsymbol{U}(\boldsymbol{V}^h)\right)_{\Omega} + B(\boldsymbol{W}^h, \boldsymbol{V}^h)\right)\mathrm{d}t$$

$$+ \left(\boldsymbol{W}^h(t^-_{n+1}), \boldsymbol{U}(\boldsymbol{V}^h(t^-_{n+1}))\right)_{\Omega} \tag{366}$$

$$L(\boldsymbol{W}^h)_n \equiv \int_{t_n}^{t_{n+1}} L(\boldsymbol{W}^h)\mathrm{d}t + \left(\boldsymbol{W}^h(t^+_n), \boldsymbol{U}(\boldsymbol{V}^h(t^-_n))\right)_{\Omega} \tag{367}$$

$$\left| \boldsymbol{W}^h \right|^2 \;\; \equiv \;\; \sum_{n=0}^{N-1} B(\boldsymbol{W}^h, \boldsymbol{W}^h)_n - \sum_{n=1}^{N-1} B(\boldsymbol{W}^h(t_n^+), \boldsymbol{U}(\boldsymbol{V}^h(t_n^-))_\Omega$$

$$= \;\; \frac{1}{2} \sum_{n=1}^{N-1} \left\| \boldsymbol{A}_0^{\frac{1}{2}} [\![\boldsymbol{W}^h(t_n)]\!] \right\|_\Omega^2$$

$$+ \frac{1}{2} \left(\left\| \boldsymbol{A}_0^{\frac{1}{2}} \boldsymbol{W}^h(T^-) \right\|_\Omega^2 + \left\| \boldsymbol{A}_0^{\frac{1}{2}} \boldsymbol{W}(0^+) \right\|_\Omega^2 \right) + \int_0^T \left| \! \left| \! \left| \boldsymbol{W}^h \right| \! \right| \! \right|^2 \mathrm{d}t \quad (368)$$

$$B_{SUPG}(\boldsymbol{W}^h, \boldsymbol{V}^h)_n \;\; = \;\; L_{SUPG}(\boldsymbol{W}^h)_n \,, \qquad n = 0, 1, \ldots, N-1 \qquad (369)$$

$$B_{SUPG}(\boldsymbol{W}^h, \boldsymbol{V}^h)_n \;\; \equiv \;\; B(\boldsymbol{W}^h, \boldsymbol{V}^h)_n + \int_{t_n}^{t_{n+1}} \left(\tau \left(\boldsymbol{A}_0 \dot{\boldsymbol{W}}^h + \tilde{\boldsymbol{A}} \cdot \nabla \boldsymbol{W}^h \right), \mathcal{L}_t \boldsymbol{V}^h \right)_{\Omega'} \mathrm{d}t \quad (370)$$

$$L_{SUPG}(\boldsymbol{W}^h)_n \;\; \equiv \;\; L(\boldsymbol{W}^h)_n + \int_{t_n}^{t_{n+1}} \left(\tau \left(\boldsymbol{A}_0 \dot{\boldsymbol{W}}^h + \tilde{\boldsymbol{A}} \cdot \nabla \boldsymbol{W}^h \right), \mathcal{F} \right)_{\Omega'} \mathrm{d}t \qquad (371)$$

$$B_{GLS}(\boldsymbol{W}^h, \boldsymbol{V}^h)_n \;\; = \;\; L_{GLS}(\boldsymbol{W}^h)_n \,, \qquad n = 0, 1, \ldots, N-1 \qquad (372)$$

$$B_{GLS}(\boldsymbol{W}^h, \boldsymbol{V}^h)_n \;\; \equiv \;\; B(\boldsymbol{W}^h, \boldsymbol{V}^h)_n + \int_{t_n}^{t_{n+1}} \left(\tau \mathcal{L}_t \boldsymbol{W}^h, \mathcal{L}_t \boldsymbol{V}^h \right)_{\Omega'} \mathrm{d}t \qquad (373)$$

$$L_{GLS}(\boldsymbol{W}^h)_n \;\; \equiv \;\; L(\boldsymbol{W}^h)_n + \int_{t_n}^{t_{n+1}} \left(\tau \mathcal{L}_t \boldsymbol{W}^h, \mathcal{F} \right)_{\Omega'} \mathrm{d}t \qquad (374)$$

$$B_{MS}(\boldsymbol{W}^h, \boldsymbol{V}^h)_n \;\; = \;\; L_{MS}(\boldsymbol{W}^h)_n \,, \qquad n = 0, 1, \ldots, N-1 \qquad (375)$$

$$B_{MS}(\boldsymbol{W}^h, \boldsymbol{V}^h)_n \;\; \equiv \;\; B(\boldsymbol{W}^h, \boldsymbol{V}^h)_n - \int_{t_n}^{t_{n+1}} \left(\tau \mathcal{L}_t^* \boldsymbol{W}^h, \mathcal{L}_t \boldsymbol{V}^h \right)_{\Omega'} \mathrm{d}t \qquad (376)$$

$$L_{MS}(\boldsymbol{W}^h)_n \;\; \equiv \;\; L(\boldsymbol{W}^h)_n - \int_{t_n}^{t_{n+1}} \left(\tau \mathcal{L}_t^* \boldsymbol{W}^h, \mathcal{F} \right)_{\Omega'} \mathrm{d}t \qquad (377)$$

GLS-norm and error estimate

Likewise,

$$\left| \boldsymbol{W}^h \right|_{GLS}^2 \;\; \equiv \;\; \sum_{n=0}^{N-1} B_{GLS}(\boldsymbol{W}^h, \boldsymbol{W}^h)_n - \sum_{n=1}^{N-1} B(\boldsymbol{W}^h(t_n^+), \boldsymbol{U}(\boldsymbol{W}^h(t_n^-)))_\Omega$$

$$= \;\; \left| \boldsymbol{W}^h \right|^2 + \sum_{n=0}^{N-1} \int_{t_n}^{t_{n+1}} \left\| \tau^{\frac{1}{2}} \mathcal{L}_t \boldsymbol{W}^h \right\|_{\Omega'}^2 \mathrm{d}t \qquad (378)$$

$$\left| \boldsymbol{E} \right|_{GLS}^2 \;\; \leq \;\; C_{\boldsymbol{V}} h^{2l} \qquad (379)$$

Remarks

1. Stabilized methods have been used widely in engineering applications. There is a very
   large literature on mathematical and practical aspects. Experience has indicated that

the SUPG and multiscale variants are superior to Galerkin/least-squares in practical applications (see, e.g., Bochev and Gunzburger (2003)). A recent evaluation of SUPG, and comparison with finite volume and discontinuous Galerkin methods, is presented in Venkatakrishnan et al. (2003).

2. There are interesting examples of **non-residual** based stabilized methods. See, for example, Codina and Blasco (2000a, 2000b), and Bochev and Dohrman (2004).

6. Turbulence

In Sections 2–5, the variational multiscale method was described, and its connection with stabilized finite element methods was established. The idea of a variational framework for subgrid-scale modeling was also discussed. In this Section, the application of the multiscale method to the incompressible, Navier-Stokes equations is considered. The objective is a satisfactory interpretation/generalization of the Large Eddy Simulation (LES) concept within a variational formulation of the Navier-Stokes equations. This requires dealing with nonlinearities as well as issues of turbulence modeling.

The classical LES formulation of the incompressible Navier-Stokes equations is reviewed first. As points of reference, filtering, the subgrid-scale stress and the Smagorinsky model are discussed. The estimation of Smagorinsky parameters by way of the approach due to Lilly (1966,1967,1988) is also recalled. The shortcomings of the classical approach, noted previously in the literature are summarized. A fundamental problem of the classical approach is scale separation. The way this problem has been addressed in the literature is by way of dynamic modeling, which provides for adaptive selection of the so-called Smagorinsky constant (see, e.g., Germano et al., 1991; Moin et al., 1991; Piomelli, 1998).

In the variational multiscale approach, scale separation is invoked *ab initio*. A space-time formulation of the incompressible Navier-Stokes equations is employed. From the discrete point of view, this leads to the time-discontinuous Galerkin method on space-time slabs. This procedure proves convenient and obviates the need to consider specific time discretization (i.e., ODE) algorithms. However, it is a straightforward matter to develop traditional semi-discrete approaches with similar properties to the ones described here. The appendix to this section illustrates this fact.

Two simple generalizations of the Smagorinsky eddy viscosity model which act only on small scales are considered. One is completely desensitized to large-scale behavior, the other, partially desensitized. Parameters are again estimated by way of the approach due to Lilly (1966,1967,1988). Because scale separation has been invoked from the outset, a constant-coefficient model in the present approach is speculated to have validity for a greater variety of flows than the classical constant-coefficient Smagorinsky model. The approach is summarized by contrasting it with the work of the Temam group (see, e.g., Dubois, Jauberteau and Temam, 1993,1998). How the present approach addresses criticisms of the classical LES/Smagorinsky method and the identification of some other useful properties are described.

6.1. Incompressible Navier-Stokes equations

Let Ω be an open, connected, bounded subset of $\mathbb{R}^d$, $d = 2$ or 3, with piecewise smooth boundary $\Gamma = \partial\Omega$; Ω represents the fixed spatial domain of our problem. The time interval of

interest is denoted $]0, T[$, $T > 0$, and thus the space-time domain is $Q = \Omega \times]0, T[$; its lateral boundary is denoted $P = \Gamma \times]0, T[$. The setup is illustrated in Figure 31.
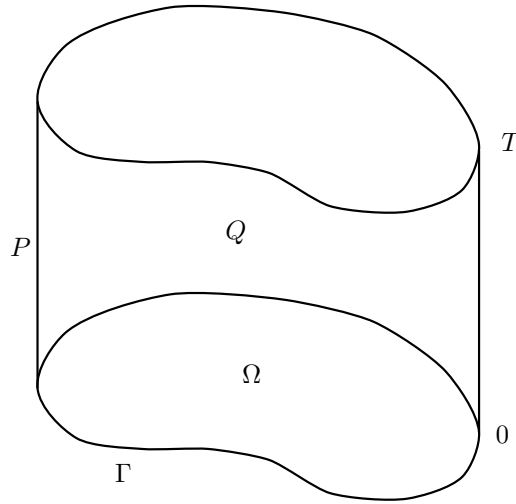

Figure 31. Space-time domain for the initial/boundary-value problem.

The initial/boundary-value problem consists of solving the following equations for $\boldsymbol{u} : \overline{Q} \rightarrow \mathbb{R}^d$, the velocity, and $p : Q \rightarrow \mathbb{R}$, the pressure (divided by density),

$$\frac{\partial \boldsymbol{u}}{\partial t} + \boldsymbol{\nabla} \cdot (\boldsymbol{u} \otimes \boldsymbol{u}) + \boldsymbol{\nabla} p = \nu \Delta \boldsymbol{u} + \boldsymbol{f} \qquad \text{in } Q \tag{380}$$

$$\boldsymbol{\nabla} \cdot \boldsymbol{u} = 0 \qquad \text{in } Q \tag{381}$$

$$\boldsymbol{u} = \boldsymbol{0} \qquad \text{on } P \tag{382}$$

$$\boldsymbol{u}(0^+) = \boldsymbol{u}(0^-) \qquad \text{on } \Omega \tag{383}$$

where $\boldsymbol{f} : Q \rightarrow \mathbb{R}^d$ is the given body force (per unit volume); ν is the kinematic viscosity, assumed positive and constant; $\boldsymbol{u}(0^-) : \Omega \rightarrow \mathbb{R}^d$ is the given initial velocity; and $\otimes$ denotes the tensor product (e.g., in component notation $[\boldsymbol{u} \otimes \boldsymbol{v}]_{ij} = u_i v_j$). Equations (380)-(383) are, respectively, the linear momentum balance, the incompressibility constraint, the no-slip boundary condition and the initial condition.

The setup for a space-time formulation is recalled once again. When a function is written with only one argument, it is assumed to refer to time. For example, $\boldsymbol{u}(t) = \boldsymbol{u}(\cdot, t)$, where the spatial argument $\boldsymbol{x} \in \Omega$ is suppressed for simplicity. Furthermore,

$$\boldsymbol{u}\left(t^{\pm}\right) = \lim_{\varepsilon \downarrow 0} \boldsymbol{u}\left(t \pm \varepsilon\right) \quad \forall t \in [0, T] \quad . \tag{384}$$

This notation allows us to distinguish between $\boldsymbol{u}(0^+)$ and $\boldsymbol{u}(0^-)$, the solution and its given initial value, respectively. In the variational formulation of the initial/boundary-value problem (see Section 6.4), (383) will only be satisfied in a weak sense. The notation of (383) and (384) is also conducive to the generalization of the formulation to the discrete case in which the

numerical problem is posed in terms of a sequence of "space-time slabs," where the solution may be discontinuous across the slab interfaces.

For mathematical results of existence, uniqueness and regularity, see Temam (1984), Quarteroni and Valli (1994), and references therein.

Solutions of (380)-(383), for the case in which ν is very small, typically give rise to turbulence, an inherently chaotic and unpredictable phenomenon. Nevertheless, some statistical quantities, such as particular spatial and temporal averages, are deterministic and, in principle, computable.

6.2. Large Eddy Simulation (LES)

The unpredictability of turbulence suggests reformulating the initial/boundary-value problem in terms of averaged quantities. In Large Eddy Simulation (LES) a spatial averaging procedure is employed. For example, let

$$\overline{\boldsymbol{u}}(\boldsymbol{x},t) = \int_{D_\Delta(\boldsymbol{x})} g(\boldsymbol{x},\boldsymbol{y})\boldsymbol{u}(\boldsymbol{y},t)\ d\boldsymbol{y} \tag{385}$$

in which

$$g(\boldsymbol{x},\boldsymbol{y}) = g(\boldsymbol{x}-\boldsymbol{y}) \quad \text{(homogeneity)} \tag{386}$$

and

$$1 = \int_{D_\Delta(\boldsymbol{x})} g(\boldsymbol{x},\boldsymbol{y})\ d\boldsymbol{y} \tag{387}$$

where $\overline{\boldsymbol{u}}$ is the filtered velocity and g is the filter having support in $D_\Delta(\boldsymbol{x}) \subset \Omega$, a neighborhood of $\boldsymbol{x} \in \Omega$. (See Fig. 32 for a schematic of a candidate filter.)
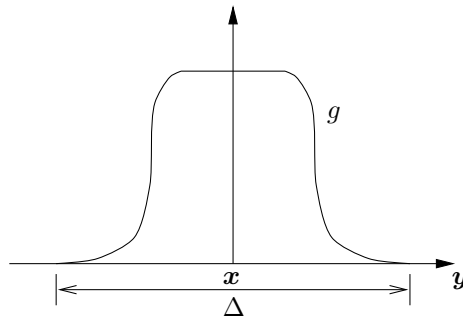
Figure 32. Typical filter function for LES.

The size of $D_\Delta(\boldsymbol{x})$ is characterized by Δ, the filter width. There are various possibilities for $D_\Delta(\boldsymbol{x})$. For example, a possible difinition is

$$D_\Delta(\boldsymbol{x}) = \left\{ \boldsymbol{y} \in \mathbb{R}^d \ | \ \rho(\boldsymbol{x},\boldsymbol{y}) < \Delta/2 \right\} \ . \tag{388}$$
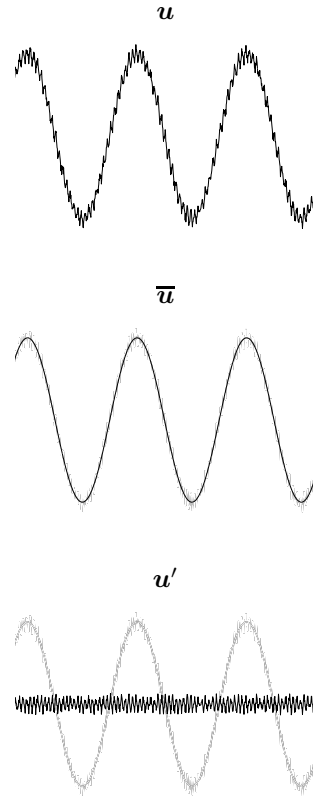
Figure 33. The effect of filtering.

The distance function, ρ, may be defined in terms of the Euclidean norm, in which case $D_\Delta(\boldsymbol{x})$ is an open ball of radius $\Delta/2$ centered at $\boldsymbol{x}$.

The effect of filtering is schematically illustrated in Figure 33.

The filtered field, $\overline{\boldsymbol{u}}$, is commonly referred to as the large, coarse, or resolvable scales. It is assumed adequate to represent the larger structures of the flow. The difference between $\boldsymbol{u}$ and $\overline{\boldsymbol{u}}$, that is,

$$\boldsymbol{u}' = \boldsymbol{u} - \overline{\boldsymbol{u}} \tag{389}$$

is the rapidly fluctuating part of $\boldsymbol{u}$; $\boldsymbol{u}'$ is commonly referred to as the small, fine, or unresolvable scales. Although primary interest is in computing $\overline{\boldsymbol{u}}$, due to the nonlinear nature of the Navier-Stokes equations, the effect of $\boldsymbol{u}'$ on $\overline{\boldsymbol{u}}$ cannot be ignored.

Remark

The homogeneous structure of the filter results in the commutativity of spatial differentiation and filtering, a property exploited in the derivation of the equations governing

filtered quantities. However, in order to obtain the filtered equations corresponding to (380)-(383), the filtering operation needs to be performed for all $\boldsymbol{x} \in \Omega$, and in particular for $\boldsymbol{x} \in \Omega \backslash \Omega_\Delta$, where

$$\Omega_\Delta = \{\boldsymbol{x} \mid D_\Delta(\boldsymbol{x}) \subset \Omega\} \quad . \tag{390}$$

In this case, the support of the filtering operation extends beyond the boundary of Ω. For a schematic illustration, see Figure 34. Clearly, this creates mathematical ambiguities. (Note that this problem does not arise in cases of domains with periodic boundary conditions.) An alternative approach is to reduce the size of the filter as the boundary is approached, but this too creates mathematical complications. This issue will not be addressed further herein. It needs to be emphasized, though, that it is an important issue. (For recent literature concerning this problem, see Galdi and Layton, 2000; John and Layton, 1998; Layton, 1996; Ghosal and Moin, 1995.)

6.2.1. Filtered Navier-Stokes equations

$$\frac{\partial \overline{\boldsymbol{u}}}{\partial t} + \boldsymbol{\nabla} \cdot (\overline{\boldsymbol{u} \otimes \boldsymbol{u}}) + \boldsymbol{\nabla}\overline{p} = \nu \Delta \overline{\boldsymbol{u}} + \overline{\boldsymbol{f}} \qquad \text{in } Q \tag{391}$$

$$\boldsymbol{\nabla} \cdot \overline{\boldsymbol{u}} = 0 \qquad \text{in } Q \tag{392}$$

$$\overline{\boldsymbol{u}} = \boldsymbol{0} \qquad \text{on } P \tag{393}$$

$$\overline{\boldsymbol{u}}(0^+) = \overline{\boldsymbol{u}}(0^-) \qquad \text{on } \Omega \ . \tag{394}$$

The nonlinear term in (391) gives rise to a **closure problem**: how to compute $\overline{\boldsymbol{u} \otimes \boldsymbol{u}}$? This necessarily entails some form of approximation. To this end, define the **subgrid-scale stress**

$$\boldsymbol{T} = \overline{\boldsymbol{u}} \otimes \overline{\boldsymbol{u}} - \overline{\boldsymbol{u} \otimes \boldsymbol{u}} \ . \tag{395}$$

In terms of the subgrid-scale stress, the filtered momentum equation (391) is rewritten as

$$\frac{\partial \overline{\boldsymbol{u}}}{\partial t} + \boldsymbol{\nabla} \cdot (\overline{\boldsymbol{u}} \otimes \overline{\boldsymbol{u}}) + \boldsymbol{\nabla}\overline{p} = \nu \Delta \overline{\boldsymbol{u}} + \boldsymbol{\nabla} \cdot \boldsymbol{T} + \overline{\boldsymbol{f}} \ . \tag{396}$$

Thus, $\boldsymbol{T}$ needs to be modeled to close the system. To be more precise, only the deviatoric part of $\boldsymbol{T}$, namely,

$$\text{dev } \boldsymbol{T} = \boldsymbol{T} - \left(\tfrac{1}{3} \text{ tr } \boldsymbol{T}\right) \boldsymbol{I} \ , \tag{397}$$

where $\boldsymbol{I}$ is the identity tensor, needs to be modeled, and the dilatational part, $\frac{1}{3} \text{ tr } \boldsymbol{T}$, may be subsumed by $\overline{p}$.

6.3. Smagorinsky closure

The classical and most widely used closures are based on the **Smagorinsky eddy viscosity model** Smagorinsky (1963):

$$\boldsymbol{T}_S = 2\nu_T \boldsymbol{\nabla}^s \overline{\boldsymbol{u}} \tag{398}$$

where

$$\nu_T = (C_S \Delta)^2 |\boldsymbol{\nabla}^s \overline{\boldsymbol{u}}| \tag{399}$$

$$\boldsymbol{\nabla}^s \overline{\boldsymbol{u}} = \tfrac{1}{2} \left(\boldsymbol{\nabla}\overline{\boldsymbol{u}} + (\boldsymbol{\nabla}\overline{\boldsymbol{u}})^T\right) \tag{400}$$

$$|\boldsymbol{\nabla}^s \overline{\boldsymbol{u}}| = (2\boldsymbol{\nabla}^s \overline{\boldsymbol{u}} \cdot \boldsymbol{\nabla}^s \overline{\boldsymbol{u}})^{1/2} \tag{401}$$
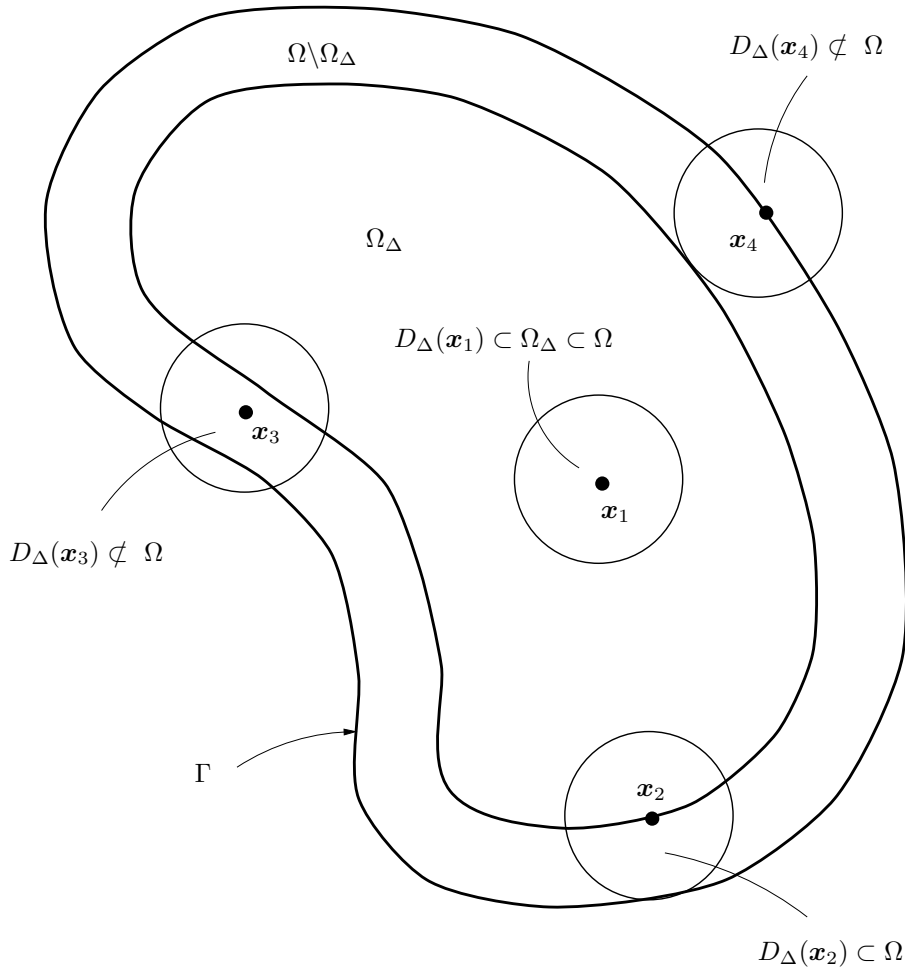
Figure 34. The support of the filter extends beyond the boundary of Ω.

and C_S is referred to as the ***Smagorinsky constant***. Note, $\boldsymbol{T}_S$ is deviatoric, i.e., $\boldsymbol{T}_S = \text{dev } \boldsymbol{T}_S$.

Various criticisms have been lodged against the Smagorinsky model (see, e.g., Germano et al., 1991; Piomelli, 1998). Typical of these are:

1. $\boldsymbol{T}_S$ does not replicate the asymptotic behavior of $\boldsymbol{T}$ near walls, in particular, $\boldsymbol{T}_S$ does not vanish at walls.
2. Values of C_S obtained from the decay of homogeneous isotropic turbulence tend to be ***too large*** for other situations, such as in the presence of mean shear.
3. $\boldsymbol{T}_S$ produces ***excessive damping*** of resolved structures in transition, resulting in incorrect growth rate of perturbations.

As a result of these shortcomings, many modifications have been proposed, such as wall

functions, intermittency functions, etc. Perhaps the most notable achievement is the **dynamic subgrid-scale model** (Germano et al., 1991), in which it is assumed that C_S is a function of space and time, that is

$$C_S = C_S(\boldsymbol{x}, t) \ . \tag{402}$$

The identification of C_S is performed adaptively by sampling the smallest resolved scales and using this information to model the subgrid scales. The dynamic model has been applied to a variety of flows and improved results have been obtained in most cases. For a recent review of the state-of-the-art and assessment, see Piomelli (1998). It is a widely held opinion that any proposal of a new LES model based on the Smagorinsky concept must address, at the very least, the shortcomings delineated above.

6.3.1. Estimation of parameters   The Smagorinsky parameters C_S and Δ may be determined by a procedure due to Lilly (1966,1967,1988). In Lilly's analysis it is assumed that turbulent kinetic energy dissipation and dissipation produced by the Smagorinsky model are in balance. The limit of resolution is assumed to fall in the Kolmogorov inertial subrange and $|\boldsymbol{\nabla}^s\overline{\boldsymbol{u}}|$ is determined by spectral integration. This enables quantification of $C_S\Delta$ and ν_T. A brief summary of the steps involved follows.
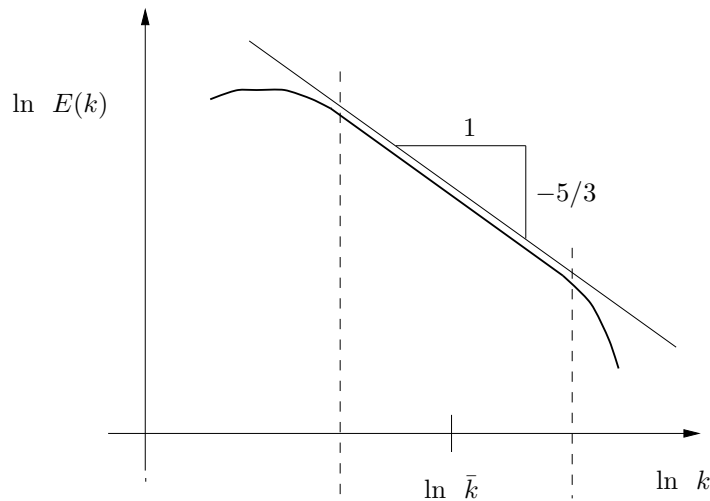

Figure 35. Kolmogorov energy spectrum.

Consider Figure 35. $E(k)$ is the spectral amplitude of kinetic energy, defined as the integral over surfaces of spheres in wave-number space parametrized by the radius k. In the inertial subrange

$$E(k) = \alpha\varepsilon^{2/3}k^{-5/3} \tag{403}$$

where α is the Kolmogorov constant and ε is the turbulent dissipation. $|\boldsymbol{\nabla}^s\overline{\boldsymbol{u}}|$ may be determined from the relation

$$\tfrac{1}{2}\,|\boldsymbol{\nabla}^s\overline{\boldsymbol{u}}|^2 = \int_0^{\bar{k}} k^2 E(k)\ dk \tag{404}$$

where $\bar{k}$ corresponds to the resolution limit, which is the cut-off wave number for spectral discretization. Equating turbulent kinetic energy dissipation with dissipation produced by the Smagorinsky model, and evaluating (404) using (403), yields

$$\begin{aligned} \varepsilon &= \boldsymbol{T}_S \cdot \boldsymbol{\nabla}^s\overline{\boldsymbol{u}} \\ &= 2(C_S\Delta)^2\,|\boldsymbol{\nabla}^s\overline{\boldsymbol{u}}|\,(\boldsymbol{\nabla}^s\overline{\boldsymbol{u}}\cdot\boldsymbol{\nabla}^s\overline{\boldsymbol{u}}) \\ &= (C_S\Delta)^2\,|\boldsymbol{\nabla}^s\overline{\boldsymbol{u}}|^3 \\ &= (C_S\Delta)^2\left(\frac{3\alpha}{2}\right)^{3/2}\bar{k}^2\varepsilon \end{aligned} \tag{405}$$

from which it follows that

$$C_S\Delta = \left(\frac{2}{3\alpha}\right)^{3/4}\bar{k}^{-1} \tag{406}$$

and

$$\nu_T = \left(\frac{2}{3\alpha}\right)\varepsilon^{1/3}\,\bar{k}^{-4/3}\ . \tag{407}$$

Assuming $\bar{k} = \mathrm{const}\ \bar{h}^{-1}$, where $\bar{h}$ is the mesh parameter, it follows from (406) and (407) that

$$C_S\Delta = O(\bar{h}) \tag{408}$$

and

$$\nu_T = O(\bar{h}^{4/3})\ . \tag{409}$$

Remarks

1. Assuming $\Delta = \bar{h} = \pi\bar{k}^{-1}$ and $\alpha = 1.4$, it follows from (406) that $C_S \cong 0.18$. However, smaller values, often around 0.10, are often used in practice (Germano et al., 1991).
2. The excessive damping of resolved structures may be explained by (398) and (409). An $O(\bar{h}^{4/3})$ viscosity acts on all scales present. It is known from the analysis of artificial viscosity methods that, even for linear model problems, an $O(\bar{h}^{4/3})$ artificial viscosity results in convergence that is at most $O(\bar{h}^{4/3})$ in L_2 and $O(\bar{h}^{2/3})$ in H^1. This is indeed very slow convergence and is deemed by most analysts as unacceptable. Furthermore, these results are probably optimistic for the (nonlinear) Navier-Stokes equations. The physical design of the Smagorinsky model results in the correct extraction of total kinetic energy, but the flaw seems to be that the extraction of kinetic energy occurs in all scales and, in particular, in the so-called "resolved scales."

3. The analysis described assumed an isotropic discretization. The anisotropic case has also been addressed by Lilly (1988). See also Scotti and Meneveau (1993), Scotti, Meneveau and Fatica (1997).
4. The concepts of filtering and the filtered equations involve subtleties not described here. For more extensive discussion of these issues, the interested reader may consult Carati, Winckelmans and Jeanmart (2001), Winckelmans et al. (2001), and Winckelmans, Jeanmart and Carati (2002).
5. It has been observed that some common filters are isomorphisms (e.g., the Gaussian filter). In these cases, $\boldsymbol{u}$ can be reconstructed from $\overline{\boldsymbol{u}}$. Consequently, the filtered equations contain the same information as the Navier-Stokes equations. A formulation of LES which circumvents the use of the filtered equations, and associated conceptual difficulties, is presented next.

6.4. Variational multiscale method

6.4.1. Space-time formulation of the incompressible Navier-Stokes equations Consider a Galerkin space-time formulation with weakly imposed initial condition. Let $\mathcal{V} = \mathcal{V}(Q)$ denote the trial solution and weighting function spaces, which are assumed to be identical. Assume $\boldsymbol{U} = \{\boldsymbol{u}, p\} \in \mathcal{V}$ implies $\boldsymbol{u} = \boldsymbol{0}$ on P and $\int_{\Omega} p(t)\, d\Omega = 0$ for all $t \in\,]0, T[$. The variational formulation is stated as follows:

Find $\boldsymbol{U} \in \mathcal{V}$ such that $\forall \boldsymbol{W} = \{\boldsymbol{w}, q\} \in \mathcal{V}$

$$B(\boldsymbol{W}, \boldsymbol{U}) = (\boldsymbol{W}, \boldsymbol{F}) \tag{410}$$

where

$$\begin{aligned} B(\boldsymbol{W}, \boldsymbol{U}) &= (\boldsymbol{w}(T^-), \boldsymbol{u}(T^-))_\Omega - \left(\frac{\partial \boldsymbol{w}}{\partial t}, \boldsymbol{u}\right)_Q - (\boldsymbol{\nabla}\boldsymbol{w}, \boldsymbol{u} \otimes \boldsymbol{u})_Q \\ &\quad + (q, \boldsymbol{\nabla} \cdot \boldsymbol{u})_Q - (\boldsymbol{\nabla} \cdot \boldsymbol{w}, p)_Q + (\boldsymbol{\nabla}^s \boldsymbol{w}, 2\nu\boldsymbol{\nabla}^s \boldsymbol{u})_Q \end{aligned} \tag{411}$$

and

$$(\boldsymbol{W}, \boldsymbol{F}) = (\boldsymbol{w}, \boldsymbol{f})_Q + (\boldsymbol{w}(0^+), \boldsymbol{u}(0^-))_\Omega. \tag{412}$$

This formulation implies weak satisfaction of the momentum equations and incompressibility constraint, in addition to the initial condition. The boundary condition is built into the definition of $\mathcal{V}$.

Remarks

1. $\boldsymbol{u}(0^-)$ is viewed as known when computing the solution in Q.
2. The standard weak formulation corresponding to the discontinuous Galerkin method with respect to time is obtained by replacing $[0, T]$ by $[t_n, t_{n+1}]$, $n = 0, 1, 2, \ldots$ and summing over the space-time slabs

$$Q_n = \Omega \times]t_n, t_{n+1}[\ . \tag{413}$$

In this case, (410)-(412) are viewed as the variational equations for a typical slab.

3. The conditions $\boldsymbol{\nabla} \cdot \boldsymbol{u} = 0$ on Q and $\boldsymbol{u} = \boldsymbol{0}$ on P imply

$$(\boldsymbol{\nabla}\boldsymbol{u}, \boldsymbol{u} \otimes \boldsymbol{u})_Q = 0 \ . \tag{414}$$

In the discrete case this term may need to be altered to preserve this property. See Quarteroni and Valli (1994), p.435.

Kinetic energy decay inequality:

Substitution of $\boldsymbol{U}$ for $\boldsymbol{W}$ in (410) leads to the inequality

$$\tfrac{1}{2}\left\|\boldsymbol{u}(T^-)\right\|_\Omega^2 \ + \ 2\nu\|\boldsymbol{\nabla}^s\boldsymbol{u}\|_Q^2 \ \leq \ \tfrac{1}{2}\left\|\boldsymbol{u}(0^-)\right\|_\Omega^2 \ + \ (\boldsymbol{u}, \boldsymbol{f})_Q \tag{415}$$

from which follows

$$\tfrac{1}{2}\left\|\boldsymbol{u}(T^-)\right\|_\Omega^2 \ + \ \nu\|\boldsymbol{\nabla}^s\boldsymbol{u}\|_Q^2 \ \leq \ \tfrac{1}{2}\left\|\boldsymbol{u}(0^-)\right\|_\Omega^2 \ + \ \frac{C_\Omega}{4\nu}\|\boldsymbol{f}\|_Q^2 \ , \tag{416}$$

where C_Ω is the constant in the Poincaré inequality:

$$\|\boldsymbol{u}\|_\Omega^2 \ \leq \ C_\Omega\|\boldsymbol{\nabla}^s\boldsymbol{u}\|_\Omega^2 \ . \tag{417}$$

6.4.2. Separation of scales Let

$$\mathcal{V} = \overline{\mathcal{V}} \oplus \mathcal{V}' \tag{418}$$

The reader is reminded that $\overline{\mathcal{V}}$ is identified with a standard **finite element space** and $\mathcal{V}'$ is ∞-dimensional. In the discrete case, $\mathcal{V}'$ can be replaced with various finite-dimensional approximations, such as hierarchical p-refinement, bubbles, etc. In any case, (418) enables decomposition of (410) into two sub-problems:

$$B(\overline{\boldsymbol{W}}, \overline{\boldsymbol{U}} + \boldsymbol{U}') \ = \ (\overline{\boldsymbol{W}}, \boldsymbol{F}) \tag{419}$$
$$B(\boldsymbol{W}', \overline{\boldsymbol{U}} + \boldsymbol{U}') \ = \ (\boldsymbol{W}', \boldsymbol{F}) \tag{420}$$

where

$$\boldsymbol{U} \ = \ \overline{\boldsymbol{U}} + \boldsymbol{U}' \tag{421}$$
$$\boldsymbol{W} \ = \ \overline{\boldsymbol{W}} + \boldsymbol{W}' \tag{422}$$

in which $\overline{\boldsymbol{U}}, \overline{\boldsymbol{W}} \in \overline{\mathcal{V}}$ and $\boldsymbol{U}', \boldsymbol{W}' \in \mathcal{V}'$.

It is important to realize that although the use of the over-bar and prime notations continues to connote large and small scales, the meaning is quite different than for the classical LES formulation considered previously. Here $\overline{\boldsymbol{U}}$ and $\boldsymbol{U}'$ may be thought of as "projections" of $\boldsymbol{U}$ onto $\overline{\mathcal{V}}$ and $\mathcal{V}'$, respectively. The terminology "projections" is used loosely because $\overline{\boldsymbol{U}}$ and $\boldsymbol{U}'$ are obtained from $\boldsymbol{U}$ by solving coupled **nonlinear** problems, viz.,

$$B(\overline{\boldsymbol{W}}, \overline{\boldsymbol{U}} + \boldsymbol{U}') \ = \ B(\overline{\boldsymbol{W}}, \boldsymbol{U}) \tag{423}$$
$$B(\boldsymbol{W}', \overline{\boldsymbol{U}} + \boldsymbol{U}') \ = \ B(\boldsymbol{W}', \boldsymbol{U}) \ . \tag{424}$$

Consequently, it is not possible to identify a simple filtering relationship between $\overline{\boldsymbol{U}}$ and $\boldsymbol{U}$, such as (385)-(386). Nevertheless, $\overline{\boldsymbol{U}}$ represents the part of $\boldsymbol{U}$ which lives in $\overline{\mathcal{V}}$, and thus clearly is a large-scale representation of $\boldsymbol{U}$. Likewise, $\boldsymbol{U}'$ is a small-scale representation of $\boldsymbol{U}$.

The relationship between the present $\overline{\boldsymbol{U}}$ and its filtered counterpart is a complex mathematical problem. Reference may be made to Galdi and Layton (2000) and John and Layton (1998) for initiatory attempts at its resolution.

Let

$$B_1(\boldsymbol{W},\overline{\boldsymbol{U}},\boldsymbol{U}') = \left.\frac{d}{d\varepsilon}B(\boldsymbol{W},\overline{\boldsymbol{U}}+\varepsilon\boldsymbol{U}')\right|_{\varepsilon=0} \tag{425}$$

$$B_2(\boldsymbol{W},\overline{\boldsymbol{U}},\boldsymbol{U}') = \left.\frac{d^2}{d\varepsilon^2}B(\boldsymbol{W},\overline{\boldsymbol{U}}+\varepsilon\boldsymbol{U}')\right|_{\varepsilon=0} . \tag{426}$$

With these, write

$$B(\boldsymbol{W},\overline{\boldsymbol{U}}+\boldsymbol{U}') = B(\boldsymbol{W},\overline{\boldsymbol{U}}) \; + \; B_1(\boldsymbol{W},\overline{\boldsymbol{U}},\boldsymbol{U}') \; + \; \tfrac{1}{2}B_2(\boldsymbol{W},\overline{\boldsymbol{U}},\boldsymbol{U}') \tag{427}$$

where

$$\tfrac{1}{2}B_2(\boldsymbol{W},\overline{\boldsymbol{U}},\boldsymbol{U}') = - \left(\boldsymbol{\nabla}\boldsymbol{w},\boldsymbol{u}'\otimes\boldsymbol{u}'\right)_Q \tag{428}$$

and

$$B_1(\boldsymbol{W},\overline{\boldsymbol{U}},\boldsymbol{U}') \;\; = \;\; \left(\boldsymbol{w}(T^-),\boldsymbol{u}'(T^-)\right)_\Omega - \left(\frac{\partial\boldsymbol{w}}{\partial t},\boldsymbol{u}'\right)_Q - (\boldsymbol{\nabla}\boldsymbol{w},\overline{\boldsymbol{u}}\otimes\boldsymbol{u}'+\boldsymbol{u}'\otimes\overline{\boldsymbol{u}})_Q$$

$$+ (q,\boldsymbol{\nabla}\cdot\boldsymbol{u}')_Q - (\boldsymbol{\nabla}\cdot\boldsymbol{w},p')_Q + (\boldsymbol{\nabla}^s\boldsymbol{w},2\nu\boldsymbol{\nabla}^s\boldsymbol{u}')_Q . \tag{429}$$

$B_1(\boldsymbol{W},\overline{\boldsymbol{U}},\boldsymbol{U}')$ is the ***linearized*** Navier-Stokes operator. With the aid of (427)-(429), rewrite (419) and (420) as

$$B(\overline{\boldsymbol{W}},\overline{\boldsymbol{U}}) + B_1(\overline{\boldsymbol{W}},\overline{\boldsymbol{U}},\boldsymbol{U}') \;\; = \;\; (\boldsymbol{\nabla}\overline{\boldsymbol{w}},\boldsymbol{u}'\otimes\boldsymbol{u}')_Q + (\overline{\boldsymbol{W}},\boldsymbol{F}) \tag{430}$$

$$B_1(\boldsymbol{W}',\overline{\boldsymbol{U}},\boldsymbol{U}') - (\boldsymbol{\nabla}\boldsymbol{w}',\boldsymbol{u}'\otimes\boldsymbol{u}')_Q \;\; = \;\; -\left[B(\boldsymbol{W}',\overline{\boldsymbol{U}}) - (\boldsymbol{W}',\boldsymbol{F})\right] . \tag{431}$$

This amounts to a pair of coupled, nonlinear variational equations. Given the small scales (i.e., $\boldsymbol{U}'$), (430) enables solution for the large scales (i.e., $\overline{\boldsymbol{U}}$). Likewise, the large scales drive the small scales through (431). Note, the right hand side of (431) is the ***residual of the large scales projected onto*** $\mathcal{V}'$.

Remark

The subgrid-scale stress, $\boldsymbol{T}$ (see (395)), may be decomposed into the Reynolds stress, cross stress and Leonard stress. In the variational formulation, the analogs of these terms are:

$$(\boldsymbol{\nabla}\overline{\boldsymbol{w}},\boldsymbol{u}'\otimes\boldsymbol{u}')_Q \qquad\qquad \text{(Reynolds stress)} \tag{432}$$

$$(\boldsymbol{\nabla}\overline{\boldsymbol{w}},\overline{\boldsymbol{u}}\otimes\boldsymbol{u}'+\boldsymbol{u}'\otimes\overline{\boldsymbol{u}})_Q \qquad\qquad \text{(Cross stress)} \tag{433}$$

$$(\boldsymbol{\nabla}\overline{\boldsymbol{w}},\overline{\boldsymbol{u}}\otimes\overline{\boldsymbol{u}})_Q - (\boldsymbol{\nabla}\boldsymbol{w},\overline{\boldsymbol{u}}\otimes\overline{\boldsymbol{u}})_Q = -(\boldsymbol{\nabla}\boldsymbol{w}',\overline{\boldsymbol{u}}\otimes\overline{\boldsymbol{u}})_Q \qquad\qquad \text{(Leonard stress)} \tag{434}$$

Note that (432)-(433) appear in (430), and (434) appears in the right-hand side of (431). Up to this point our results are ***exact***, that is, nothing has been omitted and no modeling has been performed.

6.4.3. Modeling of subgrid scales Observe that closure is not the motivation for modeling in the case of the variational multiscale formulation. In fact, there is **no** closure problem whatsoever. The need for modeling is due simply to the inability of typical discrete approximations to properly represent all necessary scales. This is viewed as a conceptual advantage of projection/variational methods over the classical filtered equation approach.

Thus, add $\left(\boldsymbol{\nabla} \boldsymbol{w}', \boldsymbol{R}_S'\right)_Q$ to (431), where

$$\boldsymbol{R}_S' = 2\nu_T' \boldsymbol{\nabla}^s \boldsymbol{u}' \ . \tag{435}$$

(Specification of ν_T' will be postponed for the moment.) The end result is

$$B'(\boldsymbol{W}', \overline{\boldsymbol{U}}, \boldsymbol{U}') = -\left[B(\boldsymbol{W}', \overline{\boldsymbol{U}}) - \left(\boldsymbol{W}', \boldsymbol{F}\right)\right] \tag{436}$$

where

$$B'(\boldsymbol{W}', \overline{\boldsymbol{U}}, \boldsymbol{U}') \equiv B_1(\boldsymbol{W}', \overline{\boldsymbol{U}}, \boldsymbol{U}') - (\boldsymbol{\nabla} \boldsymbol{w}', \boldsymbol{u}' \otimes \boldsymbol{u}')_Q + (\boldsymbol{\nabla}^s \boldsymbol{w}', 2\nu_T' \boldsymbol{\nabla}^s \boldsymbol{u}')_Q \ . \tag{437}$$

This is the modeled small-scale equation which replaces (431). The large-scale equation, (430), remains the same, that is, there is **no** modeling.

Remark

Collis (2001) has presented an interpretation of this formulation that is more consistent with traditional turbulence modeling concepts. He assumes

$$\boldsymbol{u} \ = \ \overline{\boldsymbol{u}} + \boldsymbol{u}' + \boldsymbol{u}'' \tag{438}$$

$$\boldsymbol{w} \ = \ \overline{\boldsymbol{w}} + \boldsymbol{w}' + \boldsymbol{w}'' \tag{439}$$

and

$$\mathcal{V} = \overline{\mathcal{V}} \oplus \mathcal{V}' \oplus \mathcal{V}'' \tag{440}$$

where $\overline{\mathcal{V}}$ and $\mathcal{V}'$ are the same finite-dimensional spaces considered here and $\mathcal{V}''$ is infinite-dimensional. Thus the discrete approximation amounts to simply omitting $\mathcal{V}''$. The idea is schematically illustrated in Figure 36. Collis (2001) may also be consulted for clarifications to the formulation.

6.4.4. Eddy viscosity models Two candidate definitions of ν_T' will be considered. In both cases, parameters will be estimated by way of the Lilly analysis (see Section 6.3.1). However, this time there are two relevant wave-number scales: $\bar{k}$, the resolution limit of the space $\overline{\mathcal{V}}$, and k', the resolution limit of the space $\mathcal{V} = \overline{\mathcal{V}} \oplus \mathcal{V}'$. The interpretation of $\bar{k}$ is assumed to be similar to before (see Section 6.3.1). Figure 37 schematically contrasts the present situation with classical LES.
Note that in generalizing the Lilly analysis to the current situation, it is necessary to calculate spectral integrals over the interval $[\bar{k}, k']$ (see Fig. 38). Consequently, it is assumed this interval lies entirely within the inertial subrange.

The assumed forms of ν_T' are:

$$\nu_T' = (C_S' \Delta')^2 \left|\boldsymbol{\nabla}^s \boldsymbol{u}'\right| \tag{441}$$
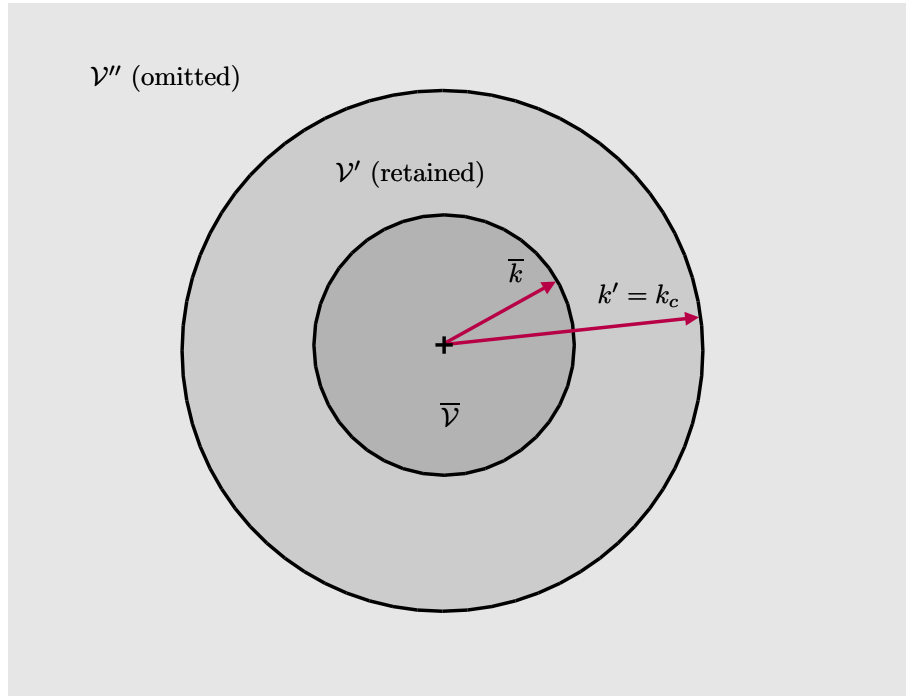
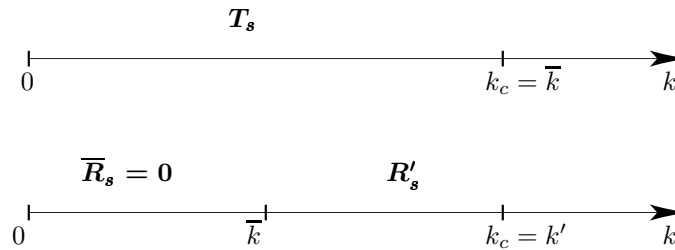Figure 36. Collis interpretation of the variational multiscale formulation.

Figure 37. Above: in classical LES, the subgrid-scale stress, $\boldsymbol{T}_S$, acts on all scales present, namely $k \in [0, \overline{k}]$. Below: in the multiscale model, the model acts only on the small scales, namely $k \in [\overline{k}, k']$.

and

$$\nu'_T = (C'_S \Delta')^2 \, |\boldsymbol{\nabla}^s \overline{\boldsymbol{u}}| \quad . \tag{442}$$

In the first case, ν'_T depends exclusively on small-scale velocity components. In the second case, ν'_T depends on the large-scale components.

As before, $|\boldsymbol{\nabla}^s \overline{\boldsymbol{u}}|$ is evaluated through (403) and (404); the small-scale counterpart is
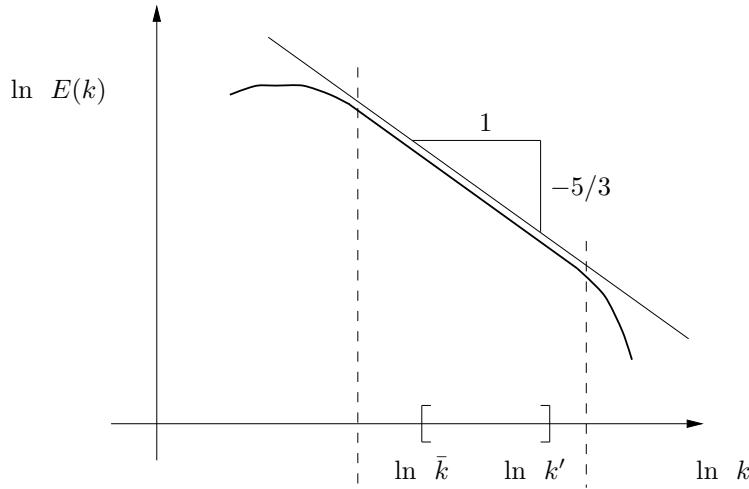
Figure 38. Kolmogorov energy spectrum. The interval of small scales is assumed to lie within the inertial subrange.

evaluated with (403) and

$$\tfrac{1}{2}\left|\boldsymbol{\nabla}^s \boldsymbol{u}'\right|^2 = \int_{\bar{k}}^{k'} k^2 E(k)\ dk\ . \tag{443}$$

With this result in hand, calculations similar to (405) yield:

$$C_S' \Delta' = \left(\frac{2}{3\alpha}\right)^{3/4} \bar{k}^{-1}\ [(k'/\bar{k})^{4/3} - 1]^{-3/4} \tag{444}$$

$$C_S' \Delta' = \left(\frac{2}{3\alpha}\right)^{3/4} \bar{k}^{-1}\ [(k'/\bar{k})^{4/3} - 1]^{-1/2} \tag{445}$$

corresponding to (441) and (442), respectively. For a given discretization, from which $\bar{k}$ and k' can be determined, (444) and (445) provide estimates of $C_S'\Delta'$ for the two cases considered.

Remarks

1. Note that fixing $\bar{k}$ in (444) and (445) implies that

$$k'\quad \uparrow \downarrow \quad \Leftrightarrow \quad C_S'\Delta'\quad \downarrow \uparrow \tag{446}$$

   for both cases, confirming the intuitively obvious result that the inclusion of more small scales reduces the size of $C_S'\Delta'$, and vice versa. If $\Delta' = \pi\bar{k}^{-1}$, as in Remark 1 of Section 6.3.1, (444) and (445) show that C_S' is just a function of the Kolmogorov constant, α, and the ratio $k'/\bar{k}$.

2. The argument can also be reversed: For fixed $\bar{k}$ and $C'_S\Delta' = C_S\Delta$ (i.e., the value for the classical Smagorinsky model), what is k'? The answer to this question estimates the size of $\mathcal{V}'$ in comparison with $\overline{\mathcal{V}}$. It turns out that for both (444) and (445),

$$k' = 2^{3/4}\bar{k} \;\approx\; 1.7\bar{k} \;. \tag{447}$$

Roughly speaking, the resolution limit needs to be almost twice as great. If it is assumed that

$$k'/\bar{k} = \bar{h}/h', \tag{448}$$

(447) implies

$$h' = \bar{h}/2^{3/4} \;\approx\; 0.6\bar{h} \;, \tag{449}$$

which amounts to a finer mesh by almost a factor of two in each direction.

3. An even more attractive option may be the analytical determination of $\boldsymbol{U}'$ and its *a priori* elimination from the large-scale equation, that is, (430). This gives rise to a **nonlinear stabilized method**. Note that for (447)-(449), as before,

$$C'_S\Delta' \;=\; O(\bar{h}) \tag{450}$$
$$\nu'_T \;=\; O(\bar{h}^{4/3}) \;. \tag{451}$$

However, keep in mind that $\boldsymbol{R}'_S$ only acts on the small scales.

6.4.5. Précis of results For convenience, the main LES/variational multiscale equations are summarized here:

Large scales

$$B(\overline{\boldsymbol{W}},\overline{\boldsymbol{U}}) + B_1(\overline{\boldsymbol{W}},\overline{\boldsymbol{U}},\boldsymbol{U}') \;=\; (\boldsymbol{\nabla}\overline{\boldsymbol{w}}, \boldsymbol{u}' \otimes \boldsymbol{u}')_Q + (\overline{\boldsymbol{W}}, \boldsymbol{F}) \tag{452}$$

Small scales

$$B_1(\boldsymbol{W}',\overline{\boldsymbol{U}},\boldsymbol{U}') - (\boldsymbol{\nabla}\boldsymbol{w}', \boldsymbol{u}' \otimes \boldsymbol{u}')_Q \;=\; -\left[B(\boldsymbol{W}',\overline{\boldsymbol{U}}) - (\boldsymbol{W}', \boldsymbol{F})\right] \tag{453}$$

Modeled small scales

$$B'(\boldsymbol{W}',\overline{\boldsymbol{U}},\boldsymbol{U}') = -\left[B(\boldsymbol{W}',\overline{\boldsymbol{U}}) - (\boldsymbol{W}', \boldsymbol{F})\right] \tag{454}$$

where

$$B'(\boldsymbol{W}',\overline{\boldsymbol{U}},\boldsymbol{U}') = B_1(\boldsymbol{W}',\overline{\boldsymbol{U}},\boldsymbol{U}') - (\boldsymbol{\nabla}\boldsymbol{w}', \boldsymbol{u}' \otimes \boldsymbol{u}')_Q + (\boldsymbol{\nabla}^s\boldsymbol{w}', 2\nu'_T\boldsymbol{\nabla}^s\boldsymbol{u}')_Q \tag{455}$$

and

$$\nu'_T = (C'_S\Delta')^2 \,|\boldsymbol{\nabla}^s\boldsymbol{u}'| \tag{456}$$

or

$$\nu'_T = (C'_S\Delta')^2 \,|\boldsymbol{\nabla}^s\overline{\boldsymbol{u}}| \;. \tag{457}$$

Modeled system

A concise way of writing the combined system of (452) and (454) is

$$\overline{B}(\boldsymbol{W},\boldsymbol{U}) = (\boldsymbol{W},\boldsymbol{F}) \tag{458}$$

where

$$\overline{B}(\boldsymbol{W},\boldsymbol{U}) \equiv B(\boldsymbol{W},\boldsymbol{U}) + (\boldsymbol{\nabla}^s \boldsymbol{w}', 2\nu_T' \boldsymbol{\nabla}^s \boldsymbol{u}')_Q \ . \tag{459}$$

Kinetic energy decay inequality for the modeled system

This follows immediately from (458) with $\boldsymbol{W}$ replaced by $\boldsymbol{U}$:

$$\tfrac{1}{2}\left|\left|\boldsymbol{u}(T^-)\right|\right|_\Omega^2 + 2\nu\left|\left|\boldsymbol{\nabla}^s\boldsymbol{u}\right|\right|_Q^2 + \left|\left|(2\nu_T')^{1/2}\boldsymbol{\nabla}^s\boldsymbol{u}'\right|\right|_Q^2 \leq \tfrac{1}{2}\left|\left|\boldsymbol{u}(0^-)\right|\right|_\Omega^2 + (\boldsymbol{u},\boldsymbol{f})_Q \tag{460}$$

which leads to

$$\tfrac{1}{2}\left|\left|\boldsymbol{u}(T^-)\right|\right|_\Omega^2 + \nu\left|\left|\boldsymbol{\nabla}^s\boldsymbol{u}\right|\right|_Q^2 + \left|\left|(2\nu_T')^{1/2}\boldsymbol{\nabla}^s\boldsymbol{u}'\right|\right|_Q^2 \leq \tfrac{1}{2}\left|\left|\boldsymbol{u}(0^-)\right|\right|_\Omega^2 + \frac{C_\Omega}{4\nu}\left|\left|\boldsymbol{f}\right|\right|_Q^2 \ . \tag{461}$$

Remarks

1. Note, if $\overline{\boldsymbol{U}}$ is an exact solution of the Navier-Stokes equations, then

$$B(\boldsymbol{W},\overline{\boldsymbol{U}}) = (\boldsymbol{W},\boldsymbol{F}) \qquad \forall \boldsymbol{W} \in \mathcal{V} \ . \tag{462}$$

   In particular,

$$B(\boldsymbol{W}',\overline{\boldsymbol{U}}) = (\boldsymbol{W}',\boldsymbol{F}) \qquad \forall \boldsymbol{W}' \in \mathcal{V}' \ . \tag{463}$$

   Consequently, for both the exact and the modeled small-scale equations (i.e., (453) and (454), respectively), it follows that $\boldsymbol{U}' = \boldsymbol{0}$. From (462), it also follows that

$$B(\overline{\boldsymbol{W}},\overline{\boldsymbol{U}}) = (\overline{\boldsymbol{W}},\boldsymbol{F}) \qquad \forall \overline{\boldsymbol{W}} \in \overline{\mathcal{V}} \ . \tag{464}$$

   These results verify that (452) is identically satisfied. This means the equation governing the large scales retains its **consistency**, or residual structure, despite the modeling of small scales, in contrast to the classical LES case described in Section 6.2.

2. By virtue of the fact that $\boldsymbol{U}' = \{\boldsymbol{u}',p'\} \in \mathcal{V}' \subset \mathcal{V}$, $\boldsymbol{u}' = \boldsymbol{0}$ on P. Furthermore, the small-scales equations (either (453) or (454)) imply $\boldsymbol{\nabla} \cdot \boldsymbol{u}' = 0$ on Q. From this it may be concluded that $\boldsymbol{u}'$ attains the correct asymptotic structure near walls by the usual argument. In particular, the [1,2] component of $\boldsymbol{u}' \otimes \boldsymbol{u}'$ in (452) behaves like x_2^3, where x_1 is the streamwise direction and x_2 is the direction normal to the wall.

6.5. Relationship with other methods

6.5.1. Nonlinear Galerkin method The approach has both similarities to, and differences with, the work of Temam and colleagues. The similarities are that both approaches invoke scale separation from the outset and both employ projected forms of the Navier-Stokes equations, rather than the filtered versions used in classical LES. The salient differences are as follows: In the earlier work of the Temam group (see Dubois, Jauberteau and Temam, 1993 for a representative exposition):

  (i) In the equation governing large-scales, the classical Reynolds stress term is neglected.
  (ii) In the equation governing small scales, the only term acting on small scales which is retained is the Stokes operator term. In particular, the cross-stress, time-derivative and small-scale Reynolds stress terms are neglected.

These assumptions are strong ones and can be shown to limit the applicability of the approach to discretizations which are only somewhat coarser than required for a fully-resolved direct numerical simulation (DNS). Otherwise excessive dissipation is encountered. This may be contrasted with the present approach in which all these terms are retained. Obviously, it is assumed here to be important to retain the terms omitted in the Temam's group earlier work. In addition, a model is added to the equation governing the small scales in the present case.

In more recent work (see Dubois, Jauberteau and Temam, 1998), Temam and co-workers retain all the terms omitted in their previous work and employ an adaptive strategy in space and time to resolve small-scale behavior. This seems to be a DNS approach, although Dubois, Jauberteau and Temam (1998) characterize it as somewhere between LES and DNS. The present approach is similar, except for the model in the small-scale equation. It is felt appropriate to characterize the present formulation as LES, or at least closer to LES than that of Dubois, Jauberteau and Temam (1998).

6.5.2. Adaptive wavelet decomposition Farge, Schneider and Kevlahan (1999) present a very interesting analysis of two-dimensional turbulence based on an adaptive wavelet decomposition of the vorticity into coherent, non-Gaussian structures, and an incoherent, Gaussian background. The efficiency of the wavelet representation is illustrated in a DNS computation of a mixing layer in which the time evolution of the coherent part only involves 8% of the wavelet coefficients. The remaining coefficients, associated with the incoherent part, are simply discarded at each time step. In order to maximize data compression, the velocity-vorticity form of the Navier-Stokes equations is employed in preference to the velocity-pressure form.

The wavelet decomposition at each time step is an example of *a priori* scale separation, as advocated in the present work. However, when Farge, Schneider and Kevlahan (1999) discuss modeling they do so in the context of the filtered form of the equations, as in classical LES, and are faced with the problem of representing the subgrid-scale stress $\boldsymbol{T}$. They propose the following possibilities: *(i)* The Smagorinsky model; *(ii)* a dynamic generalization in which the eddy viscosity ν_T is estimated in terms of the enstrophy fluxes in wavelet space, such that when energy flows from large to small scales ν_T will be positive and vice versa (i.e., backscatter); and *(iii)* the subgrid-scale stress $\boldsymbol{T}$ modeled as a Gaussian forcing term proportional to the variance of the incoherent parts of the vorticity and velocity. In modeling $\boldsymbol{T}$ in these ways it seems inevitable that at least some of the shortcomings associated with the use of the filtered
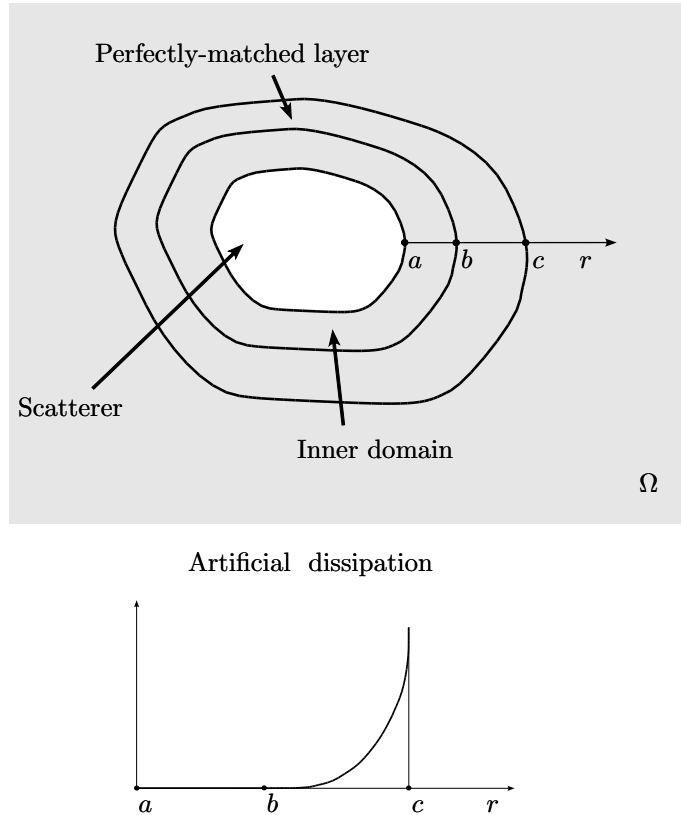
Figure 39. The perfectly-matched layer.

equations will eventually be encountered. For example, $\boldsymbol{T}$ may act too strongly on the coherent (i.e., resolved) structures, and there seems no *a priori* control of kinetic energy if backscatter occurs. However, it would seem possible to reformulate the numerical procedure in terms of the variational multiscale method, associating coherent structures with the space $\overline{\mathcal{V}}$ and the incoherent background with $\mathcal{V}'$. In this way some difficulties might be circumvented, but the efficiency of the method might also be compromised.

6.5.3. Perfectly-matched layer in electromagnetics and acoustics   Consider an exterior infinite domain $\Omega \subset \mathbb{R}^d$, $d = 1, 2$, or 3. In electromagnetic wave propagation there is interest in solving exterior infinite-domain problems with finite elements. A finite region is introduced, discretized by finite elements and surrounded by a truncated boundary. The situation is seen to be the same as for the acoustics problem considered previously in Section 2, but here there is no attempt to solve the far-field problem exactly and severe restrictions are not placed on the shape of the external region. For example, the external region need not be amenable

to a separation-of-variables solution, as is required for the Dirchlet-to-Neumann formulation considered in Section 2. In order to absorb out-going waves and to prevent spurious reflections, a finite layer is introduced in which the properties of the medium are artificially altered to be dissipative. The dissipation in the layer is designed to match that of the inner region at the interface, which is typically non-dissipative, and to progressively increase further into the layer. To ensure a smooth transition between the inner region and the layer, the dissipation coefficient is assumed to be zero, and to have zero derivative, at the interface. A quadratic variation is seen to be a simple way to achieve the desired dissipative properties in the layer, and is one often used in practice (see Fig. 39.) The dissipative layer is said to be "perfectly matched." The simplicity, generality and effectiveness of the approach have led to its popularity in electromagnetics, despite the lack of a rigorous theory to support the precise variation and amplitude of artificial dissipation. Harari, Turkel and Slavutin (2000) may be referred to for a penetrating analysis and references to important literature. The perfectly-matched layer has features in common with ideas and techniques used in turbulence as evidenced by the following.
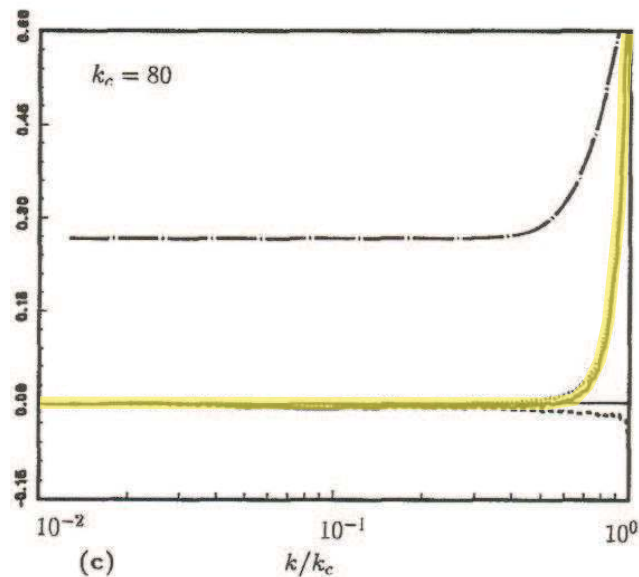

Figure 40. DNS Results for homogeneous turbulence, Domaradzki et al. , $Re_\lambda = 70$ (Taylor microscale Reynolds number).

Remarks

1. The concept of "spectral eddy viscosity," introduced by Heisenberg (1948), has undergone extensive study in the turbulence literature (see, e.g., Kraichnan, 1976; Domaradzki, Liu and Brachet, 1993; Domaradzki et al., 1994; McComb and Young, 1998). The idea is to take the spatial Fourier transform of the Navier-Stokes equations,
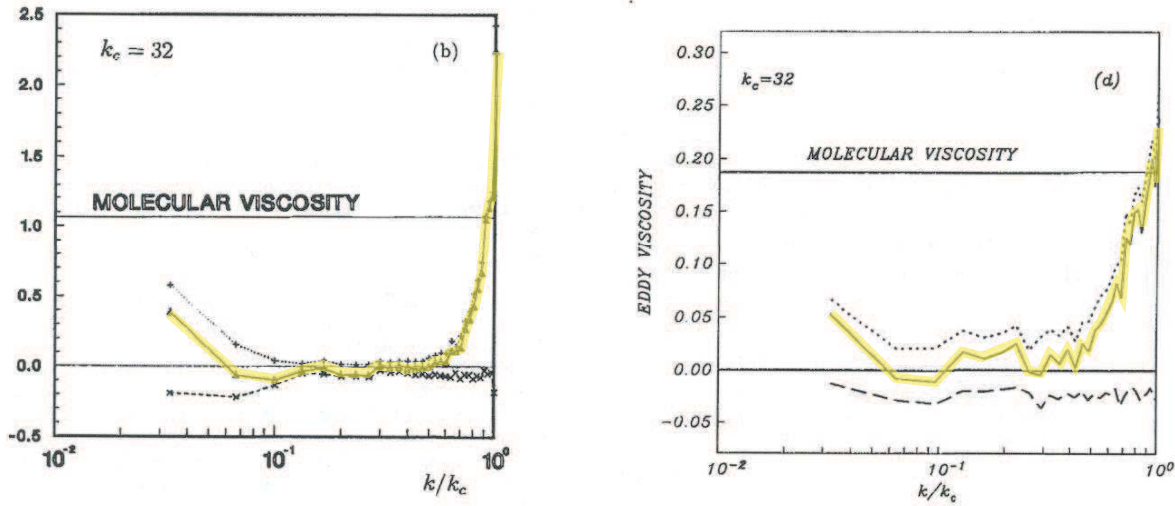
Figure 41. DNS results for wall-bounded flow, Domaradzki et al. , $Re_\tau = 210$ (Reynolds number based on friction velocity).

and eliminate the pressure by projection onto the space of divergence-free modes,

$$\frac{\partial \hat{\boldsymbol{u}}(\boldsymbol{k})}{\partial t} = -\nu k^2 \hat{\boldsymbol{u}}(\boldsymbol{k}) + N(\boldsymbol{k}|\hat{\boldsymbol{u}}(\boldsymbol{q}), \hat{\boldsymbol{u}}(\boldsymbol{p})) \tag{465}$$

Here, $\boldsymbol{k}$, $\boldsymbol{p}$, and $\boldsymbol{q}$ are wave vectors and $N(\boldsymbol{k}|\hat{\boldsymbol{u}}(\boldsymbol{q}), \hat{\boldsymbol{u}}(\boldsymbol{p}))$ is the Fourier transform of the nonlinear term. Equation (465) is then multiplied by the complex conjugate of the Fourier coefficient, namely $\hat{\boldsymbol{u}}^*(\boldsymbol{k})$, and integrated over spherical surfaces of radius $k = |\boldsymbol{k}|$ in wave-vector space, to derive an evolution equation for the energy spectrum, $E(k)$,

$$\frac{\partial E(k)}{\partial t} = -2\nu k^2 E(k) + T(k|\hat{\boldsymbol{u}}(\boldsymbol{q}), \hat{\boldsymbol{u}}(\boldsymbol{p})) \tag{466}$$

where $T(k|\hat{\boldsymbol{u}}(\boldsymbol{q}), \hat{\boldsymbol{u}}(\boldsymbol{p}))$ is referred to as the **energy transfer term**. It represents the energy transferred from the spherical surface of radius k, to Fourier modes with wave numbers $\boldsymbol{p}$ and $\boldsymbol{q}$. This equation can be given a numerical analysis interpretation by introducing a cutoff, k_c, and thinking of it as representing the limit of resolution of a discretization, in this case, spectral truncation. All Fourier modes with wave-vector amplitude larger than k_c are viewed as missing. The interesting case is energy transfer for wave numbers $k < k_c$. It makes sense to split the energy transfer term into two parts as follows:

$$\frac{\partial E(k)}{\partial t} = -2\nu k^2 E(k) + T_<(k|\hat{\boldsymbol{u}}(\boldsymbol{q}), \hat{\boldsymbol{u}}(\boldsymbol{p})) + T_>(k|\hat{\boldsymbol{u}}(\boldsymbol{q}), \hat{\boldsymbol{u}}(\boldsymbol{p})) \tag{467}$$

where $T_<(k|\hat{\boldsymbol{u}}(\boldsymbol{q}), \hat{\boldsymbol{u}}(\boldsymbol{p}))$ assumes $\boldsymbol{p}$ and $\boldsymbol{q}$ are smaller in magnitude than k_c, hence $T_<$ is exactly included in the numerical model, and $T_>(k|\hat{\boldsymbol{u}}(\boldsymbol{q}), \hat{\boldsymbol{u}}(\boldsymbol{p}))$ assumes at least one of $\boldsymbol{p}$ and $\boldsymbol{q}$ is larger in magnitude than k_c, hence $T_>$ is omitted in the numerical model. One
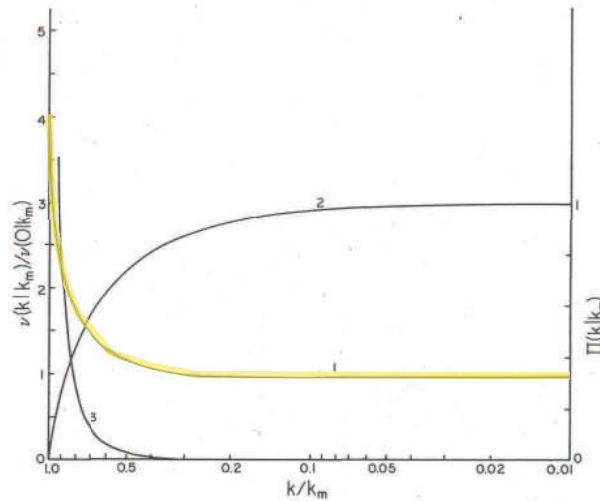
Figure 42. Direct-interaction approximation (DIA) results for homogeneous turbulence from Kraichnan.

view of the modeling problem in turbulence is to approximately represent this omitted term. Since it typically represents a flow of energy from the surface of radius k to modes beyond the cutoff, it has been customary to rescale it as a **spectral eddy viscosity**, that is,

$$\nu_T(k) = \frac{-T_>(k|\hat{\boldsymbol{u}}(\boldsymbol{q}), \hat{\boldsymbol{u}}(\boldsymbol{p}))}{2k^2 E(k)} \tag{468}$$

Theoretical studies of Kraichnan (1976), assuming infinite Reynolds number, suggested the form of $\nu_T(k)$ involves a plateau at low wave number and cusp at higher wave number, peaking at the cutoff (see Fig. 42). Initial studies of DNS data bases (well-resolved turbulent solutions at low Reynolds number) confirmed the presence of the cusp, but the plateau was at zero, rather than the value predicted by the Kraichnan theory (see Fig's. 40 and 41 from Domaradzki, Liu and Brachet, 1993; Domaradzki et al., 1994). The issue was clarified by McComb and Young (1998) who studied a higher Reynolds number flow and systematically varied the location of the cutoff k_c. The cusp is clearly apparent in all cases, but the plateau also emerges at a very low value of the cutoff (see Fig. 43). Keeping in mind that a spectral eddy viscosity model acts as an artificial viscosity and, due to the predominance of the cusp, it is very reminiscent of the cusp-like structure of the artificial dissipation employed in the perfectly-matched layer. Both mechanisms attempt to remove information which would be transferred to scales present in the numerical approximations. This amounts to an analogy between wave-vector space behavior, in the case of turbulence, with physical space behavior, in the case of the perfectly-matched layer. The latter case is hyperbolic, and the former represents, in aggregate, an almost hyperbolic phenomenon in wave-vector space. It is interesting that similar dissipative mechanisms are used to represent seemingly very different phenomena, namely, radiation damping in the electromagnetic case, a linear
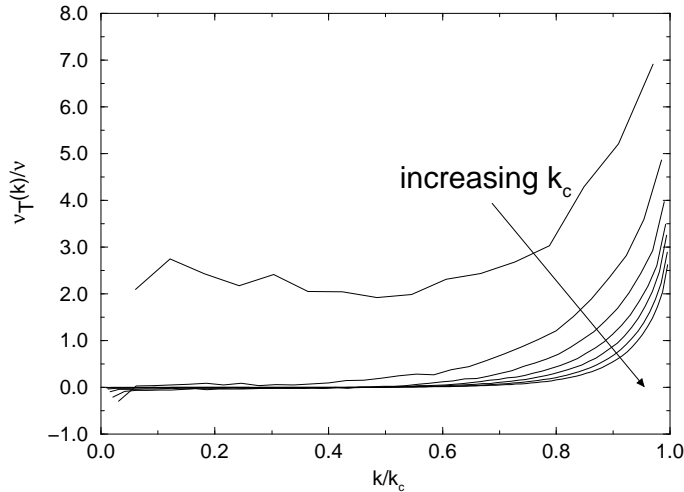
Figure 43. DNS results from McComb & Young on a 256^3 mesh at $Re_\lambda = 190$, $16.5 < k_c < 112.5$.

hyperbolic mechanism in physical space, and energy transfers due to nonlinearities in turbulence, which become nonlocal interactions in wave-vector space. The predominance of the cusp in both cases suggests a similar mechanism may be present. In fact, it can be shown in the case of turbulence that the cusp is produced by *linearized* interactions (i.e., "cross stress" terms) and the transfers are confined to a spherical layer in wave-vector space of precisely twice the radius of the cutoff, k_c (see Hughes, Wells and Wray, 2003).

2. The version of the variational multiscale method described previously may be thought of as an approximation of spectral eddy viscosity in that the artificial viscosity inspired by the Smagorinsky model is assumed to act only in a high wave-number layer in spectral space (see Fig. 44). Likewise, it may be thought of as a wave-vector interpretation of the perfectly-matched layer, although no attempt has so far been made to attain a smooth match.

3. "Hyperviscosities" in spectral formulations (see, e.g., Borue and Orszag, 1994,1996), which are also cusp-like, may be viewed as approximations of spectral eddy viscosity. As pointed out by Cerutti, Meneveau and Knio (2000), however, their behavior in physical space does not correlate very well with turbulent energy transfers. When inverse transformed to physical space, hyperviscosities lead to higher-order spatial differential operators, which cannot be easily implemented in many numerical methods such as, for example, finite elements.

6.5.4. Dissipative structural dynamics time integrators   It was observed many years ago that it was important to introduce dissipative mechanisms in structural dynamics time integrators to prevent spurious oscillations and dangerous "overshoot phenomena" in high frequencies, which turn out to be equivalent to high wave-vector components (see Hughes, 1987, Chapter 9, and references therein). In structural dynamics it was argued that time integrators could
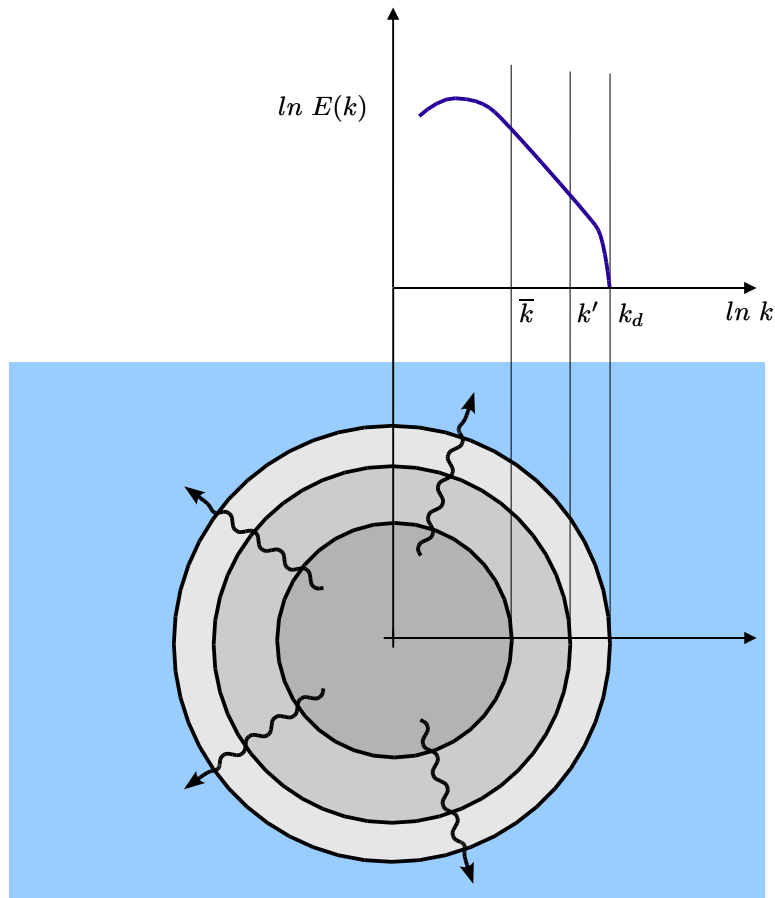
Figure 44. In three-dimensional turbulence, energy transfers in spectral space cascade from small wave number to large wave number, reminiscent of wave propagation phenomena in exterior problems in physical space. In the variational multiscale method, artificial viscosity is incorporated in the annular layer $[\overline{k}, k']$ to approximate the energy-transfer mechanism. This is reminiscent of the perfectly-matched layer.
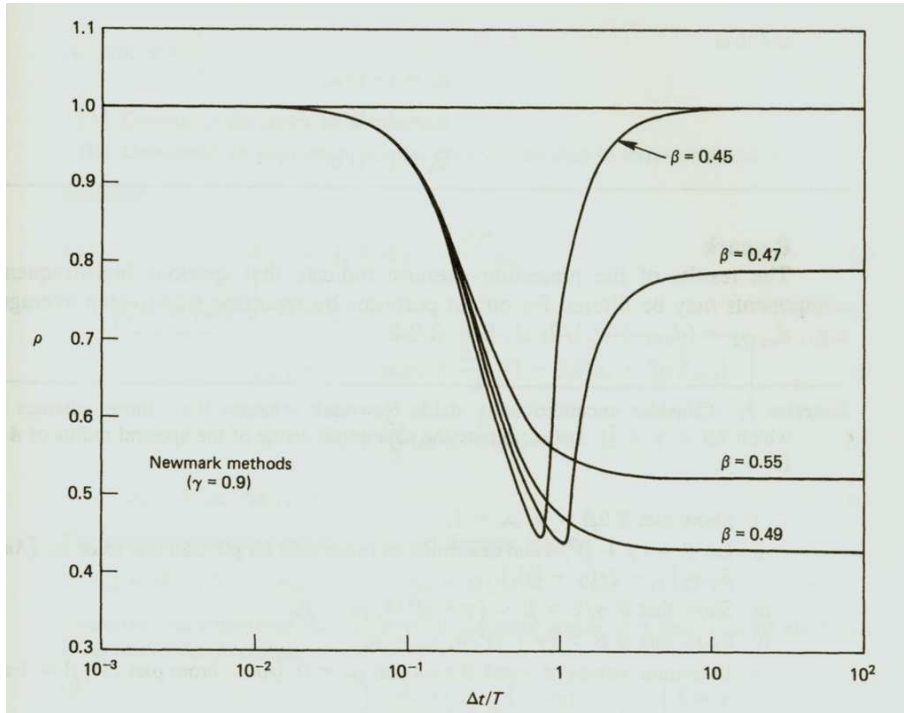
Figure 45. Spectral radii for Newmark methods with varying β.

be developed to remove high-frequency components of the solution, but that care needed to be exercised in order not to degrade accuracy in low-frequency components. The HHT α-method (see Hilber, Hughes and Taylor, 1977; Hilber and Hughes, 1978) and Park's method (Park, 1975) are two well-known integrators designed to satisfy these objectives. For further discussion and evaluation, see Hughes (1987). There again is an analogy with the variational multiscale method in that dissipation is added in the high wave-number regime to remove spurious pile-up of energy near the cutoff (i.e., limit of resolution) whereas it is avoided in the low wave-number regime so as not to degrade accuracy in the well-resolved modes. There are similarities with the other ideas described previously *mutatis mutandis*. As a measure of the high-frequency dissipation, one often uses the spectral radius of the amplification operator. A value of 1 indicates no dissipation and a value of 0 indicates maximal dissipation. Figure 45 illustrates the cusp-like behavior of spectral radii of some dissipative integrators used in structural dynamics. Note the absence of dissipation in low frequencies and the presence of dissipation in high frequencies.

6.6. Summary

In this section a variational multiscale approach to Large Eddy Simulation, has been described. The approach may be contrasted with classical LES in which modeling of the subgrid-scale stress in the filtered equations is performed first, and scale separation is accomplished *a*

posteriori by, for example, the dynamic modeling procedure.

Criticisms lodged against the classical LES/Smagorinsky model are addressed in the context of the present approach. Specifically, even with a positive, constant-coefficient, eddy viscosity term, the present approach:

1. Yields the correct asymptotic behavior at walls for the classical Reynolds stress, cross-stress, Leonard stress and, consequently, the subgrid-scale stress. In particular, no modeling of these terms is performed.
2. Reduces dissipation in the presence of mean shear.
3. Ameliorates damping of resolved structures since the eddy viscosity term acts only on fluctuations.

Furthermore, the present approach de-emphasizes the role of the Smagorinsky constant in producing dissipation, but accentuates dissipation effects associated with fluctuations. Consequently, a single value of the constant is anticipated to behave in a more satisfactory manner for a variety of complex flows.

In addition, the variational equation governing large scales, which is unmodeled, is identically satisfied by all exact solutions of the Navier-Stokes equations. This is often referred to as the "consistency condition" and is a key condition for obtaining error estimates. This may be contrasted with the classical LES/constant-coefficient Smagorinsky model case which does not possess this property.

On the other hand, the eddy viscosity models considered herein are very simple, perhaps too simple. The energy transfers from low wave numbers to unresolved modes, present in coarse and inviscid LES and manifested by the plateaus in Figures 42 and 43, are not well represented by small-scale viscous mechanisms. Consequently, the search for better methods continues. Nevertheless, experience so far with the present method has been remarkably good. Results with spectral formulations of homogeneous isotropic flows and turbulent channel flows were presented in Hughes *et al.* (2001), Hughes, Oberai and Mazzei (2001) and Oberai and Hughes (2002). Improved results with a dynamic version have been reported on in Holmen *et al.* (2004), and Hughes, Wells and Wray (2003). The variational multiscale formulation of LES was also extended by Farhat and Koobus (2002) and Koobus and Farhat (2004) to the compressible Navier-Stokes equations for unstructured finite element and finite volume discretizations. Results for vortex shedding dominated flows are presented in Koobus and Farhat (2004) and shown to match experimental data. Other works which present results for the variational multiscale formulation of LES and variations are Winckelmans and Jeanmart (2001), Jeanmart and Winckelmans (2001), Collis (2002), and Ramakrishnan and Collis (2002,2004a,2004b,2004c).

A summary of the main tenets of the approach described herein is presented as follows:

(i) Variational projection in preference to filtering. This obviates the closure problem and complex issues associated with filtering and inhomogeneous wall-bounded flows are also eliminated.
(ii) *A priori* scale separation in preference to *a posteriori* scale separation. This facilitates modeling restricted to unresolved, high-wave number phenomena rather than all wave numbers as in classical LES.

(iii) Modeling confined to the small-scale equation in preference to modeling within the large-scale equation. This means that the large-scale equation is unmodeled and is consistent in the weighted residual sense, in contrast to the modeled filtered equations.

6.7. Appendix: Semi-discrete formulation

In this appendix, the ideas are illustrated in terms of a more traditional semi-discrete formulation in which a midpoint rule algorithm is used for time discretization. Let $\boldsymbol{u}_n$ and p_n represent the algorithmic solution at time t_n. The time step is denoted $\Delta t = t_{n+1} - t_n$. It proves convenient to employ the jump and mean value operators, viz.,

$$[\boldsymbol{u}] \;=\; \boldsymbol{u}_{n+1} - \boldsymbol{u}_n \tag{469}$$

$$\langle \boldsymbol{u} \rangle \;=\; \tfrac{1}{2}\left(\boldsymbol{u}_{n+1} + \boldsymbol{u}_n\right) \;. \tag{470}$$

The algorithm is an approximation to the semi-discrete variational formulation, given as follows:

$$\left(\boldsymbol{w}, \frac{\partial \boldsymbol{u}}{\partial t}\right)_{\Omega} - (\boldsymbol{\nabla}\boldsymbol{w}, \boldsymbol{u} \otimes \boldsymbol{u})_{\Omega} + (q, \boldsymbol{\nabla}\cdot\boldsymbol{u})_{\Omega} - (\boldsymbol{\nabla}\cdot\boldsymbol{w}, p)_{\Omega} + (\boldsymbol{\nabla}^s \boldsymbol{w}, 2\nu\boldsymbol{\nabla}^s\boldsymbol{u})_{\Omega} = (\boldsymbol{w}, \boldsymbol{f})_{\Omega} \tag{471}$$

Midpoint rule

$$\frac{1}{\Delta t}(\boldsymbol{w}, [\boldsymbol{u}])_{\Omega} \;-\; (\boldsymbol{\nabla}\boldsymbol{w}, \langle\boldsymbol{u}\rangle \otimes \langle\boldsymbol{u}\rangle)_{\Omega} \;+\; (q, \boldsymbol{\nabla}\cdot\langle\boldsymbol{u}\rangle)_{\Omega} \;-\; (\boldsymbol{\nabla}\cdot\boldsymbol{w}, \langle p\rangle)_{\Omega}$$
$$+\; (\boldsymbol{\nabla}^s\boldsymbol{w}, 2\nu\boldsymbol{\nabla}^s\langle\boldsymbol{u}\rangle)_{\Omega} \;=\; (\boldsymbol{w}, \langle\boldsymbol{f}\rangle)_{\Omega} \tag{472}$$

The kinetic energy evolution law immediately follows from (472) by replacing $\boldsymbol{w}$ with $\langle\boldsymbol{u}\rangle$ and q with $\langle p\rangle$, i.e.,

$$\tfrac{1}{2}\|\boldsymbol{u}_{n+1}\|_{\Omega}^2 \;+\; 2\nu\Delta t\|\boldsymbol{\nabla}^s\langle\boldsymbol{u}\rangle\|_{\Omega}^2 \;=\; \tfrac{1}{2}\|\boldsymbol{u}_n\|_{\Omega}^2 \;+\; \Delta t\,(\langle\boldsymbol{u}\rangle, \langle\boldsymbol{f}\rangle)_{\Omega} \;. \tag{473}$$

In addition,

$$\tfrac{1}{2}\|\boldsymbol{u}_{n+1}\|_{\Omega}^2 \;+\; \nu\Delta t\|\boldsymbol{\nabla}^s\langle\boldsymbol{u}\rangle\|_{\Omega}^2 \;\leq\; \tfrac{1}{2}\|\boldsymbol{u}_n\|_{\Omega}^2 \;+\; \frac{C_{\Omega}\Delta t}{4\nu}\|\langle\boldsymbol{f}\rangle\|_{\Omega}^2 \tag{474}$$

where C_{Ω} is defined by (417).

The multiscale procedure is developed in analogous fashion to the space-time case (see Section 6.4). Let

$$\boldsymbol{u}_n \;=\; \overline{\boldsymbol{u}}_n + \boldsymbol{u}_n' \tag{475}$$

$$p_n \;=\; \overline{p}_n + p_n' \tag{476}$$

$$\boldsymbol{w} \;=\; \overline{\boldsymbol{w}} + \boldsymbol{w}' \tag{477}$$

$$q \;=\; \overline{q} + q' \tag{478}$$

These are substituted into (472) resulting in equations governing large and small scales, as before. The details, which are straightforward, are left to the interested reader. Modeling also follows the ideas developed previously, namely, to the left-hand side of (472) add the term

$$(\boldsymbol{\nabla}^s\boldsymbol{w}', 2\nu_T'\boldsymbol{\nabla}^s\langle\boldsymbol{u}'\rangle)_{\Omega} \;. \tag{479}$$

This amounts to adding viscous dissipation to the small scales equation. The modification to the kinetic energy identity, (473), is

$$\tfrac{1}{2} \left|\left|\boldsymbol{u}_{n+1}\right|\right|^2_\Omega + 2\nu\Delta t \left|\left|\boldsymbol{\nabla}^s\langle\boldsymbol{u}\rangle\right|\right|^2_\Omega + \Delta t \left|\left|(2\nu'_T)^{1/2}\boldsymbol{\nabla}^s\langle\boldsymbol{u'}\rangle\right|\right|^2_\Omega = \tfrac{1}{2}\left|\left|\boldsymbol{u}_n\right|\right|^2_\Omega + \Delta t\,(\langle\boldsymbol{u}\rangle,\langle\boldsymbol{f}\rangle)_\Omega \quad (480)$$

from which follows:

$$\tfrac{1}{2} \left|\left|\boldsymbol{u}_{n+1}\right|\right|^2_\Omega + \nu\Delta t \left|\left|\boldsymbol{\nabla}^s\langle\boldsymbol{u}\rangle\right|\right|^2_\Omega + \Delta t \left|\left|(2\nu'_T)^{1/2}\boldsymbol{\nabla}^s\langle\boldsymbol{u'}\rangle\right|\right|^2_\Omega \leq \tfrac{1}{2}\left|\left|\boldsymbol{u}_n\right|\right|^2_\Omega + \frac{C_\Omega\Delta t}{4\nu}\left|\left|\langle\boldsymbol{f}\rangle\right|\right|^2_\Omega \quad (481)$$

Remark

As remarked previously, the term $(\boldsymbol{\nabla}\langle\boldsymbol{w}\rangle,\langle\boldsymbol{u}\rangle\otimes\langle\boldsymbol{u}\rangle)_\Omega$ may need to be altered in the discrete case in order to achieve

$$(\boldsymbol{\nabla}\langle\boldsymbol{u}\rangle,\langle\boldsymbol{u}\rangle\otimes\langle\boldsymbol{u}\rangle)_\Omega = 0 \ . \tag{482}$$

See Quarteroni and Valli (1994), p.435.

ACKNOWLEDGEMENTS

REFERENCES

Aliabadi SK and Tezduyar TE. Space-time finite element computation of compressible flows involving moving boundaries and interfaces. *Computer Methods in Applied Mechanics and Engineering* 1993; **107**:209–223.

Asensio MI, Russo A, and Sangalli G. The residual-free bubble numerical method with quadratic elements. *Mathematical Models and Methods in Applied Sciences* 2004; (to appear).

Baiocchi C, Brezzi F and Franca LP. Virtual bubbles and the Galerkin/least squares method. *Computer Methods in Applied Mechanics and Engineering* 1993; **105**:125–142.

Barbosa, HJC and Hughes TJR. Boundary Lagrange multipliers in finite elements methods: error analysis in natural norms. *Numerische Mathematik* 1992; **62**:1–15.

Bochev P and Dohrman C. A stabilized finite element method for the Stokes problem based on polynomial pressure projections. Submitted to *International Journal of Numerical Methods in Engineering* 2004.

Bochev P and Gunzburger M. An absolutely stable pressure-Poisson stabilized finite element method for the Stokes equations. *SIAM Journal on Numerical Analysis* (to appear).

Borue V and Orszag SA. Self-similar decay of three-dimensional homogeneous turbulence with hyperviscosity. *Physical Review E* 1994; **51**(2):R856–R859.

Borue V and Orszag SA. Kolmogorov's refined similarity hypothesis for hyperviscous turbulence. *Physical Review E* 1996; **53**(1):R21–R24.

Brezzi F, Bristeau MO, Franca LP, Mallet M and Roge G. A relationship between stabilized finite element methods and the Galerkin method with bubble functions. *Computer Methods in Applied Mechanics and Engineering* 1992; **96**:117–129.

Brezzi F, Franca LP, Hughes TJR and Russo A. $b = \int g$. *Computer Methods in Applied Mechanics and Engineering* 1997; **145**:329–339.

Brezzi F, Hauke G, Marini LD, and Sangalli G. Link-cutting bubbles for convection-diffusion-reaction problems. *Mathematical Models and Methods in Applied Sciences* 2003; **3**(13):445–461.

Brezzi F, Hughes TJR, Marini LD, Russo A, and Süli E. *A priori* error analysis of a finite element method with residual-free bubbles for advection dominated equations. *SIAM Journal on Numerical Analysis* 1999; **36**:1933–1948.

Brezzi F and Marini LD. Augmented spaces, two-level methods, and stabilizing subgrids. *International Journal for Numerical Methods in Fluids* 2002; **40**:31–46.

Brezzi F, Marini LD, Houston P, and Süli E. Modeling subgrid viscosity for advection-diffusion problems. *Computer Methods in Applied Mechanics and Engineering* 2000; **190**: 1601–1610.

Brezzi F, Marini LD, and Russo A. Applications of pseudo residual-free bubbles to the stabilization of convection-diffusion problems. *Computer Methods in Applied Mechanics and Engineering* 1998; **166**:51–63.

Brezzi F, Marini LD, and Russo A. On the choice of a stabilizing subgrid for convection-diffusion problems. *Computer Methods in Applied Mechanics and Engineering* 2004; (to appear).

Brezzi F, Marini LD, and Süli E. Residual-free bubbles for advection-diffusion equations. *Numerische Mathematik* 2000; **85**:31–47.

Brezzi F and Russo A. Choosing bubbles for advection-diffusion problems. *Mathematical Models and Methods in Applied Sciences* 1994; **4**:571–587.

Brooks AN and Hughes TJR. Streamline upwind / Petrov-Galerkin formulations for convection dominated flows with particular emphasis on the incompressible Navier-Stokes equations. *Computer Methods in Applied Mechanics and Engineering* 1982; **32**:199–259.

Carati D, Winckelmans GS and Jeanmart H. On the modeling of the subgrid-scale and filtered-scale stress tensors in large-eddy simulation. *Journal of Fluid Mechanics* 2001; **441**:119-138.

Cerutti S, Meneveau C and Knio OM. Spectral and hyper eddy viscosity in high-Reynolds-number turbulence. *Journal of Fluid Mechanics* 2000; **421**:307–338.

Ciarlet PG. *The Finite Element Method for Elliptic Problems*. North-Holland:Amsterdam. 1978.

Codina R. Comparison of some finite element methods for solving the diffusion-convection-reaction equation. *Computer Methods in Applied Mechanics and Engineering* 1998; **156**:185–210.

Codina R. On stabilized finite element methods for linear systems of convection-diffusion-reaction equations. *Computer Methods in Applied Mechanics and Engineering* 2000; **188**:61–82.

Codina R and Blasco J. Analysis of a pressure-stabilized finite element approximation of the stationary Navier-Stokes equations. *Numerische Mathematik* 2000a; **87**:59–81.

Codina R and Blasco J. Stabilized finite element method for the transient Navier-Stokes equations based on a pressure gradient projection. *Computer Methods in Applied Mechanics and Engineering* 2000b; **182**:277–300.

Collis SS. Monitoring unresolved scales in multiscale turbulence modeling. *Physics of Fluids* 2001; **13**(6):1800–1806.

Collis SS. The DG/VMS method for unified turbulence simulation. AIAA 2002-3124. AIAA 32nd Fluid Dynamics Conference, St. Louis, Missouri, June 24-27, 2002.

Domaradzki JA, Liu W and Brachet ME. An analysis of subgrid-scale interactions in numerically simulated isotropic turbulence. *Physics of Fluids A* 1993; **5**:1747–1759.

Domaradzki JA, Liu W, Härtel C and Kleiser L. Energy transfer in numerically simulated wall-bounded turbulent flows. *Physics of Fluids* 1994; **6**(4):1583–1599.

Douglas Jr. J and Wang JP. An absolutely stabilized finite element method for the Stokes problem. *Mathematical of Computation* 1989; **52**:495–508.

Dubois T, Jauberteau F and Temam R. Solution of the incompressible Navier-Stokes equations by the nonlinear Galerkin method. *Journal of Scientific Computing* 1993; **8**:167–194.

Dubois T, Jauberteau F and Temam R. Incremental unknowns, multilevel methods and the numerical simulation of turbulence. *Computer Methods in Applied Mechanics and Engineering* 1998; **159**:123–189.

E W and Engquist B. The heterogeneous multiscale methods. *Communications in Mathematical Sciences* 2003; **1**(1):87–132.

Farge M, Schneider K and Kevlahan N. Non-Gaussianity and coherent vortex simulation for two-dimensional turbulence using an adaptive wavelet basis. *Physics of Fluids* 1999; **11**(8):2187–2201.

Farhat C, Harari I and Franca L. The discontinuous enrichment method. *Computer Methods in Applied Mechanics and Engineering* 2001; **190**:6455–6479.

Farhat C, Harari I and Hetmaniuk U. A discontinuous Galerkin method with Lagrange multipliers for the solution of Helmholtz problems in the mid-frequency regime. *Computer Methods in Applied Mechanics and Engineering* 2003a; **192**;1389–1419.

Farhat C, Harari I and Hetmaniuk U. The discontinuous enrichment method for multiscale analysis. *Computer Methods in Applied Mechanics and Engineering* 2003b; **192**:3195–3210.

Farhat C and Koobus B. Finite volume discretization on unstructured meshes of the multiscale formulation of large eddy simulations. *Proceedings of the Fifth World Congress on Computational Mechanics (WCCM V)*, Mang HA, Rammerstorfer FG and Eberhardsteiner J (eds.), Vienna University of Technology, Austria, July 7-12, 2002.

Franca LP, Do Carmo EGD. The Galerkin gradient least-squares method. *Computer Methods in Applied Mechanics and Engineering* 1989; **74**:41–54.

Franca LP, Farhat C. On the limitations of bubble functions. *Computer Methods in Applied Mechanics and Engineering* 1994; **117**:225–230.

Franca LP, Farhat C. Anti-stabilizing effects of bubble functions. *Proceedings of the Third World Congress on Computational Mechanics*, Extended Abstracts. Chiba, Japan, (August 1994) Vol. 2:1452–1453.

Franca LP, Farhat C. Bubble functions prompt unusual stabilized finite element methods. *Computer Methods in Applied Mechanics and Engineering* 1995; **123**:299–308.

Franca LP and Frey SL. Stabilized finite element methods: II. The incompressible Navier-Stokes equations. *Computer Methods in Applied Mechanics and Engineering* 1992; **99**:209–233.

Franca LP, Frey SL and Hughes TJR. Stabilized finite element methods: I. Application to the advection-diffusion model. *Computer Methods in Applied Mechanics and Engineering* 1992; **95**:253–276.

Franca LP and Hughes TJR. Two classes of mixed finite element methods. *Computer Methods in Applied Mechanics and Engineering* 1988; **69**:89–129.

Franca LP and Hughes TJR. Convergence analysis of Galerkin/least–squares methods for symmetric advective-diffusive forms of the Stokes and incompressible Navier-Stokes equations. *Computer Methods in Applied Mechanics and Engineering* 1988; **105**:285–298.

Franca LP, Hughes TJR and Stenberg R. Stabilized finite element methods for the Stokes problem. In *Incompressible Computational Fluid Dynamics*, Gunzburger MD and Nicolaiades RA (eds). Cambridge University Press:Cambridge; 87–107.

Franca LP, Hughes TJR, Loula AFD and Miranda I. A new family of stable elements for nearly incompressible elasticity based on a mixed Petrov-Galerkin finite element formulation. *Numerische Mathematik* 1988; **53**:123–141.

Franca LP, Nesliturk A, and Stynes M. On the stability of residual-free bubbles for convection-diffusion problems and their approximation by a two-level finite element method. *Computer Methods in Applied Mechanics and Engineering* 1998; **166**(1-2):35–49.

Franca LP and Russo A. Deriving upwinding, mass lumping and selective reduced integration by residual-free bubbles. *Applied Mathematics Letters* 1996; **9**:83–88.

Franca LP and Valentin F. On an improved unusual stabilized finite element method for the advective-reactive-diffusive equation. *Computer Methods in Applied Mechanics and Engineering* 2000; **190**:1785–1800.

Galdi GP and Layton WJ. Approximation of the larger eddies in fluid motion. II: A model for space-filtered flow. *Mathematical Models and Methods in Applied Sciences* 2000; **10**(3):343–351.

Germano M, Piomelli U, Moin P and Cabot WH. A dynamic subgrid-scale model. *Physics of Fluids A* 1991; **3**:1760–1765.

Ghosal S and Moin P. The basic equations for the Large Eddy Simulation of turbulent flows in complex-geometry. *Journal of Computational Physics* 1995; **118**:24–37.

Givoli D. *Numerical Methods for Problems in Infinite Domains.* Elsevier:Amsterdam. 1992.

Givoli D and Keller JB. An exact non-reflecting boundary condition. *Journal of Computational Physics* 1988; **82**:172–192.

Givoli D. and Keller JB. A finite element method for large domains. *Computer Methods in Applied Mechanics and Engineering* 1989; **76**:41–66.

Guermond J-L. Subgrid stabilization of Galerkin approximations of linear monotone operators. *IMA Journal on Numerical Analysis* 2001; **21**(1):165–197.

Harari I, Farhat C and Hetmaniuk U. Multiple-stencil dispersion analysis of the Lagrange multipliers in a discontinuous Galerkin method for the Helmholtz equation. *Journal of Computational Acoustics* 2003; **ll**: 239–254.

Harari I and Hughes TJR. Analysis of continuous formulations underlying the computation of time-harmonic acoustics in exterior domains. *Computer Methods in Applied Mechanics and Engineering* 1992; **97**:103–124.

Harari I and Hughes TJR. Studies of domain-based formulations for computing exterior problems of acoustics. *International Journal of Numerical Methods in Engineering* 1994. **37**:2935–2950.

Harari I, Turkel E and Slavutin M. Analytical and numerical studies of a finite element PML for the Helmholtz equation. *Journal of Computational and Acoustics* 2000; **8**(1):121–137.

Hemker PW. Mixed defect correction iteration for the accurate solution of the convection-diffusion equation. In *Multigrid Methods*, Hackbusch W and Trottenberg U (eds.), *Lecture Notes in Mathematics, Vol. 960.* Springer-Verlag:New York, 1981.

Heisenberg W. On the theory of statistical and isotropic turbulence. *Proceedings of the Royal Society of London, Series A, Mathematical and Physical Sciences* 1948; **195**(1042):402–406.

Hilber H and Hughes TJR. Collocation, dissipation and 'overshoot' for time integration schemes in structural dynamics. *Earthquake Engineering and Structural Dynamics* 1978; **6**:99–118.

Hilber H, Hughes, TJR and Taylor R. Improved numerical dissipation for time integration algorithms in structural dynamics. *Earthquake Engineering and Structural Dynamics* 1977; **5**:283–292.

Holmen J, Hughes TJR, Oberai AA and Wells GN. Sensitivity of the scale partition for variational multiscale LES of channel flow. *Physics of Fluids* 2004; **16**(3):824–827.

Holmes B, Dias J, Jaroux B, Sassa T and Ban Y. Predicting the wind noise from the pantograph cover of a train. *International Journal of Numerical Methods in Fluids* 1997; **24**:1307–1319.

Hughes TJR. *The Finite Element Method: Linear Static and Dynamic Finite Element Analysis.* Prentice-Hall:Englewood Cliffs, New Jersey. 1987.

Hughes TJR. Multiscale phenomena: Green's functions, the Dirichlet-to-Neumann formulation, subgrid-scale models, bubbles and the origin of stabilized methods. *Computer Methods in Applied Mechanics and Engineering* 1995; **127**:387–401.

Hughes TJR and Brezzi F. On drilling degrees-of-freedom. *Computer Methods in Applied Mechanics and Engineering* 1989; **72**:105–121.

Hughes TJR, Engel G, Mazzei L and Larson MG. The continuous Galerkin method is locally conservative. *Journal of Computational Physics* 2000; **163**:467–488.

Hughes TJR and Franca LP. A new finite element formulation for computational fluid dynamics. VII. The Stokes problem with various well-posed boundary conditions: symmetric formulations that converge for all velocity/pressure spaces. *Computer Methods in Applied Mechanics and Engineering* 1987; **65**:85–96.

Hughes TJR, Franca LP and Balestra M. A new finite element formulation for fluid dynamics: V. Circumventing the Babŭska-Brezzi condition. A stable Petrov-Galerkin formulation of the Stokes problem accommodating equal-order interpolations. *Computer Methods in Applied Mechanics and Engineering* 1986; **59**:85–99.

Hughes TJR, Franca LP, Harari I, Mallet M, Shakib F and Spelce TE. Finite element method for high-speed flows: Consistent calculation of boundary flux. AIAA-87-0556, AIAA 25th Aerospace Sciences Meeting, Reno, Nevada, January 12-15, 1987.

Hughes TJR, Franca LP and Hulbert GM. A new finite element formulation for computational fluid dynamics. VIII. The Galerkin/least-squares method for advective-diffusive equations. *Computer Methods in Applied Mechanics and Engineering* 1989; **73**:173–189.

Hughes TJR, Franca LP and Mallet M. A new finite element method for computational fluid dynamics: VI. Convergence analysis of the generalized SUPG formulation for linear time-dependent multidimensional advective-diffusive systems. *Computer Methods in Applied Mechanics and Engineering* 1987; **63**:97–112.

Hughes TJR, Hauke G and Jansen K. Stabilized finite element methods for fluids: inspirations, origins, status and recent developments. In *Recent Developments in Finite Element Analysis. A Book Dedicated to Robert L. Taylor*, Hughes TJR, Oñate E and Zienkiewicz O (eds), International Center for Numerical Methods in Engineering:Barcelona, Spain, 1994; 272–292.

Hughes TJR and Hulbert GM. Space-time finite element methods for elastodynamics: Formulations and error estimates. *Computer Methods in Applied Mechanics and Engineering* 1988; **66**:339–363.

Hughes TJR and Mallet M. A new finite element method for computational fluid dynamics: III. The generalized streamline operator for multidimensional advection-diffusion systems. *Computer Methods in Applied Mechanics and Engineering* 1986; **58**:305–328.

Hughes TJR, Mallet M and Mizukami A. A new finite element method for computational fluid dynamics: II. Beyond SUPG. *Computer Methods in Applied Mechanics and Engineering* 1986; **54**:341–355.

Hughes TJR, Mazzei L, Oberai AA and Wray AA. The multiscale formulation of large eddy simulation: Decay of homogeneous isotropic turbulence. *Physics of Fluids* 2001. **13**:505–512.

Hughes TJR, Oberai AA and Mazzei L 2001b. Large eddy simulation of turbulent channel flows by the variational multiscale method. *Physics of Fluids* 2001; **13**(6):1784–1799.

Hughes TJR, Wells GN and Wray AA. Energy transfers and spectral eddy viscosity in large eddy simulations of homogeneous isotropic turbulence. Preprint: 2003.

Hulbert GM and Hughes TJR. Space-time finite element methods for second-order hyperbolic equations. *Computer Methods in Applied Mechanics and Engineering* 1990; **84**:327–348.

Jansen K, Whiting C, Collis SS and Shakib F. A better consistency for low-order stabilized finite element methods. *Computer Methods in Applied Mechanics and Engineering* 1999; **174**:153–170.

Jeanmart H. and Winckelmans GS. Comparison of recent dynamic subgrid-scale models in the case of the turbulent channel flow. In *Proceedings Summer Program 2002*:105-116, Center for Turbulence Research, Stanford University & NASA Ames, 2002.

John V and Layton W. Approximation of the larger eddies in fluid motion. I: Direct simulation for the Stokes problem. Preprint: 1998.

Johnson C. Streamline diffusion methods for problems in fluid mechanics. In *Finite Elements in Fluids, Vol. VI* Gallagher R, Carey GF, Oden JT and Zienkiewicz OC (eds). Wiley:Chichester, 1986; 251–261.

Johnson C. *Numerical Solutions of Partial Differential Equations by the Finite Element Method*. Cambridge University Press: Cambridge, 1987.

Johnson C. Finite element methods for flow problems. *Unstructured Grid Methods for Advection Dominated Flows*. AGARD Report 787, 1992.

Johnson C and Hansbo P. Adaptive finite element methods in computational mechanics. Preprint No. 1992-04/ISSN 0347-2809, Department of Mathematics, Chalmers University of Technology, University of Göteborg, Göteborg, Sweden: 1992.

Johnson C, Nävert U and Pitkäranta J. Finite element methods for linear hyperbolic problems. *Computer Methods in Applied Mechanics and Engineering* 1984; **45**:285–312.

Koobus B and Farhat C. Finite volume/element discretization on unstructured meshes of the multiscale formulation of the large eddy simulation method and application to vortex shedding. *Computer Methods in Applied Mechanics and Engineering* (to appear).

Kraichnan RH. Eddy viscosity in two and three dimensions. *Journal of Atmospheric Sciences* 1976; **33**(8):1521–1536.

Lai CH. A defect-correction method for multiscale problems in computational aeroacoustics. In *Lecture Notes in Computational Science and Engineering*, Pavarino L et al. (eds.). Springer Verlag, 2002; 147–156.

Layton WJ. A nonlinear subgrid-scale model for incompressible viscous flow problems. *SIAM Journal on Scientific Computing* 1996; **17**:347–357.

Lighthill MJ. On sound generated aerodynamically. I. General theory. *Proceedings of the Royal Society of London, Series A, Mathematical and Physical Sciences* 1952; **211**(1107):1–32.

Lighthill MJ. On sound generated aerodynamically. II. Turbulence as a sound source. *Proceedings of the Royal Society of London, Series A, Mathematical and Physical Sciences* 1954; **222**(1148):564–587.

Lilly DK. On the application of the eddy viscosity concept in the inertial subrange of turbulence. NCAR Manuscript 123. Boulder, Colorado, 1966.

Lilly DK. The representation of small-scale turbulence in numerical simulation experiments. In *Proceedings of the IBM Scientific Computing Symposium on Environmental Sciences*. Yorktown Heights, New York, 1967.

Lilly DK. The length scale for subgrid-scale parametrization with anisotropic resolution. *CTR Annual Research Briefs*, Center for Turbulence Research, Stanford University/NASA Ames Research Center, 1988.

McComb D and Young A. Explicit-scales projections of the partitioned non-linear term in direct numerical simulation of the Navier-Stokes equations. *Second Monte Verita Colloquium on Fundamental Problematic Issues in Fluid Turbulence*. Ascona, Switzerland, March 23-27, 1998. Available on the web at http://arxiv.org.

Mittal S and Tezduyar TE. Massively parallel finite element computation of incompressible flows involving fluid-body interactions. *Computer Methods in Applied Mechanics and Engineering* 1994; **112**:253–282.

Moin P, Squire K, Cabot WH and Lee S. A dynamic subgrid-scale model for compressible turbulence and scalar transport. CTR Manuscript 124, Center for Turbulence Research, Stanford University/NASA Ames Research Center, 1991.

Nävert U. *A Finite Element Method for Convection-diffusion Problems*. Ph.D. Thesis, Department of Computer Science. Chalmers University of Technology, Göteborg, Sweden, 1982.

Oberai AA and Hughes TJR. The variational multiscale formulation of LES: Channel flow at $Re_\tau = 590$. AIAA paper 2002-1056. 40th AIAA Aerospace Sciences Meeting and Exhibit, Reno, Nevada, January 14-17, 2002.

Oberai AA and Pinsky PM. Finite element methods for the Helmholtz equation based on global multiscale variational forms. *Computer Methods in Applied Mechanics and Engineering* 1998; **154**:281–297.

Oberai AA, Roknaldin F and Hughes TJR. Computational procedures for determining structural acoustic response due to hydrodynamic sources. *Computer Methods in Applied Mechanics and Engineering* 2000; **190**(3-4):345–361.

Oberai AA, Roknaldin F and Hughes TJR. Trailing-edge noise from a finite chord airfoil. *AIAA Journal* 2002; **40**(11):2206–2216.

Papastavrou A and Verfürth R. *A posteriori* error estimators for stationary convection-diffusion problems: a computational comparison. *Computer Methods in Applied Mechanics and Engineering* 2000; **189**:449–462.

Park KC. Evaluating time integration methods for nonlinear dynamic analysis. In *Finite Element Analysis of Transient Nonlinear Behavior Vol. AMD 14.*, Belytschko T et al. (eds.), ASME:New York; 35–58.

Piomelli U. Large-eddy simulation: Present state and future perspectives. AIAA paper 1998-0534. 36th AIAA Aerospace Sciences Meeting and Exhibit, Reno, Nevada, January 12-15, 1998.

Quarteroni A and Valli A. *Numerical Approximation of Partial Differential Equations*. Springer-Verlag:Berlin, 1994.

Ramakrishnan S and Collis SS. Variational multiscale modeling for turbulence control. AIAA 2002-3280. AIAA 1st Flow Control Conference, St. Louis, Missouri, June 24-26, 2002.

Ramakrishnan S and Collis SS. Variational multiscale modeling for turbulence control. *AIAA Journal*, 2004a (to appear).

Ramakrishnan S and Collis SS. Partition selection in multiscale turbulence modeling. 2004b: Preprint.

Ramakrishnan S and Collis SS. Multiscale modeling for turbulence simulation in complex geometries. AIAA 2004-0241. 40th AIAA Aerospace Sciences Meeting and Exhibit, Reno, Nevada, January 5-8, 2004c.

Russo A. Bubble stabilization of finite element methods for the linearized incompressible Navier-Stokes equations. *Computer Methods in Applied Mechanics and Engineering* 1996a; **132**:335–343.

Russo A. *A posteriori* error estimators via bubble functions. *Mathematical Models and Methods in Applied Sciences* 1996b; **6**:33–41.

Saad Y. *Iterative methods for sparse linear systems*. PWS Publishing Company, Boston, MA. 1995.

Sangalli G. Global and local error analysis for the residual-free bubbles method applied to advection-dominated problems. *SIAM Journal on Numerical Analysis* 2000; **38**(5):1496–1522.

Sangalli G. A robust *a posteriori* estimator for the residual-free bubbles method applied to advection-diffusion problems. *Numerische Mathematik* 2001; **89**(2):379–399.

Sangalli G. Quasi-optimality of the SUPG method for the one-dimensional advection-diffusion problem. *SIAM Journal on Numerical Analysis* 2004 (to appear).

Scotti A and Meneveau C. Generalized Smagorinsky model for anisotropic grids. *Physics of Fluids A* 1993; **5**:2306–2308.

Scotti A, Meneveau C and Fatica M. Dynamic Smagorinsky model on anisotropic grids. *Physics of Fluids* 1997; **9**:1856–1858.

Silvester DJ and Kechkar N. Stabilized bilinear-constant velocity-pressure finite elements for the conjugate solution of the Stokes Problem. *Computer Methods in Applied Mechanics and Engineering* 1990; **79**:71–86.

Smagorinsky J. General circulation experiments with the primitive equations. I. The basic experiment. *Monthly Weather Review* 1963; **91**:99–164.

Stakgold I. *Green's Functions and Boundary Value Problems*. Wiley:New York, 1979.

Temam R. *Navier-Stokes Equations. Theory and Numerical Analysis* (3rd edn). North-Holland: Amsterdam, 1984.

Tezduyar TE, Behr M and Liou J. A new strategy for finite element computations involving moving boundaries and interfaces. The deforming-spatial-domain/space-time procedure. I. the concept and the preliminary numerical tests. *Computer Methods in Applied Mechanics and Engineering* 1992; **94**:339–351.

Tezduyar TE, Behr M, Mittal S and Liou J. A new strategy for finite element computations involving moving boundaries and interfaces. The deforming-spatial-domain/space-time procedure. II. Computation of free-surface flows, two-liquid flows, and flows with drifting cylinders. *Computer Methods in Applied Mechanics and Engineering* 1992; **94**:353–371.

Trottenberg U, Oosterlee C and Schüller A. *Multigrid*. Academic Press, 2001.

Venkatakrishnan V, Allmaras S, Kamenetskii D and Johnson F. Higher order schemes for the compressible Navier-Stokes equations. AIAA 2003-3987. AIAA 16th Computational Fluid Dynamics Conference, Orlando, Florida, June 23-26, 2003.

Verfürth R. *A posteriori* error estimators for stationary convection-diffusion equations. *Numerische Mathematik* 1998; **80**(4):641–663.

Wagner GJ and Liu WK. Coupling atomistic and continuum simulations using a bridging scale decomposition. *Journal of Computational Physics* 2003; **190**(1): 249–274.

Winckelmans GS and Jeanmart H. Assessment of some models for LES without/with explicit-filtering. In *Direct and Large-Eddy Simulation IV*, ERCOFTAC Series **8**:55-66, Geurts BJ, Friedrich R and Métais O (eds.), Kluwer:Dordrecht, 2001.

Winckelmans GS, Jeanmart H and Carati D. On the comparison of turbulence intensities from large-eddy simulation with those from experiment or direct numerical simulation. *Physics of Fluids* 2002; **14**(5):1809–1811.

Winckelmans GS, Wray AA, Vasilyev OV and Jeanmart H. Explicit-filtering large-eddy simulation using the tensor-diffusivity model supplemented by a dynamic Smagorinsky term. *Physics of Fluids* 2001; **13**(5):1385–1403.